

APPENDIX 1

**Project budget
15.2.2011**



SKYREC Budget 15.2.2011

- Projects paid: 494 327,37 €
- Projects not yet paid: 158 850,00 €
- Sum (projects ordered): 653 177,37 €

-> 46 822,63 € must be invoiced before 30.6.2011

+ extra 100 000 € after that



New project proposals

ÅA: Dew point measurements	30 000,00 €
ÅA: Corrosion tests in reducing conditions – PART II A&B	26 400,00
Boildec Oy: Material testing in furnace, test 5	20 000,00 €
VTT: Analyzes for Boildec test 5	11 500,00 €
VTT: Mill tests of superheater materials, test 2	100 000 ?
VTT: Magnetite formation, part 2	68 500,00 €
Total	258 400 €

APPENDIX 2

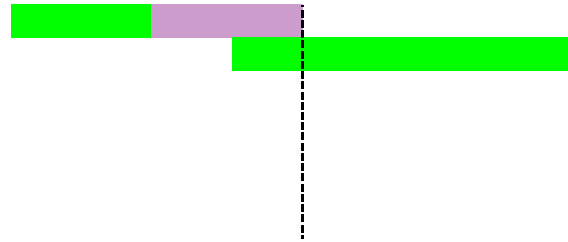
**Project schedule
15.2.2011**

SKYREC - schedule

15.12.2010



- OY: Activated carbon and UV-treatment - field tests
- OY: Activated carbon and UV-treatment - field tests, part 2
- V2 Development of chemicals testing
 - VTT Magnetite formation, part 2
- V3 Testing oxygen scavenging chemicals
- V4 Formation of magnetite layer in autoclave
- V5 Formation of magnetite layer in recovery boiler



WP5 Coordination and other

- K1 Coordinator
- K2 Secretary services
- K3 Meetings and communication
- K4 Translations

Original start date for project 1.1.2008

Decision from TEKES 24.4.2008

Organisation meeting 5.6.2008

Second meeting 18.9.2008

First order 30.10.2008

Intermediate report nro 1 to TEKES 1.1.2008 - 30.4.2008

Intermediate report nro 2 to TEKES 1.5.2008 - 31.10.2008

Intermediate report nro 3 to TEKES 1.11.2008 - 30.4.2009

Intermediate report nro 4 to TEKES 1.5.2009 - 31.10.2009

Intermediate report nro 5 to TEKES 1.11.2009 - 30.4.2010

Intermediate report nro 6 to TEKES 1.5.2010 - 30.10.2010

Intermediate report nro 7 to TEKES 1.11.2010 - 30.6.2011

Final report to TEKES



APPENDIX 3

Utilization of pyrolysis gases from the recovery boiler
Åbo Akademi
final report
15.2.2011

Finnish Recovery Boiler Committee SkyRec

Utilization of Pyrolysis Gases from the Recovery Boiler Preliminary studies

Final report 15.12.2010

Mikko Hupa, Nikolai DeMartini, Anders Brink, and Markus Engblom
Åbo Akademi University

Introduction

There is an interest to replace fossil fuels in pulp mills. One theoretical possibility is to extract gases from the lower part of the recovery boiler. These gases potentially have a heating value high enough to be used in, e.g. the lime kiln. In addition, gas extraction can also potentially increase the recovery boiler capacity.

This work was carried out to study possibilities for extracting gases from the lower part of a recovery boiler, to be used in the lime kiln. The extracted amount should be such that it would cover the need of a lime kiln with 30 MW thermal input, typical at a 500 000 – 550 000 ADt pulp mill. The study consisted of the following tasks:

- i) equilibrium calculations of gas composition as function of air factor at 900°C;
- ii) analysis of gas composition in the lower furnace in two recovery boilers using existing CFD results; and
- iii) estimation of the minimum and maximum dust content of the lower furnace gas.

It should be noted that the original project title refers to “Pyrolysis Gases”. However, this work was not restricted to only considering the gases released from black liquor during the pyrolysis stage of combustion. Instead, the “gas” that is referred to in this report is the flue gas from black liquor combustion at various air factors.

Equilibrium calculations

The fuel analysis of a typical Finnish liquor was used as basis for the equilibrium calculations. For the calculations the liquor was assumed to consist of two parts: (i) smelt and (ii) moisture + combustibles. Only the fraction consisting of moisture and combustibles was considered in the equilibrium calculations.

The elements in the liquor dry solids were first assumed to form smelt consisting of Na_2S and Na_2CO_3 . By difference the carbon and oxygen not bound in smelt were considered combustible. In addition, all hydrogen in liquor dry solids was assumed combustible. Thus, the input to the calculations concerning mass consisted of the amounts of black liquor moisture and combustible carbon, hydrogen, and oxygen. The black liquor heating value, excluding heat from sulfide oxidation, was used in calculation of the adiabatic flame temperature. The gas phase chemical species CH_4 , CO , CO_2 , H_2 , H_2O , O_2 , and N_2 and solid carbon (soot) were included in the calculations.

Two different equilibrium calculations of black liquor combustion with varying air factor were carried out:

- (i) considering the adiabatic flame temperature, which varies with the air factor and
- (ii) at a fixed temperature of 900°C .

Figure 1 presents the shares of gas phase species and solid carbon at the adiabatic temperature (T_{ad}) as function of air factor. The adiabatic temperature increases with the air factor, reaching 900°C at an air factor of about 0.45. The adiabatic temperature shown in Figure 1 was calculated assuming that black liquor and combustion air have an initial temperature of 25°C . Assuming an initial temperature of 200°C resulted in the adiabatic temperature reaching 900°C at an air factor of about 0.4.

Due to heat transfer inside the recovery furnace, it is motivated to assume that a gas, regardless of its adiabatic temperature, could have a temperature of 900°C when extracted from the recovery boiler.

Figure 2 presents the equilibrium gas composition as function of air factor at 900°C . The region of air factors which would result in adiabatic temperatures below 900°C is indicated. In addition, the region of zero heating value gas due to overstoichiometric combustion is indicated. Methane and solid carbon are not stable at 900°C and are therefore not included in Figure 2.

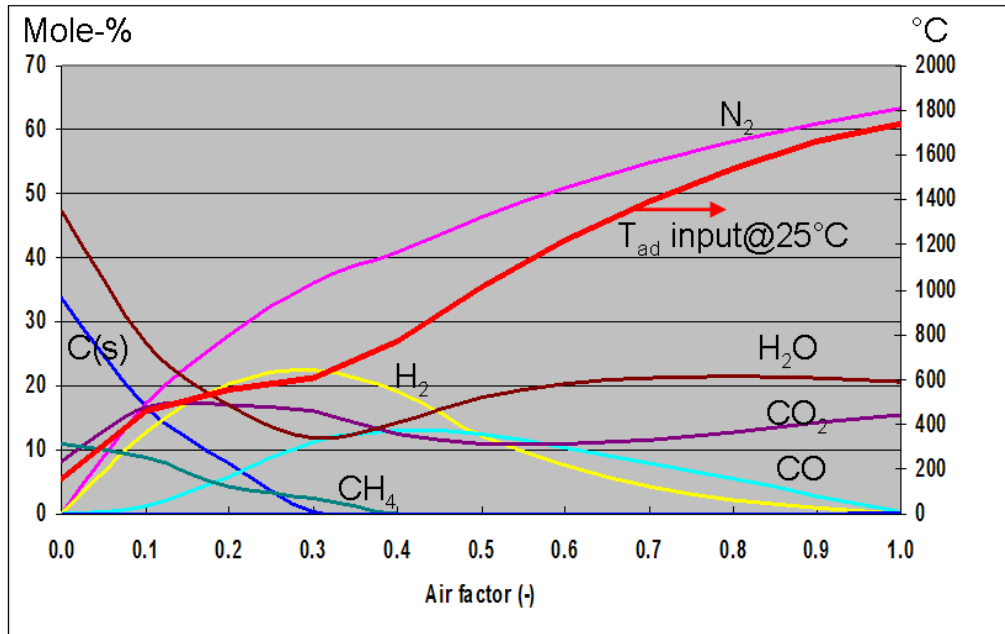


Figure 1. Equilibrium calculations: Shares of gas phase species and solid carbon at adiabatic temperature (T_{ad}) as function of air factor.

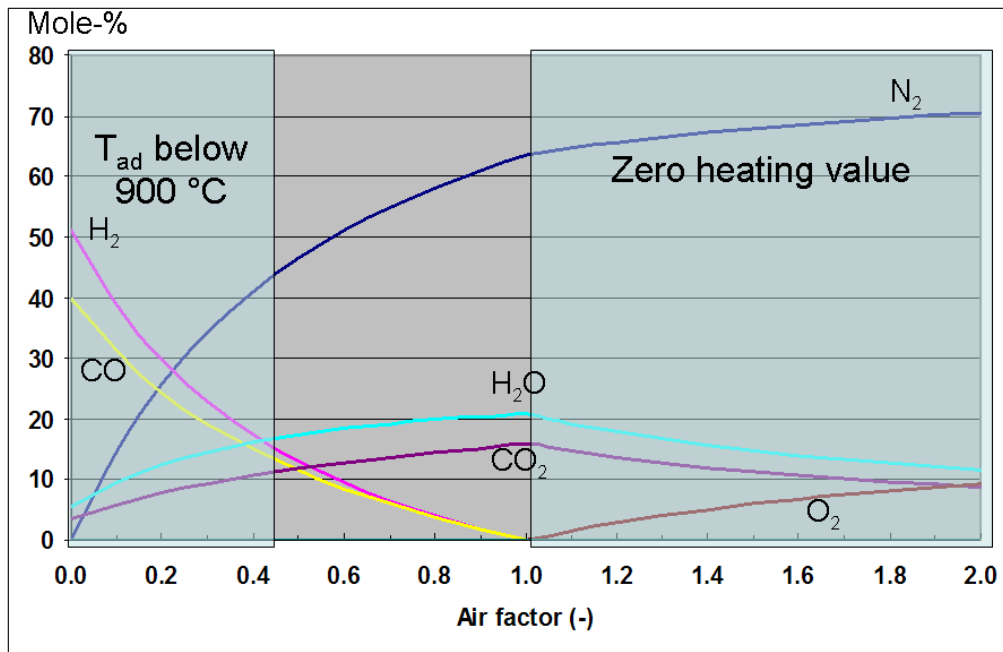


Figure 2. Equilibrium calculations: Gas composition as function of air factor at 900°C. Region of air factors which would result in adiabatic temperatures below 900°C also indicated, as well as the region of zero heating value gas due to overstoichiometric combustion.

Figure 3 presents the heating value of the gas as function of air factor corresponding to the composition presented in Figure 2 (chemical equilibrium at 900°C). The amount of gas to be extracted to cover 30 MW is indicated for two cases. The sensible enthalpy is excluded in calculation of the amount of gas needed. In addition to the heating value, the gas would contain some energy because of its temperature. Taking zero degrees Celsius as the reference temperature, in the case of 10kg/s extracted, the gas would contain 30 MW as heating value and about 9 MW as sensible enthalpy; the sensible enthalpy being 30% compared to the heating value of the gas. In the case of 3 kg/s extracted, there would be about 3 MW sensible enthalpy, which is 10% compared to the heating value.

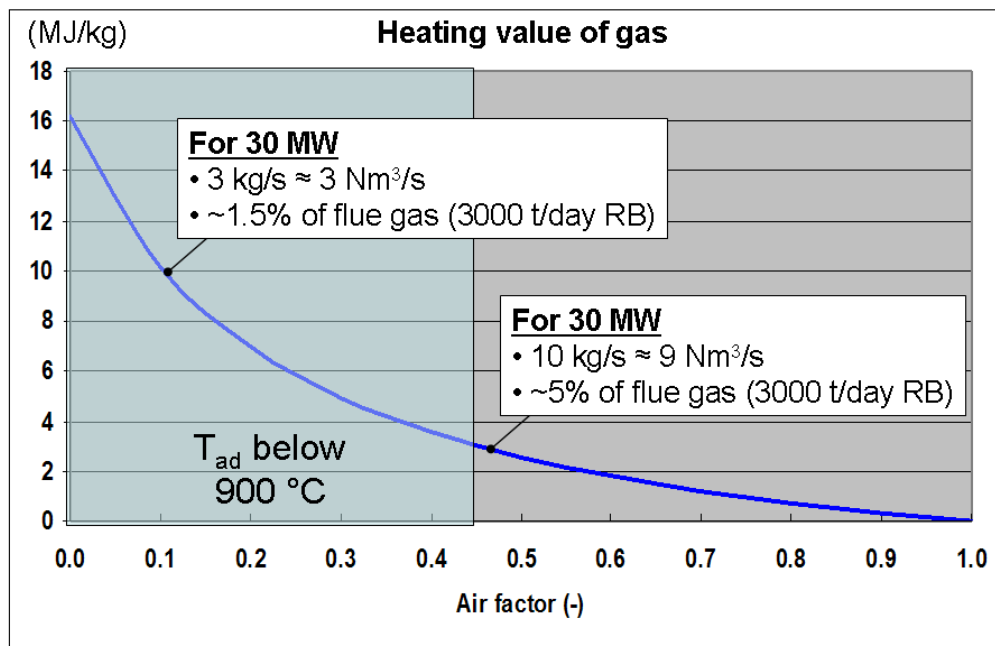


Figure 3. Gas heating value as function of air factor, from equilibrium calculations at 900°C. Region of air factors which would result in adiabatic temperatures below 900°C also indicated.

CFD simulations

Results from existing CFD simulations of two recovery furnaces were analyzed for the local gas composition in the lower furnace. The recovery boilers A and B have rated capacities of 3150 tds/d and 4450 tds/d, respectively.

Figure 4 presents the gas heating value in recovery furnaces A and B. The heating value of the gas is highest in those locations which have a high fuel-to-air ratio (low air factor).

In Furnace A, black liquor droplets hitting the back wall create a zone near the back wall between secondary and tertiary air levels with a gas heating value of about 3 MJ/kg. The location could be suitable for gas extraction.

In Furnace B, the spray is directed to a greater extent towards the char bed, resulting in the high-heating-value zones located above the bed. For each furnace (A and B), the simulated char bed as a whole was close to a balanced situation, i.e., the overall char bed burning rate closely matched the overall input rate of combustible matter. However, in Furnace B the high-heating-value zones above the char bed are associated with local carbon accumulation in the char bed, indicating bed growth in these locations. It is uncertain if Furnace B could be operated continuously in this manner.

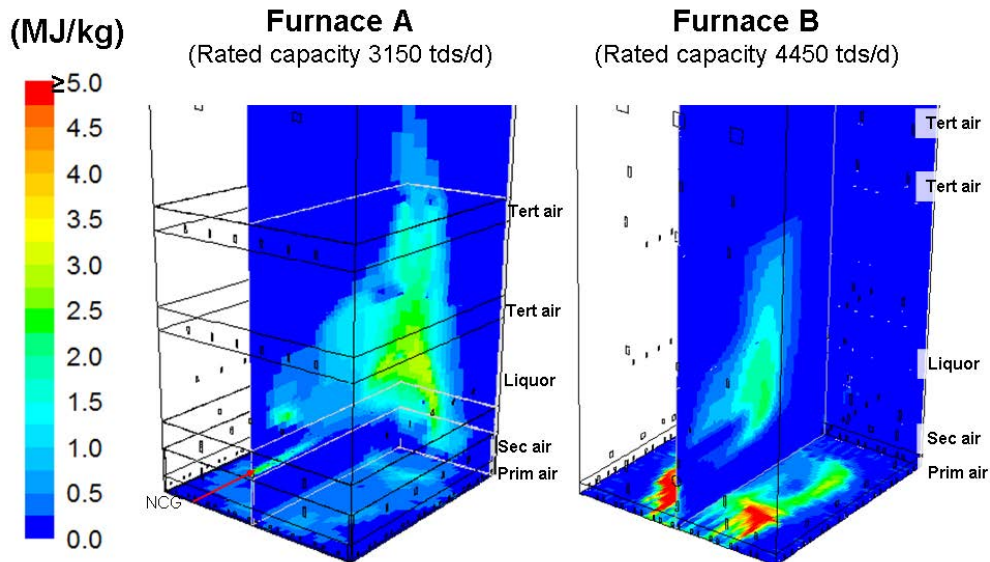


Figure 4. Gas heating values in the lower furnace of two recovery boilers, as predicted by CFD simulations. Heating values shown above the char bed, close to the furnace back wall, and on the front-to-back center plane of the furnace.

The CFD simulations do not take into consideration gas extraction from the furnace, which could potentially affect the gas composition inside the recovery furnace. In addition, modifications to the operation or design of the recovery furnace could possibly be made to increase the gas extraction potential. However, these considerations are outside the scope of this work.

Dust content

Estimates for the minimum and maximum dust content of the lower furnace gas are based on the dust content in the ESP being typically about 20 g/Nm^3 ^(1,2). Taking into consideration the share of combustion air introduced at different air levels, the dust load inside the recovery furnace can be estimated as presented in Figure 5; with the range of dust load being $20\text{-}80 \text{ g/Nm}^3$.

¹ Tarja Tamminen, Continuous Monitoring of Dust Concentration and Composition in Kraft Recovery Boilers, Licentiate Thesis, Report 01-07, Combustion and Materials Chemistry Åbo Akademi University, 2007.

² Adams (ed), Kraft Recovery Boilers, TAPPI PRESS, 1997.

Release of dust-forming elements has been observed to occur mainly (>90%) during in-flight combustion of black liquor droplets¹. In Figure 5, the estimated dust load between the primary and secondary air levels (80 g/Nm³) assumes that all dust formation has taken place in that zone. However, it is perhaps more realistic to estimate that the lower furnace dust content would be in the range 30-80 g/Nm³, given by the estimated dust contents in the two zones below the tertiary air level (see Figure 5).

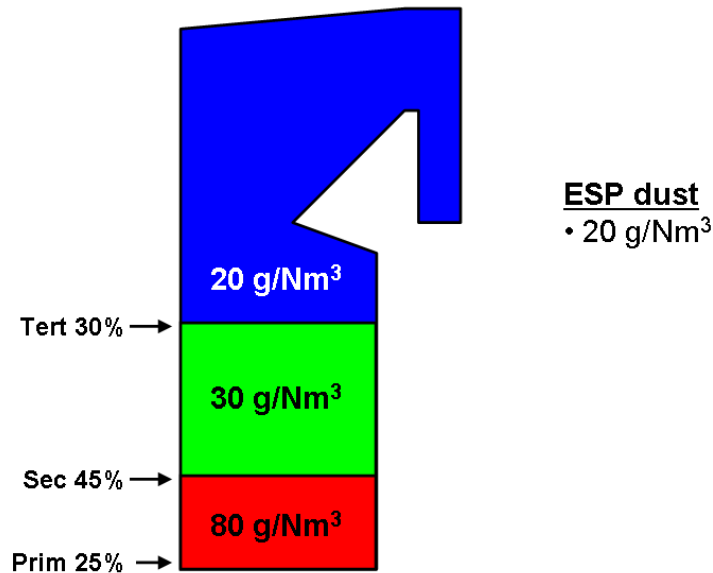


Figure 5. Estimated dust load in different locations of the recovery furnace due to split of combustion air.

Summary and conclusions

Preliminary studies were carried out to investigate the potential for extracting gases from the lower furnace of the recovery boiler to be used in the lime kiln.

The following conclusions are made:

- Extraction of gas with a heating value of 3 MJ/kg could be feasible with normal recovery boiler operation.
- Existence of suitable location for gas extraction depends on recovery boiler operation. A high fuel-to-air ratio, for example, close to a furnace wall would be desirable.
- Dust load is estimated to be in the range 30-80 g/Nm³.
- Factors not included in this study, but which could be relevant to consider include: modifications to recovery boiler operation to maximize gas heating value; gas extraction; and removal of dust from the extracted gas.

APPENDIX 4

**Åbo Akademi: Nikolai DeMartini, Niklas Vähä-Savo, Mikko Hupa
Co-firing of black liquor and biomass, part 2
final report
15.2.2011**

**Draft Report: Sky-REC Co-combustion of mixed fuels – Phase 2**

Prepared by Nikolai DeMartini, Niklas Vähä-Savo, Mikko Hupa

10 December 2010

Summary

This project was designed to provide some initial information to questions following the SKY-REC Co-combustion of mixed fuels project. The questions of interest are:

1. At what addition level does the mixture burn more like wood than black liquor?
2. What is the fate of nitrogen in a BL + wood mixture - does the char have more cyanate?
3. What are the burning characteristics of reduced lignin black liquor?
4. What is the fate of nitrogen in lignin lean black liquor?
5. What is the impact of wood on the combustion properties of lignin lean BL?
6. How much of the nitrogen in biosludge nitrogen is lost for biosludge; biosludge + black liquor after 60 minutes of heat treatment at an agreed upon high solids concentrator temperature followed by concentration of the liquor?
7. How does a 5 wt% d.s. biosludge addition affect black liquor combustion?
8. Does biosludge addition change the cyanate concentration in smelt?

Wood and biosludge were the two fuels of interest for further work. Some preliminary work was also made with a reduced lignin black liquor. For phase 1 of this project, a single black liquor was used. In this project, the same black liquor was used for the mixtures with wood. A second liquor was used for the biosludge work and a third liquor was used for the lignin depletion tests. This was because there was an insufficient quantity of the original liquor for the biosludge work and the reduced lignin black liquor came from another study. For all liquors, the unmodified liquor was also tested as a reference. In addition to data for wood, we have in some instances done some additional work with bark and in one case peat. These additional tests were funded outside of this project, but included where appropriate to provide some additional insight.

There were three changes to the reactor set up compared with the phase one work. The hook in this work hangs from a platinum wire extended out from a quartz glass tube rather than from platinum wire between two quartz glass tubes. This results in a number of differences. The first is that if the fuel swells in the upward direction, which it often did, we can see it. With the old set up, part of the fuel went between the quartz glass holder if it swelled up. With the previous set-up we had to estimate the amount of swollen droplet between the quartz glass tubes. Second, the portion of the fuel between the quartz glass tubes was not considered in the burnout time. Finally, the quartz glass tubes clearly resulted in some back mixing. The second change was that we replaced the old NO analyzer. It appears that with the new analyzer/set-up, we get a higher value for NO, but the trend with fuel addition is similar. Finally, we discovered during the trimming of the new analyzer that the flow meters to the reactor were off. The actual flow to the reactor was 261 l/h rather than the target 220 l/h. This accounts for a portion of the difference in the NO values, but not all. For these reasons we re-ran all of the wood-black liquor mixtures, including 13 and 26% wood.

The wood mixtures looked more like solid fuels than liquid fuels, which caused some variation in the biomass - black liquor distribution in the droplets used in the combustion experiments. This can explain the high standard deviations that were obtained in some of the results, particularly the



burning times where a larger piece of wood would take longer to burn out. Black liquor mixed with biosludge and lignin depleted black liquor looked like typical black liquor fuel.

Below is a brief summary to the experimental results related to each question.

1. At what addition level does the mixture burn more like wood than black liquor?

There was no sharp transition as there had been with 26% peat, though the 50 wt-% d.s. wood appeared to result in a significant increase in combustion time and therefore 35 wt-% wood was also studied. Combustion times for the 26% and 35% wood mixtures were similar and longer than for 13%, but shorter than for 50%. For all wood addition levels, devolatilization times appeared to be shorter and char burning times were significantly longer. Thus increasing the amount of wood would probably result in an increasing amount of char in the char bed and may require a change in air distribution.

2. What is the fate of nitrogen in BL+wood mixture - does the char have more cyanate?

The wood used has more nitrogen than the black liquor on a dry solids basis. Therefore, adding wood resulted in black liquors with a nitrogen content higher than the original black liquor. Because the nitrogen content of wood is lower than bark and peat, this effect is less pronounced. The question here was whether increasing the fuel nitrogen content would also increase the cyanate concentration. Because bark and peat have more nitrogen, we also looked at the impact of these fuels. Wood, bark and peat all resulted in more cyanate, with peat resulting in the largest increase. This is consistent with the nitrogen content of the mixtures, with the peat-BL mixture having the highest nitrogen content. Bark had the lowest increase despite the bark-BL mixture having more nitrogen than the wood-BL mixture. The increase with wood or bark probably would not be seen in a modern recovery boiler. The high lower furnace temperature would likely result in a portion of this added cyanate being oxidized/decomposed and therefore not seen in the exiting smelt. For a very high nitrogen fuel like peat, any difference would be more pronounced. The implication of this work and some subsequent on-going work is that cyanate formation occurs via the alkali carbonate catalysis route.

3. What are the burning characteristics of reduced lignin black liquor?

Our lignin lean black liquor was generated in our lab by bubbling CO₂ through the liquor to lower the pH. Analysis of the lignin lean black liquor provided conflicting results as to the success of the lignin depletion. It is probable that in addition to lignin we also precipitated some hemicelluloses. Therefore these results should be considered preliminary rather than representative of the commercial process. The pH of the black liquor was raised by added NaOH so that the residual alkali was essentially the same for both the original and reduced lignin black liquor. The swelling significantly decreased in the reduced lignin black liquor and the char burning time increased accordingly. Alén et al. [1] showed that both lignin and hemicelluloses together are important to swelling and whether the observed reduction is a result of lignin removal, hemicellulose removal, both or another phenomena requires more investigation.



4. What is the fate of nitrogen in lignin lean black liquor?

Because lignin contains more nitrogen based on literature we expected a reduction in both the NO formed and the amount of cyanate formed. We did see a reduction in NO of about 10 to 15%, and a larger reduction in cyanate.

5. What is the impact of wood on the combustion properties of lignin lean BL?

Wood was added to replace the lost energy value of the black liquor. The LHV of the original black liquor and lignin lean black liquor were both measured in this work and the LHV of the wood had been measured in a previous project. Because there was a significant reduction in the LHV with lignin precipitation, the addition of wood was 35 wt-% on a dry solids basis. This addition further increased the combustion time and raised the NO formed by about 20% compared to the original black liquor or about 40% relative to the lignin lean black liquor. This is similar to the 30% increase seen for the mixture of BL-35 wt-% wood indicating that reducing the lignin content of the black liquor probably does not alter the NO formation of mixtures when compared to a black liquor that has not had lignin precipitated.

6. How much of the nitrogen in biosludge nitrogen is lost for biosludge; biosludge + black liquor after 60 minutes of heat treatment at an agreed upon high solids concentrator temperature followed by concentration of the liquor?

A black liquor – biosludge mixture containing 5 wt% biosludge was prepared for a Kraft liquor from a Finnish pulp mill and a biosludge from a second Finnish Kraft pulp mill. Three separate mixtures made with the same addition levels were heated to either 105, 130 or 160 °C and held for 60 minutes. After cooling, nitrogen was bubbled through the solution and the gas was bubbled through an 0.05 M H₂SO₄ solution to capture NH₃ for analysis. Very little ammonia was recovered indicating little to no ammonia formation during the heat treatment. These experiments therefore do not explain the apparent loss of biosludge nitrogen seen in some of the earlier mill balances [ex. 2]. A mill balance at Kymi around the concentrator and recovery boiler before and after biosludge addition in the spring would help clarify these findings as the fate of biosludge nitrogen remains unclear.

7. How does a 5 wt% d.s. biosludge addition affect black liquor combustion?

Average combustion times were about the same for all of the heat treated black liquor-biosludge mixtures except for the 160 °C heat treatment where the average increased due to an increase in the char burning time. Still, there was overlap of the standard deviations indicating that this difference was not statistically significant.

8. Does biosludge addition change the cyanate concentration in smelt?

Biosludge addition resulted in both higher NO and higher cyanate. The NO increase was 24% for the 160 °C heat treatment and 65% for the 130 °C heat treatment. Cyanate formation approximately doubled. Experiments at 900 °C, 10% O₂ [3] would separate out NO formation during devolatilization and NO formed due to smelt oxidation. At 1100 °C, this distinction is much harder to make. This distribution may be important to the observation of no increase in NO formation due



to biosludge addition. Of course it should also be noted that the level of biosludge addition here was at least twice that typically added in a mill.

In addition to the above experiments, a wood-black liquor mixture where the wood moisture level was increased to 50% was burned at 1100 °C, 3 vol-% O₂. The wood addition level was 26 wt-% on a dry solids basis. The wet wood mixture swelled much more than either the dry wood mixture or the original black liquor. The devolatilization + char burning time was about the same as for the black liquor and significantly less than for the dry wood-black liquor mixture. Finally, the NO was about 7% less than for the dry wood-black liquor mixture.

The phase 2 work supports the conclusion of the phase 1 work that wood addition appears possible and very large wood additions may be possible. It also provided some background for interesting questions around lignin depleted liquors, cyanate formation and the fate of biosludge nitrogen. Clearly more work is needed with lignin depleted black liquor, especially around the characterization of the reduced lignin black liquor. The increase in cyanate formation with the addition of higher nitrogen fuels has provided some new insight into cyanate formation. We have begun investigating this further. The fate of biosludge nitrogen remains unclear and would indicate that a mill trial at a modern mill like Kymi where the concentrator condensate can be sampled would be useful in trying to clarify the question of why biosludge does not seem to result in higher NO concentration in the recovery boiler.

Experimental

In this work three different black liquors were used: BL-468 was the same as used in phase 1 and was mixed with wood, bark or peat; BL-537 was used for the black liquor-biosludge mixtures and BL-538 was used for the lignin reduction.

Black liquor with 80.4% dry solids content (BL468) was mixed with air dried wood and for a few experiments, bark or peat. For the experiments with moist wood, the air dried wood samples were wetted with ion exchange water to 50% dry solids, so that both dry and wet wood samples were used in these experiments. All of these fuel mixtures looked more like solid fuels than liquid fuel. Information on fuel mixtures and experiments conducted are shown in Table 1. The nitrogen content of BL468 and biofuels mixed with BL468 are shown in Table 2.

Table 1. Dry solids of fuels, mixtures and the experiments conducted

Sample	Dry solids% (wt% d.s)	mass fraction biomass in mixture (wt% d.s)	Mixture (wt% d.s)	combustion	cyanate
BL468	80.40%		80.40%	X	X
bark	92.28%	50.0% / 35.0%	85.91% / 84.53%	X	
bark	92.28%	25.6%	83.41%		X
bark	49.95%	25.6%	69.52%	X	
wood	92.23%	50.0% / 35.0%	85.88% / 84.51%	X	
wood	92.23%	25.6%	83.40%		X
wood	49.95%	25.6%	69.48%	X	
peat	96.55%	25.6%	84.51%		X



Table 2. Nitrogen content of black liquor 468 and biofuels

Fuel	N (g/kg) d.s.
Black liquor 468	0.08
Bark	0.4
Wood	0.2
Peat	2.06

Black liquor 537 (BL537) with 81.93% dry solids content was mixed with an 2.1% dry solid biosludge at a 95 wt-% to 5 wt-% dry solids bases. The mixture had a dry solids content of 28.23%. Information on the fuel components is shown in Table 3.

Table 3. Dry solids, Kjeldahl-N and NH₃-N of BL537 and biosludge

Sample	Dry solids (wt-% d.s.)	Kjeldahl-N g/kg d.s.	NH ₃ -N g/kg d.s.
BL537	81.93%	0.9	
Biosludge	2.10%	47	3.8

It was calculated that the mixture contained 3.2 g/kg d.s nitrogen (Kjeldahl-N) and 0.19 g/kg d.s. NH₃. The mixture was divided into the three batches (weighing between 70 and 80g). The batches were heat treated for 60 min in a sealed vessel at three different temperatures: 105°C, 130°C and 160°C. After the heat treatment the vessel was purged with nitrogen and the vent gas was lead through an acid trap containing 0.05M H₂SO₄, in order to capture the released NH₃. The acid trap was analyzed for NH₃ with a WTW NH 500/2 ion selective electrode. Information of the three batches nitrogen content and NH₃ distribution are shown in Table 4.

Table 4. Nitrogen content and NH₃ content in the three heat treated batches

sample	Kjeldahl-N in mixture G	NH ₃ in mixture g	NH ₃ captured in acid trap g	NH ₃ "missing" g
105C 60min HT	0.067926	0.004027	0.001327	0.002699
130C 60min HT	0.066128	0.003920	0.000970	0.002950
160C 60min HT	0.070492	0.004179	0.000980	0.003198

After the heat treatment the three batches were concentrated up to approx. 80% dry solids for the combustion tests. Information on the three batches dry solid contents and experiments conducted are shown in Table 5. For comparison cyanate formation and combustion characteristics of BL537 was performed.

Table 5. Data on mixture dry solids, NH₃ released during heat treatment and experiments conducted

sample	mixture dry solids after concentration (wt% d.s.)	combustion	cyanate
105C 60min HT	81.21%	X	
130C 60min HT	81.50%	X	
160C 60min HT	80.86%	X	X

Black liquor 538 is a Kraft black liquor from the same mill as BL 537, but pulled on a day later. Lignin was precipitated by bubbling CO₂ through the black liquor diluted to 30% dry solids (140 g dry solids in a batch) and held at 65 °C. Sintered glass was used to disperse the CO₂ bubbles in the black liquor. The final pH was measured to be 9.63. The liquor was allowed to set for 1 week in an



attempt to maximize lignin depletion. The analysis results provide mixed results for the amount of lignin precipitated. The measured lignin content in the reduced lignin black liquor is 25.1 wt % compared to 29.2 wt % for the liquor before lignin depletion. The heating value data, Table 6, indicates that more lignin than this was removed, but additional analysis is needed to clarify these conflicting results. Table 7 gives the CHN (ASTM D 5373) and BL538 and lignin.

Table 6. LHV data on black liquor, lignin depleted black liquor and lignin depleted black liquor with wood addition

sample	Dry solids (wt % d.s)	LHV (MJ/kg)
BL538	83.05 %	10.04
BL538RL(+3.8 wt-% NaOH)	84.87 %	5.68
BL538RL(+3.8 wt-% NaOH)+dry wood (65.31-34.69)	87.29 %	10.04

Table 7. C,H,N analysis (ASTM D 5373); *Kjeldahl-N

sample	Dry solids (wt % d.s)	C (%)	H (%)	N (%)
BL538	30.00 %	31.0	3.1	.097*
BL538RL	25.95 %	21.8	2.6	<0.1
Lignin	94.0 %	62.0	5.4	<0.1

Combustion and cyanate formation experiments were conducted in a single particle furnace, which is a quartz glass reactor where the temperature and atmosphere can be adjusted. The single particle furnace is described in detail by DeMartini et.al [1]. Droplet size used during combustion and cyanate formation experiments was between 11 and 17 mg. The combustion experiments were conducted at 1100°C and 3.3% O₂ in N₂. The total gas flow was 264.7 l/h and 23.2 l/h of the nitrogen flow into the reactor is lead through the sample insertion port, in order to cool down the sample and prevents any reactions before insertion. The CO, CO₂ and SO₂ emissions were measured with an on-line infrared analyzer (ABB AO2020) and NO was measured with a chemiluminescence analyzer (Teledyne Model 200EM). The combustion of the samples was recorded with a video camera.

The recorded combustion videos were used to determine devolatilization and char burning times for the fuel mixtures. Maximum swelling volume of the droplet is estimated by capturing an image from the recorded video. The captured two dimensional image is compared to a circle or an ellipse, so that the volume of a corresponding sphere or ellipsoid could be calculated.

Cyanate formation in the fuel mixtures was determined by pyrolysing the samples at 800°C 100% N₂ in the single particle furnace for 6 seconds to form a char. The chars were then gasified at 800°C 13% CO₂ 87% N₂ to different smelt yields. The smelt yield was calculated from weight loss of the samples, by comparing the weight of the smelt samples to the char samples. The samples were gasified to five different smelt yields. Each smelt yield consisted of 6 samples. After the pyrolysis and gasification the samples were washed with ion exchanged water and filtrated. The procedure was to take three samples from each smelt yield and wash it with 6ml ion exchange water, giving two washing solutions for each smelt yield. The washing solutions were analyzed for OCN⁻ with ion chromatography (IC) which had a Metrosep Anion Dual 2 column.



Results

1. At what addition level does the mixture burn more like wood than black liquor?

Increasing wood generally resulted in longer char burning and total combustion times while devolatilization times were about the same for all wood addition levels, Figure 1. The combustion times for the 13 and 26% wood addition levels were based on new mixtures with the modified reactor set-up. There was no sharp transition as there had been with 26% peat, though 50% wood did represent another significant increase in combustion time relative to 26% and 35% wood. There was not a clear trend between level of wood addition and average swollen volume, Figure 2.

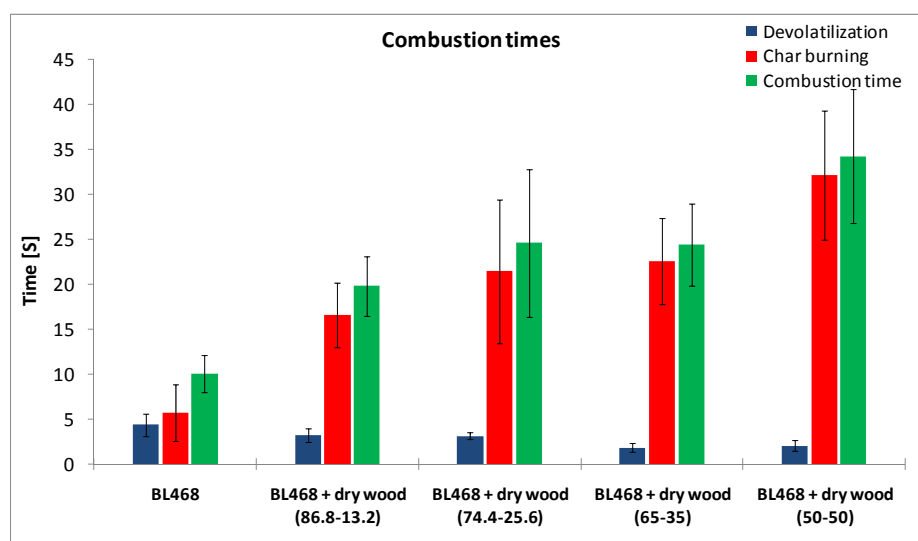


Figure 1. Devolatilization, char burning and total combustion times for 4 different addition levels of dry wood with black liquor.

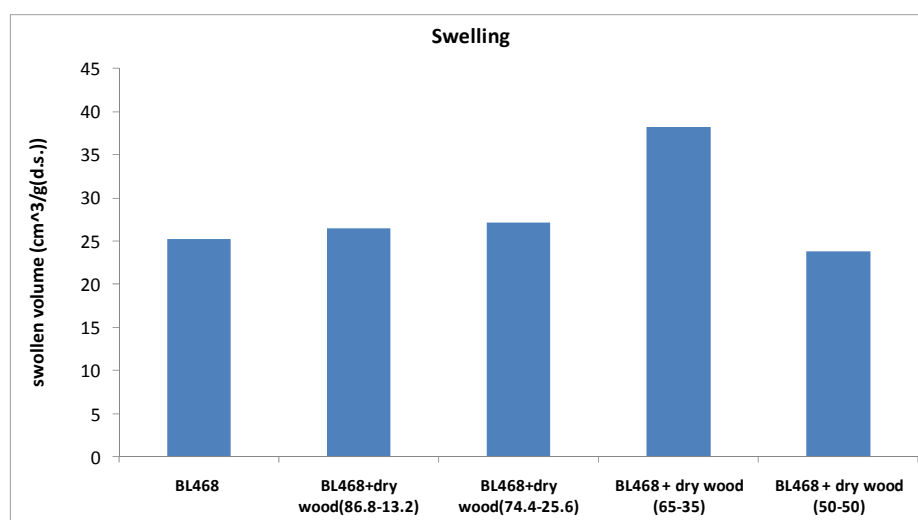


Figure 2. Average swollen volume for BL 468 and BL-wood mixtures at 4 different levels.

2. What is the fate of nitrogen in BL+wood mixture - does the char have more cyanate?

As found in the phase 1 work, adding wood increases the NO formed due to an increase in fuel-NO, Figure 3. Cyanate also increased for a wood-BL mixture relative to wood, Figure 4. Only the 26 wt% wood mixture was tested from the wood mixtures. To verify this result, both a bark-BL and



peat-BL mixture were tested and showed increased cyanate formation, Figure 5. The largest increase in cyanate came with peat mixture which also has the highest fuel nitrogen. The bark-BL mixture has a higher nitrogen content than the wood mixture but did not result in a higher cyanate formation in these tests.

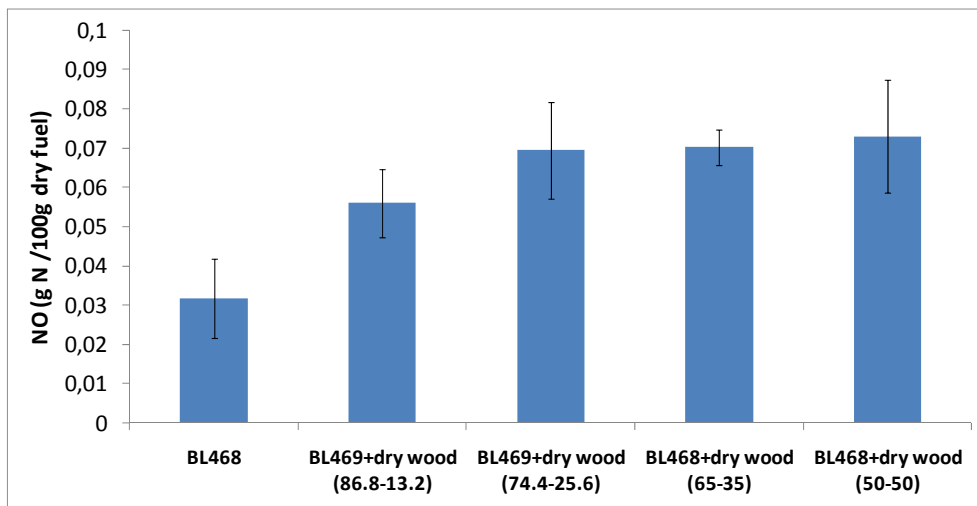


Figure 3. NO formation as gN/100 g dry fuel for increasing levels of wood addition.

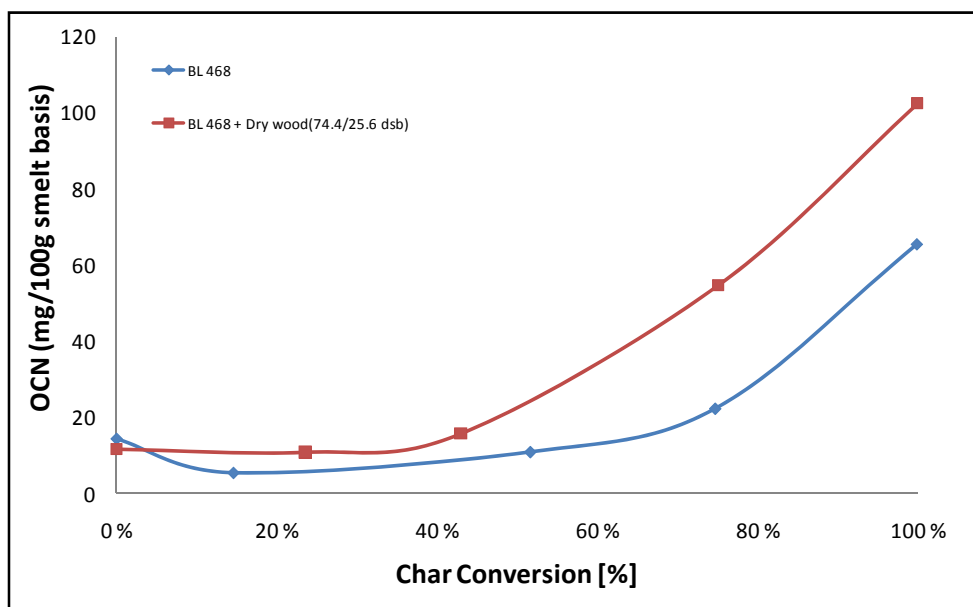


Figure 4. Concentration of cyanate in char vs. char gasification at 800 °C in 13% CO₂ / 87% N₂. Chars were formed by pyrolysis at 800 °C for 6 s in 100% N₂.

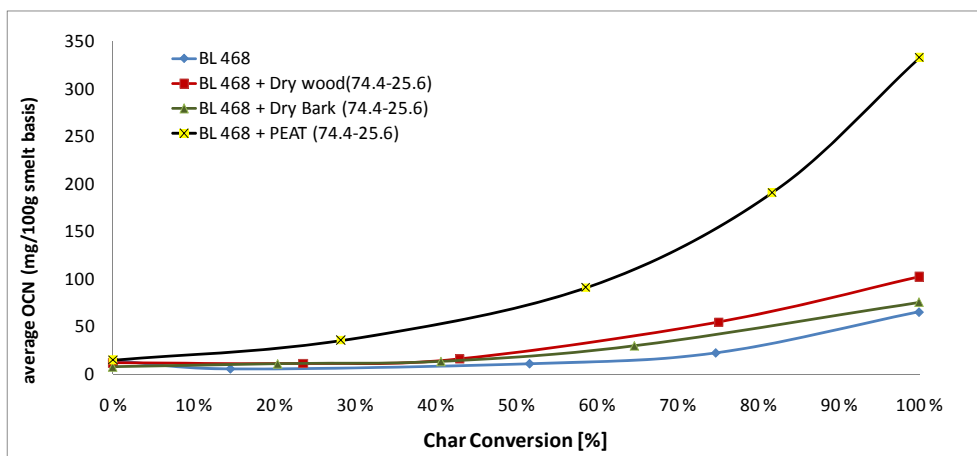


Figure 5. Concentration of cyanate in char vs. char gasification at 800 °C in 13% CO₂ / 87% N₂. Chars were formed by pyrolysis at 800 °C for 6 s in 100% N₂.

3. What are the burning characteristics of reduced lignin black liquor?
5. What is the impact of wood on the combustion properties of lignin lean BL?

The swelling significantly decreased in the reduced lignin black liquor, Figure 6, and the char burning time increased accordingly, Figure 7. Wood did not have much impact on swelling, but did result in longer residence times, most likely due to small sticks of wood.

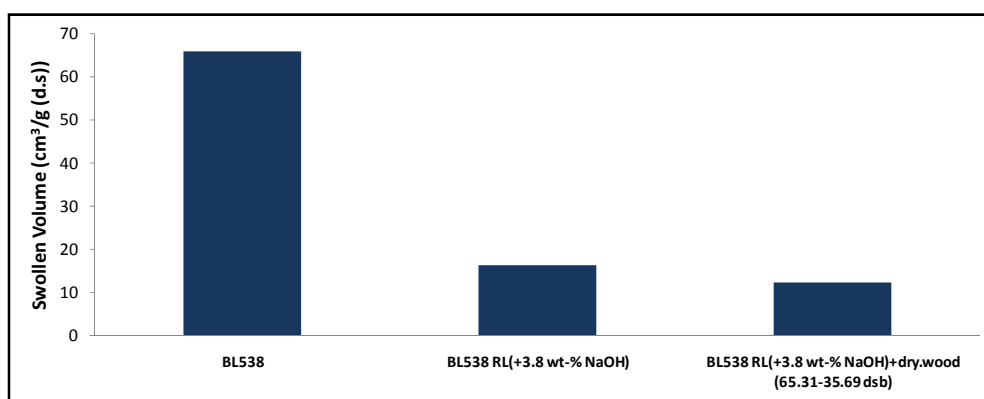


Figure 6. Swelling of BL 538, the reduced lignin BL and the reduced lignin BL + wood.

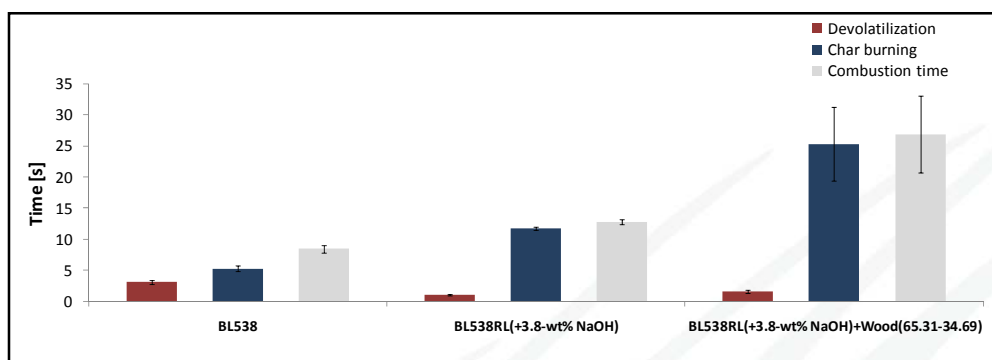


Figure 7. Devolatilization, char burning and total combustion times of BL 538, the reduced lignin BL and the reduced lignin BL + wood.

4. What is the fate of nitrogen in lignin lean black liquor?

Because lignin contains more nitrogen based on literature we expected a reduction in both the NO formed and the amount of cyanate formed. We did see a reduction in NO of about 10 to 15%, Figure 8, and a larger reduction in cyanate, Figure 9.

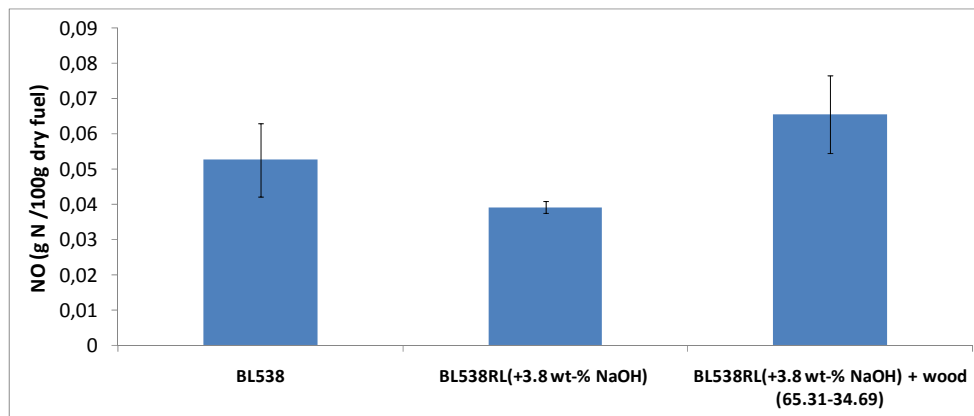


Figure 8. NO formation as gN/100 g dry fuel for reduced lignin black liquor with and without the addition of wood to replace the heating value.

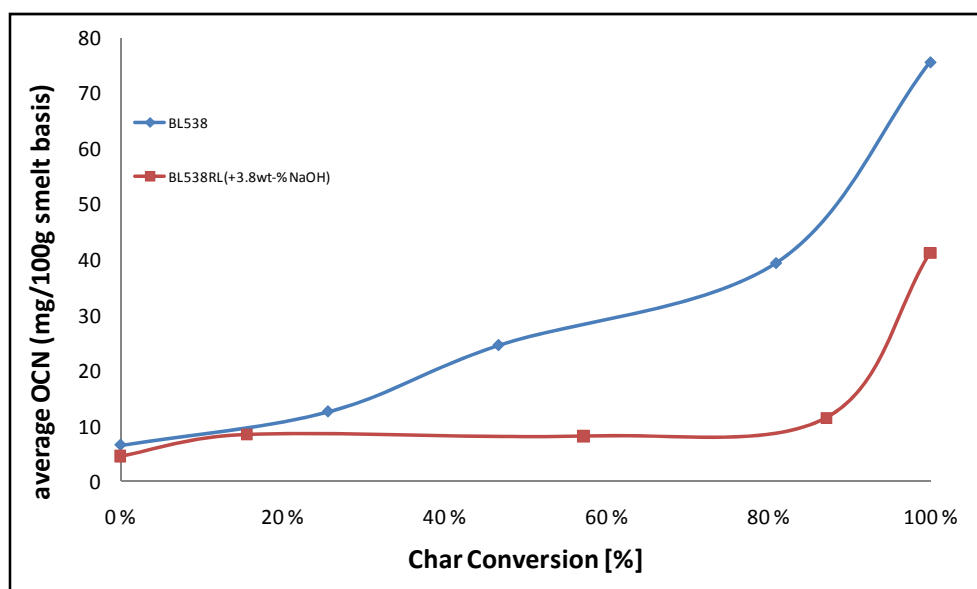


Figure 9. Concentration of cyanate in char vs. char gasification at 800 °C in 13% CO₂ / 87% N₂. Chars were formed by pyrolysis at 800 °C for 6 s in 100% N₂.

6. How much of the nitrogen in biosludge nitrogen is lost for biosludge; biosludge + black liquor after 60 minutes of heat treatment at an agreed upon high solids concentrator temperature followed by concentration of the liquor?

As shown Table IV, very little NH₃ was captured after heat treatment indicating that very little was formed. This is also consistent with the higher NO formation observed, Figure 10.

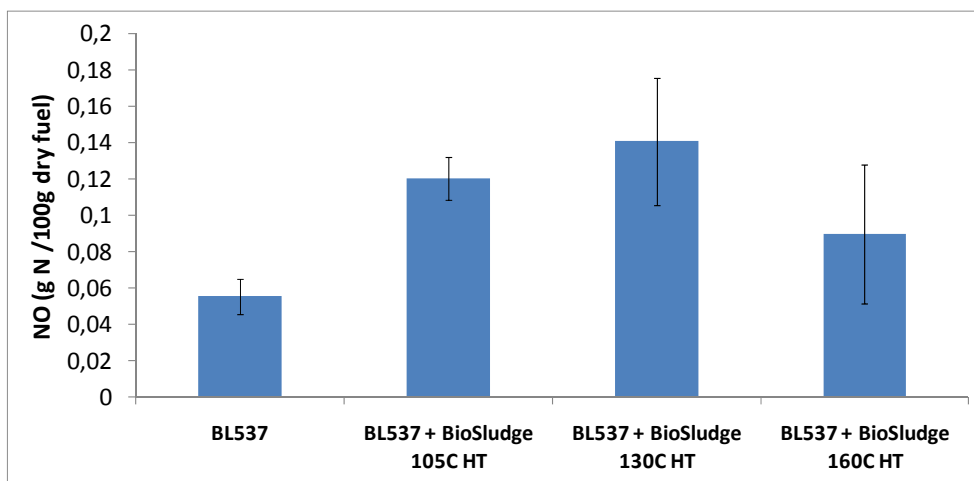


Figure 10. NO formation as gN/100 g dry fuel for BL-biosludge samples that were heat treated for 60 minutes at one of three temperatures.

7. How does a 5 wt-% d.s. biosludge addition affect black liquor combustion?

The biosludge black liquor mixture had to be concentrated to 80% solids before combustion. The concentrated mixture looks like black liquor. Combustion times for the mixtures were within a few seconds of the combustion time for the original black liquor, Figure 11 despite a large difference in the average swollen volume, Figure 12.

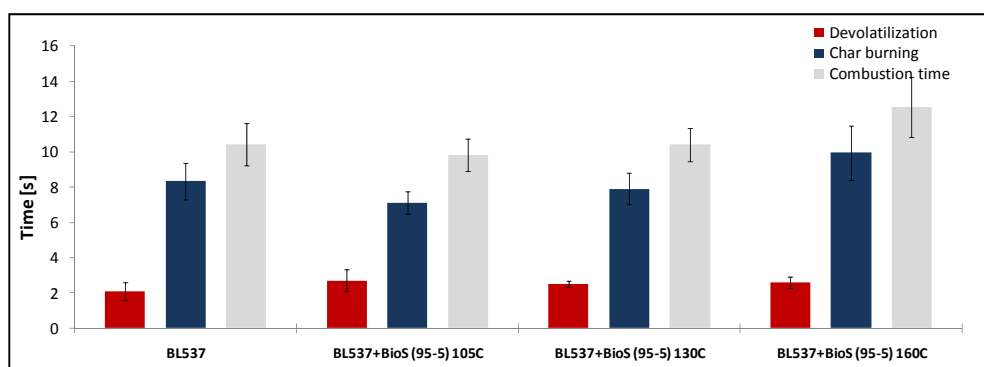


Figure 11. Devolatilization, char burning times for BL-biosludge samples that were heat treated for 60 minutes at one of three temperatures.

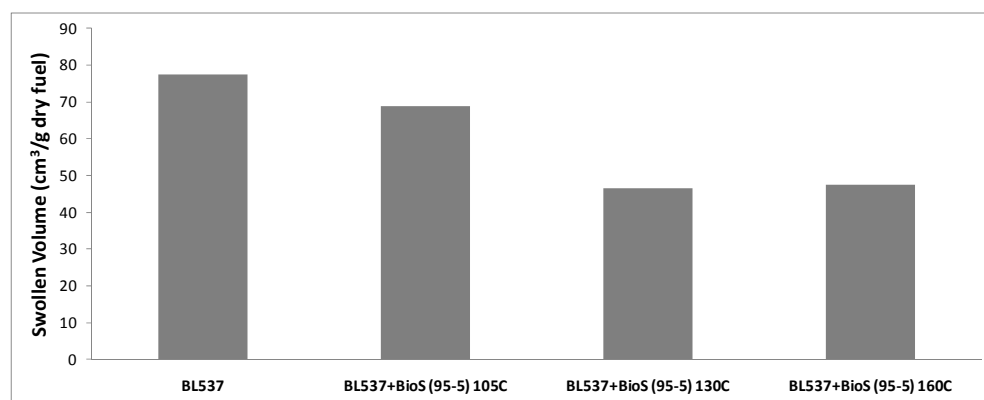


Figure 12. Swollen volume of BL 538, and the heat treated biosludge mixtures.



8. Does biosludge addition change the cyanate concentration in smelt?

Cyanate formation was measured for only the liquor treated at 160 °C. A significant increase in cyanate formation was observed, Figure 13.

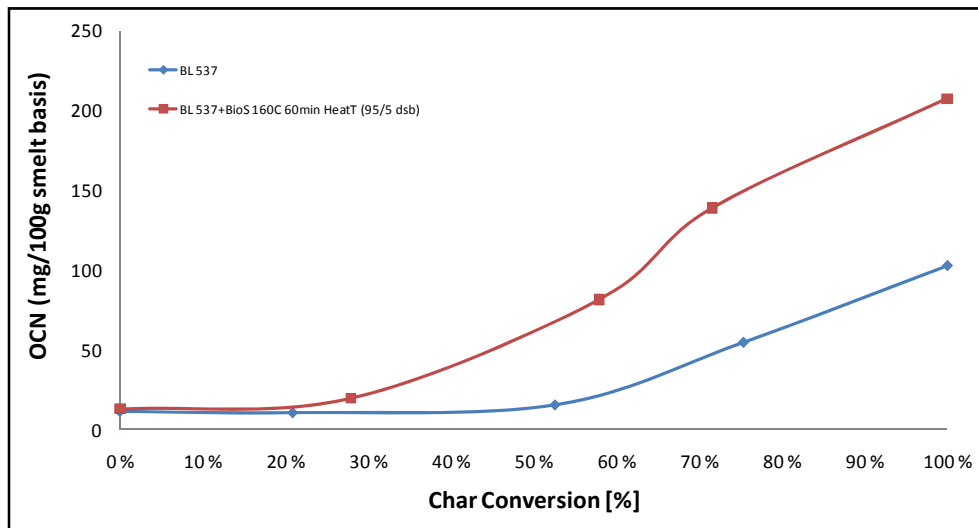


Figure 13. Concentration of cyanate in char vs. char gasification at 800 °C in 13% CO₂ / 87% N₂. Chars were formed by pyrolysis at 800 °C for 6 s in 100% N₂.

References

1. Alén, R., Hupa, M. & Noopila, T. Combustion properties of organic constituents of Kraft black liquors. *Holzforschung*, 46: 337-42 (1992)
2. Kymäläinen, M.; Holmström, M.; Forssén, M.; Hupa, M. the fate of nitrogen in the chemical recovery process in a kraft pulp mill Part III. The effect of some process variables. *J. Pulp Paper Sci.* 27(9): 317-324 (2001a)
3. Kymäläinen, M.; Forssén, M.; Kilpinen, P.; Hupa, M. Nitrogen oxide formation in black liquor single droplet combustion. *Nordic Pulp Pap. Res. J.* 4(16): 346-354 (2001b)

APPENDIX 5

Åbo Akademi
Corrosion tests in reducing conditions, PART II
Offer
25.11.2010

Skyrec

Corrosion tests in reducing conditions – PART II

Project description and offer

Laboratory of Inorganic Chemistry
Åbo Akademi University

November 2010

Background

This offer is based on earlier results obtained from laboratory tests performed at the Åbo Akademi University at Laboratory of Inorganic Chemistry. Experiments under reducing conditions were carried during 2009 in agreement with Suomen Soodakattilayhdistys – Finnish Recovery Boiler Committee. These tests were done in a gas containing CO and N₂ and additionally active carbon were placed on the synthetic salts. The reason for using active carbon instead of black liquor chars, which are more reducing, was that BL-chars contain chlorine and since one of the tested salts (Salt 5) does not contain any chlorine it was decided not to use the char. However, when looking at the results from these tests it seems that no or only a small reduction (at 600°C) of the sulphate to sulfide was achieved with this test setup.

In this offer the tests are planned to be done with BL-char despite the fact that it may contain some chlorine and thus affect the results, at least for the test with Salt 5.

The offer contains three parts; Part A in which the reducing effect of the BL-char is preliminary tested and a verification of sulphate reduction is to be established, Part B in which a further mapping of the temperature on the reducing effect is to be done, and Part C is to finalize a similar test matrix as was done in the earlier tests in 2009. Before starting with Part A, a couple of TGA-tests will be done to establish the reduction temperature of a mixture of NaSO₄ and BL-char.

The tests will be performed at Åbo Akademi using a laboratory method for studying high temperature corrosion. The method is based on the estimation of the oxide layer thickness or/and depth of the material degradation. Elemental analyses of the corrosion layer composition are also to be done.

The content of the report is confidential and the property of Suomen Soodakattilayhdistys – Finnish Recovery Boiler Committee.

Experimental

The corrosion test furnace is equipped with a tightly closed glass reactor. The composition of the gas flowing through the reactor during will be 5% CO, 95% N₂ with a flow of 2.0 l/min. In each test, five specimens can be tested, of which one commonly is a reproducibility sample. The duration of each test is one week.

After the corrosion test, the specimens are cooled down to room temperature inside the furnace with a continuous flow of the gas mixture through the reactor. The samples are then placed in a mould and cast in epoxy, then cut off in the middle. The cross-section surfaces are then polished in kerosene, using 1000 and 1200 grid SiC paper, cleaned in petroleum ether and ultrasound bath. The samples are then ready to be analyzed with the SEM/EDX.

The corrosion products are identified by using x-ray images. The corrosion layer thickness is determined by using scanning electron microscope back-scatter images. Several SEM images are combined into one panoramic picture. After that the panoramic pictures are digitally treated by using contrast differences. An example of the treatment stages of a typical SEM panoramic picture is shown in Figure 1. After the

panoramic images have been colored, the thickness of the oxide layer is determined for each vertical line of pixels and recalculated into μm .

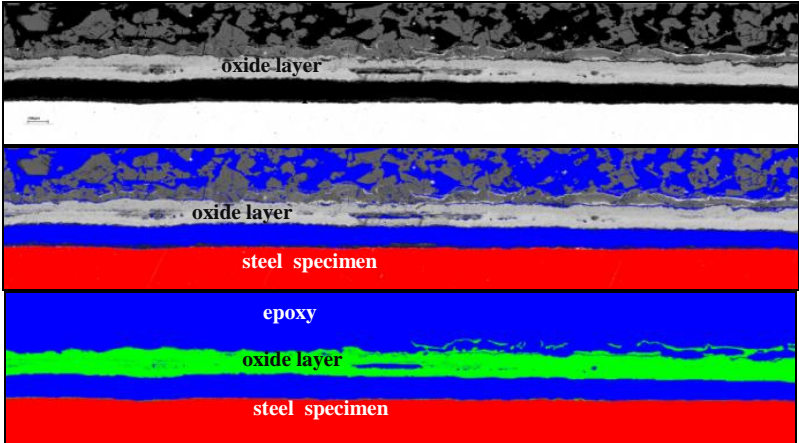


Figure 1. A schematic view of SEM picture coloring stages in order to determine the oxide layer thickness

The corrosion layer is defined as the thickness of the oxide layer for each line and the corrosion attack is expressed as a mean thickness of the oxide layer.

The compositions of the synthetic ashes used in the earlier experiments and planned to be used in this work, as well, are shown in Figure 2. The names: Salt 5, Salt 8, Salt 9 and Salt 10 are introduced with respect to previous projects dealing with the same salts and are used for comparison and recognition purposes.

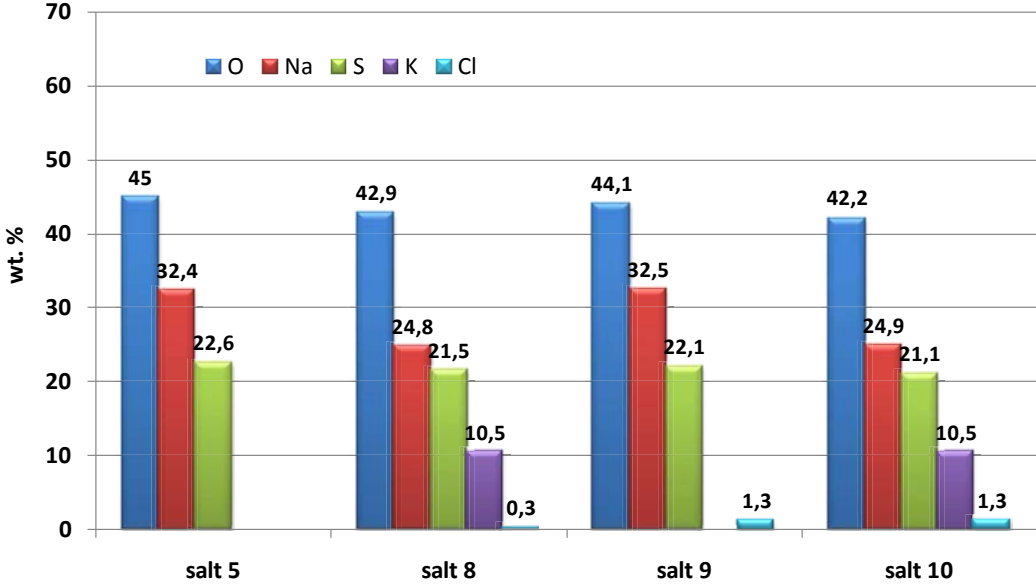


Figure 2. The chemical compositions of the synthetic ashes used in the corrosion tests (wt%)

The four different superheater materials that were used in the earlier experiments and planned to be used in this work, as well, are 10CrMo9-10, T91, Sanicro 28, and HR11N

Before the experiments all steel specimens are polished in ethanol using first a 600 and then a 1000 grid SiC paper, cleaned in ultrasound bath. Before the tests, the specimens

are pre-oxidised in a furnace for 24 h at 200°C. After the pre-treatment the specimen is covered with the salt mixture in question (of 0.25 g/specimen) mixed with about 30% of BL-char. Then the material samples (up to 5 at a time) are exposed to high temperature in a horizontal tube furnace for 168 h (7 days), at 450°C - 600°C.

Test plan

Before the corrosion tests are started a few TGA-runs will be done to establish the temperature where the reduction of NaSO₄ in a mixture with BL-char begins. This temperature will then determine which temperatures are to be used in the corrosion tests.

Part A

Temperature: "the reduction temperature" determined from the TGA-tests (e.g. 550°C)

Salts: Salt 5 and Salt 10, both mixed with 30% BL-char

Materials: 10CrMo9-10, T91, Sanicro 28, HR11N

In this part SEM/EDX evaluations and analyses will only be done on 10CrMo and HR11N, the other samples will be stored in case of activation of Part B.

Number of samples = 8 + 2 (repetitions)

Number of samples to SEM: 4 + 2 (repetitions)

Price: 6 900 € + VAT

Part B

Temperatures: three temperatures (e.g. 450, 500, and 600)

Salts: Salt 5 and Salt 10, both mixed with 10% BL-char

Materials: 10CrMo9-10, T91, Sanicro 28, HR11N

Number of samples: 24 + 6 (repetitions)

Number of samples to SEM: 30 + 4 (Part A) =34

Price B: 20 500 € + VAT

Price A+B: 26 400 € + VAT

Part C

This part is the last and the goal with Part C is to finalize a similar test matrix as was done on the earlier tests in 2009.

Temperatures: the four temperatures used an Part A and Part B

Salts: Salt 8 and Salt 9, both mixed with 10% BL-char

Materials: 10CrMo9-10, T91, Sanicro 28, HR11N

Number of samples: 32 + 8 (repetitions)

Number of samples to SEM: 40

Price C: 27 300 € + VAT

Price A+B+C: 52 700 € + VAT

Project organization

Personnel involved in this project at Åbo Akademi University will be:

- Mikko Hupa, responsible leader
- Patrik Yrjas, project leader
- Nikolai DeMartini, expert
- Dorota Bankiewicz, researcher
- Jaana Paananen and Piia Leppäsalo, laboratory personnel
- Linus Silvander, SEM/EDX expert and analytics

If so approved by the Finnish Recovery Boiler Committee the project can be connected to a masters thesis or part of some other thesis work.

Timetable

Depending on which alternative is chosen the time schedule differs.

Part A: the report is ready in March 2011

Parts A+B: the report is ready in May 2011

Parts A+B+C: the report is ready in October 2011, however, a preliminary report is to be available in June 2011.

If the parts are ordered separately the time schedule may change.

The offer is in force until 31.12.2010.

Place and date: Turku 25 November, 2011

Prof. Mikko Hupa

Patrik Yrjas, Dr. (Chem. Eng)

APPENDIX 6

**VTT: Markku Orjala, Martti Mäenpää, Janne Kärki
Mill tests of superheater materials
draft report
20.1.2010**



Full scale material exposure in Joutseno Recovery Boiler

Authors: Martti Mäkipää, Janne Kärki, Markku Orjala

Confidentiality: Confidential

Report's title Full scale material exposure in Joutseno Recovery Boiler	
Customer, contact person, address Suomen Soodakattilayhdistys SKYREC-projekti	Order reference VTT's offer VTT-V-38086-09
Project name Tulistinputki	Project number/Short name 38086
Author(s) Martti Mäkipää, Janne Kärki, Markku Orjala	Pages 43
Keywords superheater, recovery boiler, corrosion	Report identification code VTT-R-00499-11
Summary <p>Objective of the work was to study the corrosion performance of various superheater tube materials in recovery boilers at high material temperatures. Full scale material exposures were carried out in Joutseno RB by September-October 2010. Materials selected for the study were 347H, AISI310, HR11N, SAN28, Super 625 and SAN69. Two identical cooled probes with 6 material samples in each were exposed in the boiler for a time of one month. Nominal material temperatures on the exposed side of each probe were 530 °C and 570 °C.</p> <p>After the exposure the rings were mounted on site in resin, taken to laboratory and prepared to metallographic cross sections using ethanol as grinding medium. Material wall thicknesses of the metallographic cross sections were measured. Metallographic cross sections were characterised using optical microscope, or after coating with thin carbon film, using an environmental scanning microscope (ESEM) equipped with an analyser. Analytical results were used for predictive calculations using thermo-chemical database and calculation tool "FactSage 6.1".</p> <p>Corrosion conditions were highly variable depending of the flue gas flow direction and the temperature exposure history. Corrosion morphologies known as typical of each material tested in terms of oxide scale growth, grain boundary attack and internal penetration, were noticed. Maximum metal loss was typically observed to occur on the leeward side of each material. The extent of metallic corrosion at locations was, however, related to the presence of chloride. The ranking found was as: SAN28 < 347H < AISI310 < HR11N < SAN69 ~ Super 625 (best). Predictive calculations referring to deposit conditions with about 0.5 % chloride and some carbonate resulted to a ranking as: SAN28 < 347H < AISI310 < HR11N < Super 625 ~ SAN 69 (best). Performances of the six materials tested are considered as unsatisfactory in the actual test conditions, Super 625 and possibly SAN 69 excluded.</p>	
Confidentiality	Confidential
Jyväskylä 20.1.2011 Written by  Martti Mäkipää Senior Research Scientist	
Reviewed by  Janne Kärki Team Leader	
Accepted by  Jouni Hämäläinen Technology Manager	
VTT's contact address VTT, PL 1603, 40400 Jyväskylä	
Distribution Customer, VTT project staff	
<i>The use of the name of the VTT Technical Research Centre of Finland (VTT) in advertising or publication in part of this report is only permissible with written authorisation from the VTT Technical Research Centre of Finland.</i>	

Preface

The main objective of the project was to study corrosion performance of six different superheater tube materials at high-material temperatures in recovery boilers. VTT carried out research, which included cooled probe exposures in Joutseno recovery boiler, material sample characterisation and analyses, and interpretation of the results.

VTT's project manager was Markku Orjala who was in charge of the probe measurements together with Jukka-Pekka Sulin-Saaristo and Juha Hakulinen. Martti Mäkipää and his staff conducted the metal material analyses. Janne Kärki participated on the analysis of the results.

This report presents results from one month monitoring period in September-October 2010.

Jyväskylä 20.1.2011

Authors

Contents

Preface	<u>4</u>
1 Introduction.....	<u>6</u>
2 Cooled probe tests in Joutseno recovery boiler.....	<u>8</u>
2.1 General	<u>8</u>
2.2 Probe temperature regulation	<u>9</u>
2.3 Material exposures.....	<u>10</u>
3 Material sample characterisation.....	<u>13</u>
3.1 Material wall thickness measurements	<u>13</u>
3.2 Optical microscopy.....	<u>13</u>
3.3 Environmental Scanning Electron Microscopy (ESEM)	<u>14</u>
3.3.1 Results of ESEM studies: Elemental analysis of the deposits.....	<u>14</u>
3.3.2 Results of ESEM studies: Estimated metal losses.....	<u>15</u>
3.3.3 Results of ESEM studies: Quantitative elemental analyses of corrosion products	<u>16</u>
3.3.4 Results of ESEM studies: Comments	<u>17</u>
4 Thermodynamic calculations using FactSage 6.1	<u>19</u>
4.1 General considerations on deposit chemistry	<u>19</u>
4.1.1 Equilibrium calculations based on quantitative analyses performed ..	<u>19</u>
4.1.2 Predictive calculations	<u>23</u>
5 Discussion	<u>24</u>
5.1 Comparison to recent full-scale material exposure data	<u>24</u>
5.2 Corrosion mechanistic considerations	<u>26</u>
5.3 Concluding remarks	<u>27</u>
6 Conclusions.....	<u>28</u>
References	<u>29</u>

1 Introduction

Objective of the work was to study the corrosion performance of various superheater tube materials in recovery boilers at high material temperatures. Materials selected for the study were 347H, AISI 310, HR11N, SAN 28, Super 625 and SAN 69. There were two material test temperatures that were chosen to be, in nominal, 530 °C and 570 °C. The research included material sample preparation to the form of rings, carrying out corrosion measurements by exposing the samples as attached in cooled probes to in-furnace flue gas atmosphere, and thorough material inspection of the exposed material rings.

The material samples were exposed in a recovery boiler owned by Oy Metsä-Botnia Ab, and located in Joutseno, South-East Finland. During the material tests in September-October 2010 the boiler was operated using softwood liquor as fuel. Analytical of a sample taken by 20th September 2010 was provided by the plant operator, see Table 1. With reference to that data, the molar ratios of $K/(Na+K)$, $Cl/(Na+K)$ and $S/(K_2+Na_2)$ in the liquor are 5.1, 0.3 and 11.1 %, respectively. From the corrosion point of view the content of chloride of deposits in the superheater area may be presumed as low. The ratio of alkali to sulphur in the flue gas flow as well as in the deposits is, however, potentially relatively high.

Pre-existing literature data [1-8] indicates that quite different performance-limiting behaviour may be expected for the studied materials. Corrosion of austenitic stainless steel 347H is expected to initiate by grain boundary attack, which eventually leads under sulphur oxide-depleted conditions to severe general attack due to basic fluxing. Under alkaline deposit conditions probably encountered in the test, the localised corrosion of highly with chromium alloyed steels AISI 310, HR11N and SAN 28 is a self-sustaining process, if initiated. Alloy 625 having a high content of molybdenum is reported to have performed outmost well, e.g., in the temperature range from 520 to 530 °C [8]. The material temperature of material samples exposed in recovery boilers may, however, actually vary appreciably depending on the heat flux, the measured peaking material temperatures approaching 600 °C [7,9].

Table 1. Analysis of the softwood liquor sample.

Solids	%	SCAN-N 22:77	82.4
Ash	%	KCL 59:83	53.3
C	%	ASTM D 5373	33.4
H	%	ASTM D 5373	3.4
N	%	ASTM D 5373	< 0,1
Na	%	SCAN-N 37:98	20.8
K	%	SCAN-N 37:98	1.9
Al	mg/kg	SCAN-N 38:10	25
Ba	mg/kg	SCAN-N 38:10	4.5
Ca	mg/kg	SCAN-N 38:10	240
Cu	mg/kg	SCAN-N 38:10	0.9
Fe	mg/kg	SCAN-N 38:10	21
Mg	mg/kg	SCAN-N 38:10	290
Mn	mg/kg	SCAN-N 38:10	90
P	mg/kg	SCAN-N 38:10	77
Si	mg/kg	SCAN-N 38:10	340
V	mg/kg	SCAN-N 38:10	< 5
Zn	mg/kg	SCAN-N 38:10	11
S	%	SCAN-N 38:10	6.8
Cl	%	AOX-equipment	0.1
CO ₃ ⁼	%	SCAN-N 32:98	5.3
SO ₄ ⁼	%	KCL 71:81	5.8
S ⁼	%	SCAN-N 31:94	3.3

2 Cooled probe tests in Joutseno recovery boiler

2.1 General

Two air- and water-cooled probes were used which imitate the behaviour of superheater tubes. The probes were inserted on the level of 10 ½ between 2nd and 3rd superheaters on opposite side walls of the boiler, see Figs. 1 to 3. The surface temperatures of the probes vary depending on the direction of the flue gas flow. The windward temperature is maintained constant by adjusting the cooling rate and the temperatures on other sides change when deposits are formed. (In this particular case, hard deposit acting as an insulator did rapidly form on the flue gas flow side causing that the material temperature on other locations did rise, see Fig.4.)



Figure 1. Probe 1 ready for insertion through an inlet located about one meter below the sootblower at level 10 ½, between 2nd and 3rd superheater.

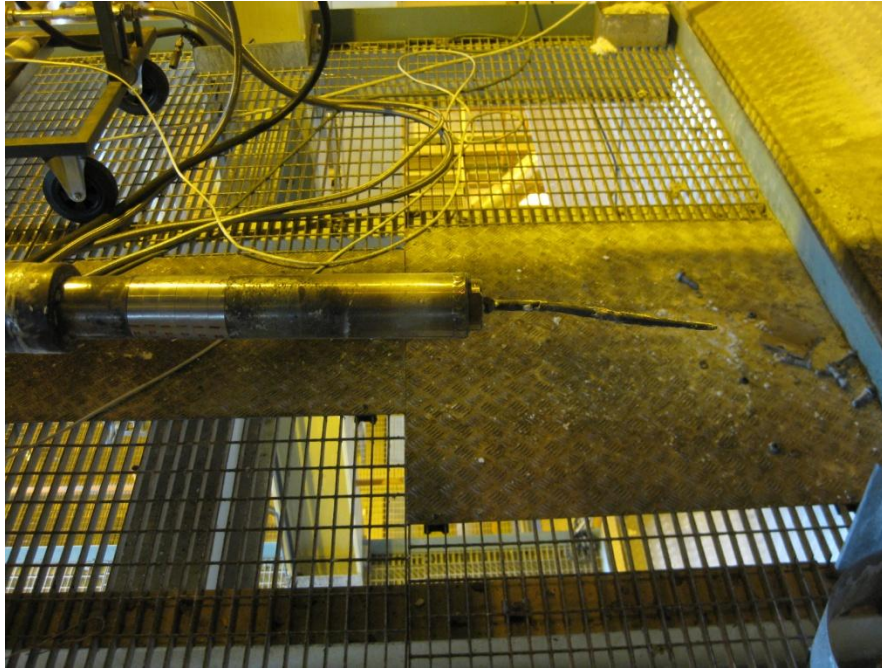


Figure 2. The flue-gas end of the Probe 1. Test material rings, in all six, appear as metallic on the left in the picture. The flue gas temperature sensing element is attached to the tip of the probe on the right in the picture and it was damaged during the measurements.

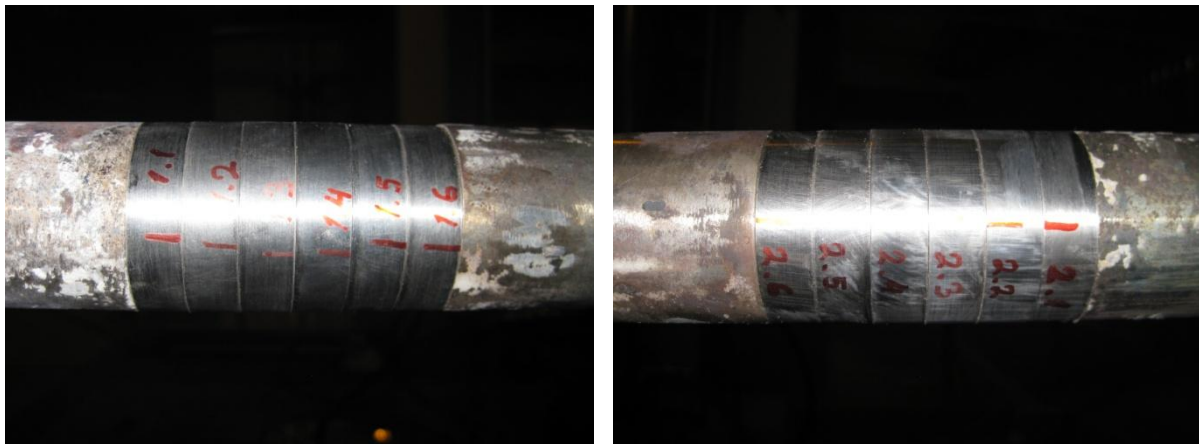


Figure 3. Attachment of the test material rings in the probes. Sample number 1.1(SAN 28) respectively 2.1(SAN 28) is farthest from, and Sample number 1.6 (347H) respectively 2.6 (347H) closest to the tip of the probe. Windward side is marked with red line.

2.2 Probe temperature regulation

The surface temperatures of the probes vary depending on the direction of the flue gas flow. The windward temperature is maintained constant by adjusting the cooling rate and the temperatures on other sides change when deposits are formed. In this particular case, a deposit layer acting as an insulator did rapidly form on the flue gas flow side causing that the material temperature on other locations did rise (up to 590 °C for few hours). The probes were removed by 16th of September from the boiler and inspected to find a 10 to 15 mm thick hard deposit to be present on the windward side of the probes. The problem was effectively corrected by changing the regulating thermocouple from the windward side to the up side (by 90 degrees) in both probes. During the next day 17th September the regulation principle was

changed to the original one and by 18th September back to the changed one. Windward material temperature was stabilised at 529 °C in the Probe and at 570 °C in the Probe 2.

2.3 Material exposures

The material test period was altogether 649 h from 16th September to 13th October 2010. Boiler operation data including boiler load (tons of dry solids/day), main steam temperature and flow, flue gas temperature before the boiler bank, oxygen content of flue gases before air preheater, material temperatures of superheater II and III and is found as enclosed in *appendix (figures 1-7)*. The highest material temperature in SH III is reportedly in the range of 490 °C. Deciding from the main steam temperature data the actual maximum SH III tube metal temperatures must be, however, appreciably higher than 490°C.

Immediately post-exposure the probes showed thick deposits on the Windward side, see Fig, 4 below. Thick deposits did fall off from the probe surface. Little of any deposited material was remaining attached on the samples as they were mounted in the resin on the site.



Figure 4. Post-exposure appearance of Probe 1 and Probe 2 shown in pictures in the left and right column, respectively.

When inspected post-exposure by plain eye several of the rings were found to be non-circular. An obvious explanation for such deformations might be impacts of lumps of material falling down in the boiler. Such impacts were noticed to occur during the time elapse from 11th to 13th October when the boiler was cooling down.

Material temperature stability is quite good after the changes that were made in the beginning of the campaign, Figs. 5. Material temperature on the Up, Down and Leeward side of the probe has exceeded the Windward side for a time elapse which accounts for less than 3 % of

the total of 600 h exposed at high temperatures, Fig. 6. Material temperature on the Windward side remained most of the test time close to regulated value ($528\text{ }^{\circ}\text{C} \pm 1\text{ }^{\circ}\text{C}$ for 538 h) in the Probe 1, and less satisfactorily in the Probe 2 ($568\text{ }^{\circ}\text{C} \pm 2\text{ }^{\circ}\text{C}$ for 400 h). Material temperature data referring to the time elapse from 16th September to 11th October totalling 600 h is shown in tabulated form below, Table 2.

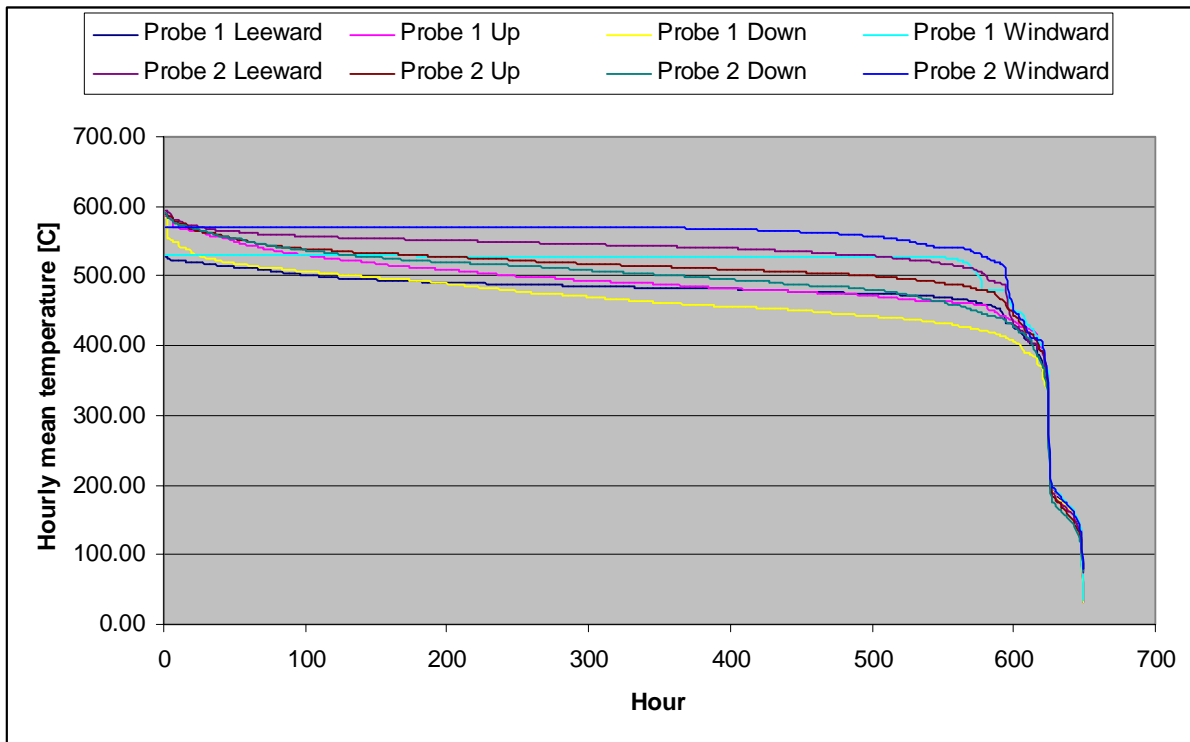


Figure 5. Temperature stability curves for Probe 1 and Probe 2.

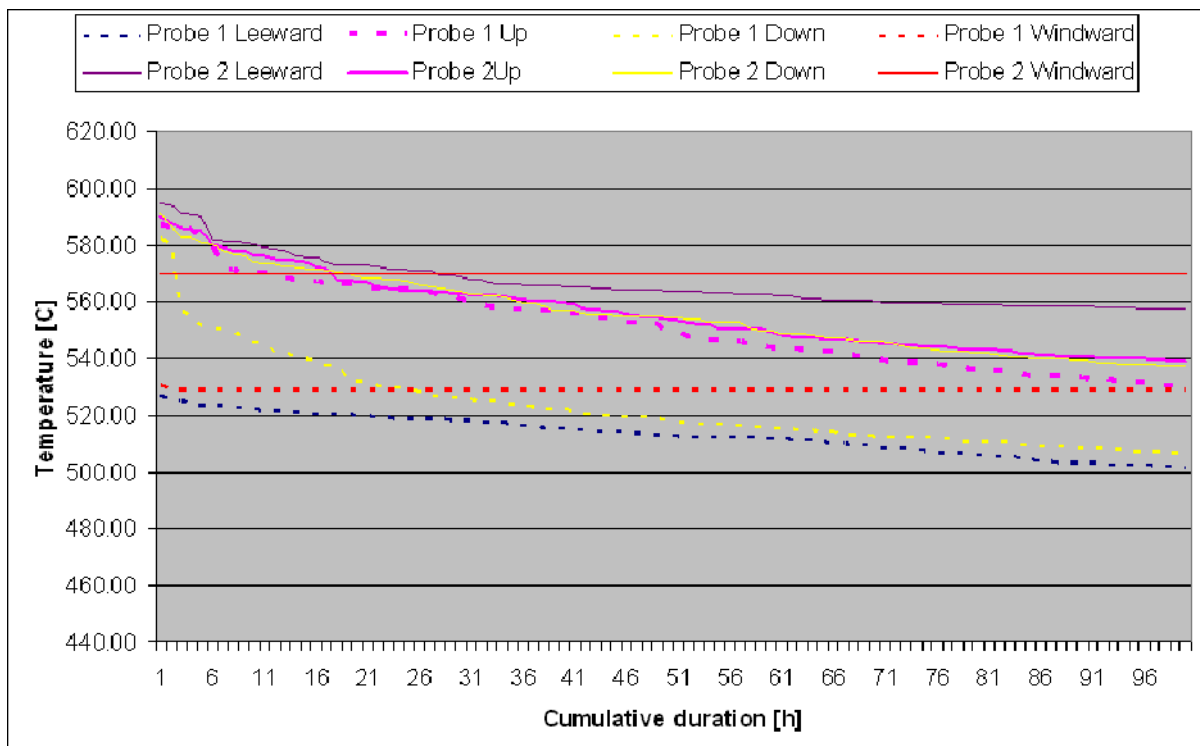


Figure 6. High-temperature end of material temperature curves shown in Fig. 5 and 6.

Table 2. Numeric temperature data for Probe 1 and Probe 2.

Temperature:	Average	Median	Maximum	Minimum
Position:	°C	°C	°C	°C
P1 Leeward	487	484	527	402
P2 Leeward	542	545	595	397
P1 Up	499	491	587	422
P2 Up	519	515	590	390
P1 Down	473	466	582	375
P2 Down	507	505	591	368
P1 Windward	526	529	531	436
P2 Windward	562	569	570	417

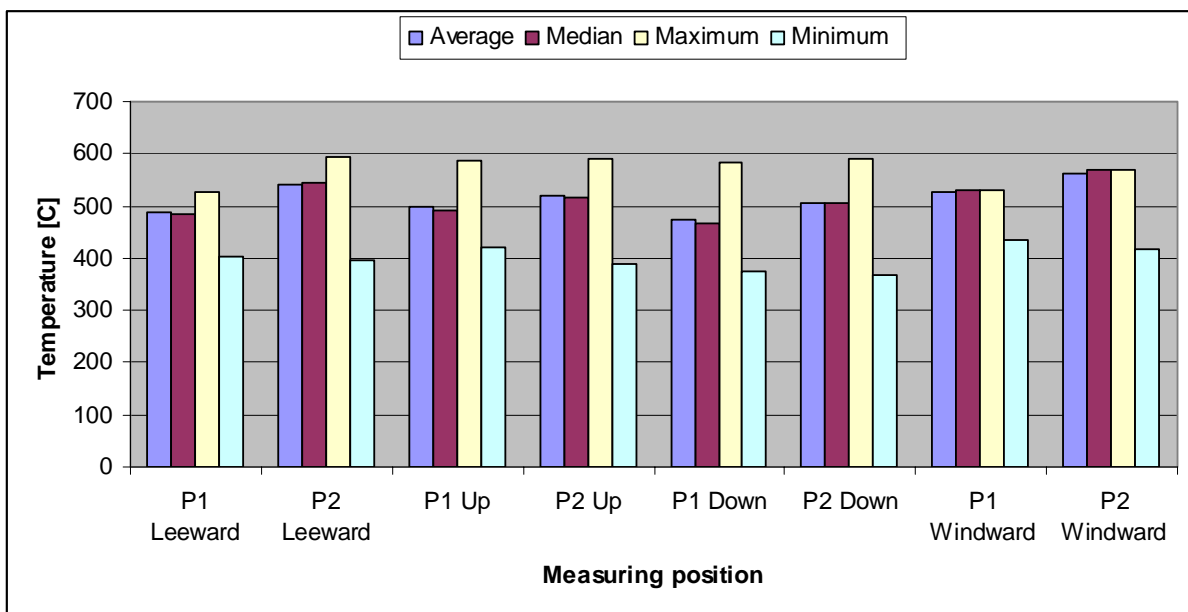


Figure 7. Comparison of temperature data for Probe 1 and Probe 2. Period 16th September – 11th October, exposure time elapse 600 h.

3 Material sample characterisation

Post-exposure the rings were mounted on site in resin, taken to laboratory and prepared for further studies to metallographic cross sections using ethanol as grinding medium. As mentioned before, the material falling from the roof etc. had made harm to some of the samples. According to closer examination samples with marked deformation were as follows. Probe 1: SAN 69, AISI 310, 347H; Probe 2: Super 625, AISI 310.

3.1 Material wall thickness measurements

Material wall thicknesses of the metallographic cross sections were measured from 8 positions (0, 45, 90, 135, 180, 225, 270 and 316 degrees from the windward position (0 degrees)) using an optical method. Measuring values thus obtained were compared internally and to pre-exposure measuring values, Table 3. Those rings which were asymmetric due to material deformation were not measured.

Table 3. The difference in the wall thickness values (Δ [mm]) for various material sample rings measured after and before the exposure.

Δ [mm]	Probe 1				Probe 2				
	SAN28	HR11N	Super 625	Mean	SAN28	Super 625	SAN 69	347H	Mean
<i>Windward (0)</i>	0.002	-0.058	-0.055	-0.037	0.030	-0.002	-0.017	0.009	0.005
<i>Up (90)</i>	0.015	-0.014	0.044	0.015	-0.007	0.008	-0.031	-0.005	-0.009
<i>Leeward (180)</i>	0.002	0.031	-0.022	0.004	-0.033	0.017	0.001	0.041	0.006
<i>Down (270)</i>	0.036	-0.060	0.013	-0.004	0.003	0.000	-0.007	0.105	0.025
<i>Mean</i>	0.014	-0.025	-0.005	-0.005	-0.002	0.006	-0.014	0.038	0.001

The difference-values (Δ) determined were found to vary in a random manner independently of the measuring position and the ring material. The mean value of all differences is 0.001 mm (1 μ m). Wall thickness measuring values are considered as useless for the corrosion evaluations.

3.2 Optical microscopy

Metallographic cross sections of the material samples exposed in the Probe 1 were inspected using a stereo microscope. Indications were found of possible material deformation – corrosion interactions having occurred obviously during the high-temperature exposure (illustrations not shown here). Both deformed sample (material 347H) and less-deformed samples (materials SAN 28, Super 625) in Probe 1 were chosen for more detailed studies using an optical microscope, see optical micrographs enclosed, Figs. 8, 9 and 10 in *Appendix*. In the case of 347H material surface cross section on the Windward position appeared as little affected besides oxide growth outwards whereas on the Leeward position material had suffered from general corrosion and additionally of internal attack along open grain

boundaries down to the depth of about 75 μm from the current metal surface, see Fig. 8 in *Appendix*. In the case of SAN 28 there was found internally penetrated (de-alloyed) zone and oxide scale growths on the Windward and Leeward position, Fig. 9 in *Appendix*. Apparent metal loss totalled about 30 μm and 75 μm on the Windward and Leeward position, respectively. In the case of Super 625 the corrosion attack mode was similar to that in the case of SAN 28, but less in extent, Figure 10 in *Appendix*. Total metal loss, however, depended much of exact location examined. Apparent metal loss at the cross section locating exactly on the Windward position (0 degrees) was found to be less than 10 μm whereas at locations situated about 30 degrees sideways apparent metal loss was about 25 μm or more. Even if still crossly circular, cross section of Super 625 showed features interpreted preliminary as marks of impaction on the Leeward side of the ring, see Fig. 10 in *Appendix*.

Material surface temperature on the Windward and Leeward side of the Probe 1 was measured to be 487 °C and 526 °C, respectively. There was no difference in the maximum temperature value. Examination of Figures 8 to 10 in *Appendix* leads to the suggestion that the extent of corrosion attack for various materials seems to depend more on the local deposit conditions (and on the nature of local thermo-physical stresses) than simply on the probe material surface temperature measured.

3.3 Environmental Scanning Electron Microscopy (ESEM)

Metallographic cross sections of the six material samples exposed in the Probe 2 were coated with a thin film of elemental carbon in order to provide good electric conductivity of the samples mounted in resin. The study was performed using environmental scanning electron microscope “FEI XL30 ESEM” equipped with an analyser “ThermoScientific” and calculation program “Noran System 7” suitable for quantitative elemental analyses. In the practical analytical work the elements with contents of 0.1 wt-% or more only are listed in the analytical reports. For example, chloride contents of less than 0.1 wt-% are not reported. A light element carbon is present in the mounting material, conductive coating and as superficial contaminant as well. Carbon, independent of its presence in the raw data, has been therefore left out from quantitative elemental composition calculations.

Outer circumference of the samples (SAN 28, HR11N, Super 625, SAN 69, AISI 310 and 347H) was examined with using magnification of 200 x starting from the Windward position (0-degrees). Base material composition was determined at the starting position in a depth where there were no signs of corrosion. For in-detail studies of corrosion morphologies ESEM magnifications ranging from 200x to 5000x were applied. Areal and point analyses of corrosion products or deposits refer to areas having horizontal dimensions in the range from 0.05 to 0.001 mm. Vertical dimension of the volume analysed is the order of 0.001 mm. The study was comprehensive covering a total inspected length about of 90 cm and the number of quantitative analyses performed totalled about tree hundred. The most illustrative quantitative analyses only are reproduced in this report.

3.3.1 Results of ESEM studies: Elemental analysis of the deposits

Graphs of quantitative elemental analyses of deposits present at various directions are shown, in Figs. 11 and 12 in *Appendix*. Typically, oxygen, sodium, sulphur, some potassium, and some small amounts of chloride (range from < 0.1 wt-% Cl to about 1 wt-% Cl) and some of chromium, iron and nickel is found in the areal analyses of deposits. In the case of high nickel alloys point analyses indicated that the mass fraction of chlorine in metal-near deposits/corrosion products may locally rise up to 10 or 25 wt-% Cl.

3.3.2 Results of ESEM studies: Estimated metal losses

Typical corrosion morphologies for each material at various directions are shown in Figs. from 13 to 16 in *Appendix*. Oxygen and/or sulphur are found at metal grain boundaries and in the composition of subsurface de-alloyed zones impoverished in respect of chromium and enriched in respect of nickel and iron. Chloride is found too but in amounts of few tens of percent only. The internal penetration depth depends on the local material temperature and deposition conditions. Total metal losses estimated in each case are given below, Table 4.

Table 4. Total metal losses estimated for various material samples exposed in Probe 2.

Material	Lee	Up	Down	Wind	Mean
	[mm]	[mm]	[mm]	[mm]	[mm]
SAN28	0.11	0.04	0.01	0.01	0.043
HR11N	0.08	0.05	0.01	0.025	0.041
Super 625	0.015	0.025	0.005	0.05	0.024
SAN 69	0.05	0.06	0.04	0.05	0.05
AISI 310	0.04	0.09	0.005	0.03	0.041
347H	0.05	0.08	0.02	0.1	0.061
Mean	0.06	0.06	0.01	0.04	0.043

For illustrative purposes the metal loss values given in Table 4 above were converted by linear extrapolation in to annual corrosion rates, see Fig. 8 below. Materials rankings according to linear extrapolation of mean or maximum metal loss in Table 4 above are shown in Fig. 9.

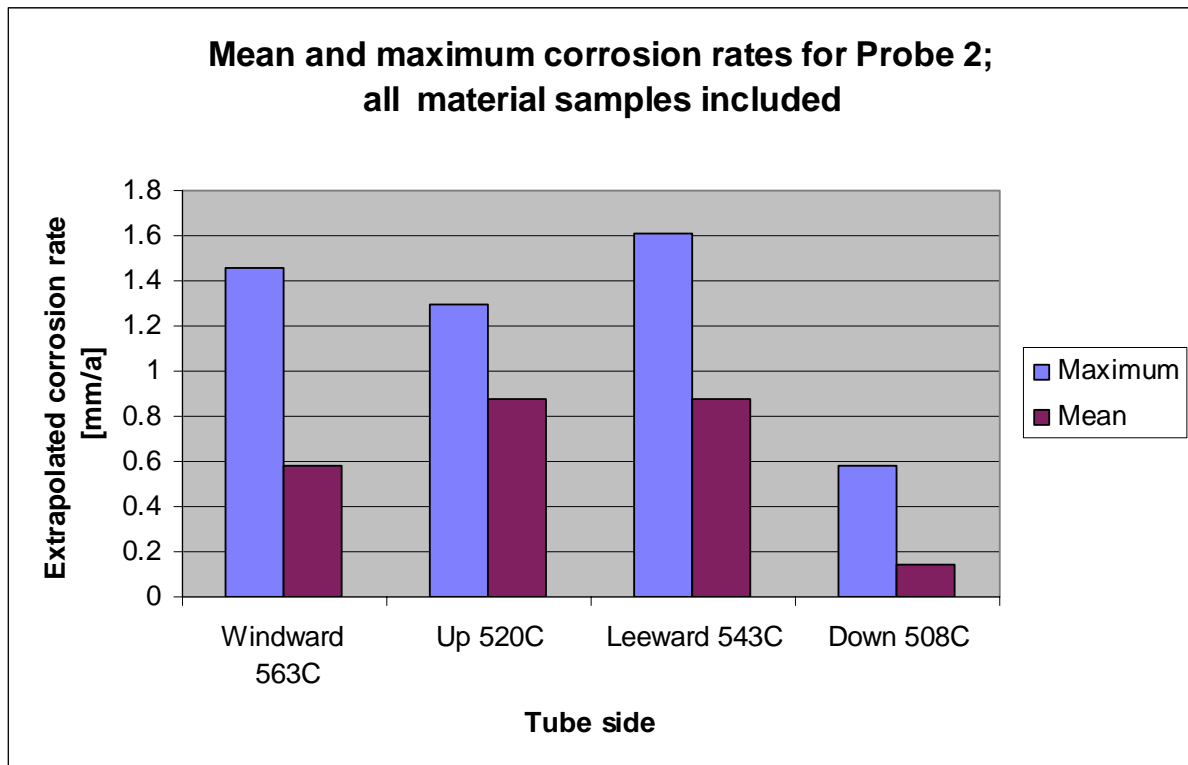


Figure 8. Mean and maximum corrosion rates in various exposure conditions for Probe 2, as estimated. All test materials are included.

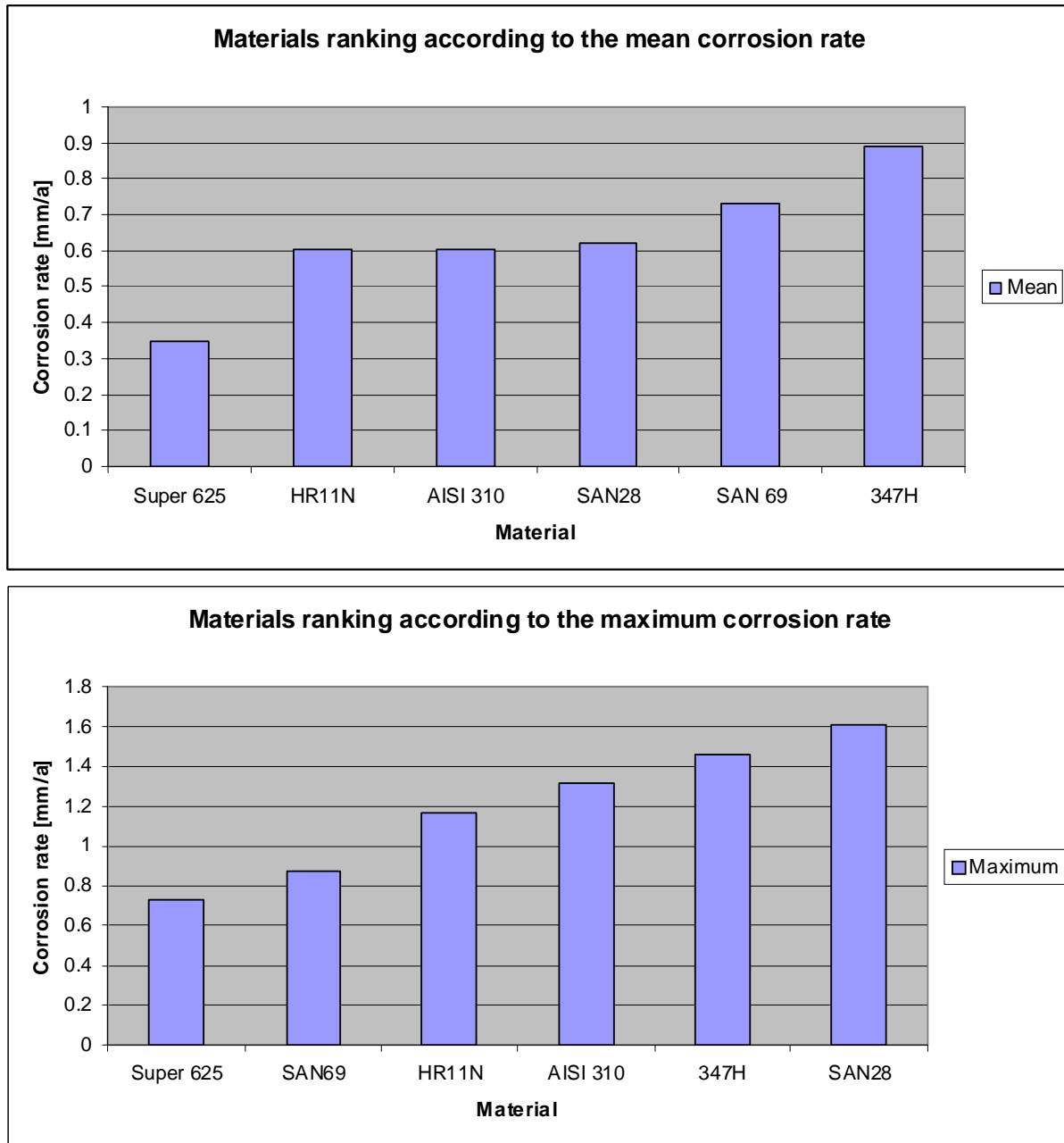


Figure 9. Materials ranking according to the mean or maximum corrosion rate estimated as explained above. Using the maximum corrosion rate as criterion all materials, except Super 625 and SAN 69, show a corrosion rate > 1 mm/a, i.e., corrode with an unacceptable rate. According to mean corrosion rate all materials corrode at a rate < 1mm/a.

3.3.3 Results of ESEM studies: Quantitative elemental analyses of corrosion products

In the case of 347H grain boundary attack, de-alloying of superficial metal grains and chloride enhanced oxide scale growth are the governing modes of accelerated corrosion. Some chloride is very typically found in the areal quantitative analyses of the corrosion products. Point analyses of attacked grain boundaries did, or did sometimes not, reveal sulphur and/or chloride in addition to oxygen, see for example quantitative results found in Fig. 19 in *Appendix*. Note that the conventional analytical limit here is 0.1 wt-% and even so for S and Cl.

Corrosion morphologies and results of detailed quantitative elemental analyses indicated that steels and alloys alloyed highly with chromium had suffered from internal sulphidation and/or oxidation attack. Oxygen or oxygen and sulphur were found as abundant in various de-alloyed zones impoverished in respect of chromium and enriched in respect of nickel and iron, Fig. 20 in *Appendix*. The content of chloride was in general low as compared to oxygen and sulphur. Localised enrichments consisting of nickel and chromium chlorides did contain up to 30 % wt-% Cl, Fig. 21 in *Appendix*.

3.3.4 Results of ESEM studies: Comments

It seems that the corrosion rate of is greatly enhanced at material temperatures in the range from 505 °C to 519 °C, Fig. 10. Referring to the state-of-the-art theory of high temperature break-away oxidation of chromium alloyed steels and high-nickel alloys, see refs. [5,6,10] for example, one may propose that enhanced corrosion attack of the material samples tested is related here to the enhanced growth of mixed-type iron oxide – chromium oxide scales at locations exposed to high surface temperatures and some aggressive chemical conditions.

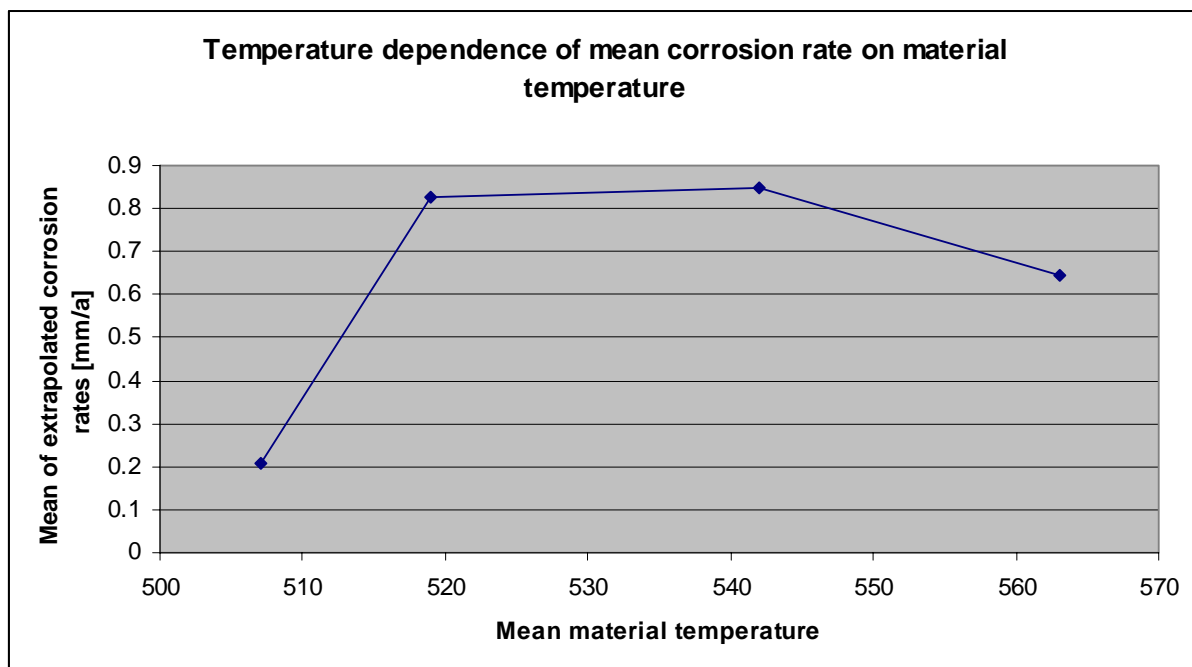


Figure 10. Dependence of mean metal loss measured on material temperature including the data for all six test materials exposed in Probe 2. See for reference Table 4.

A high content of chromium in the material composition seems not to be as beneficial as could be expected, Fig. 11. Initial oxidation conditions in the beginning of the exposure may have also played a role in the enhanced oxide scale growth, see for general reference Fig. 12 below, and ref. [4].

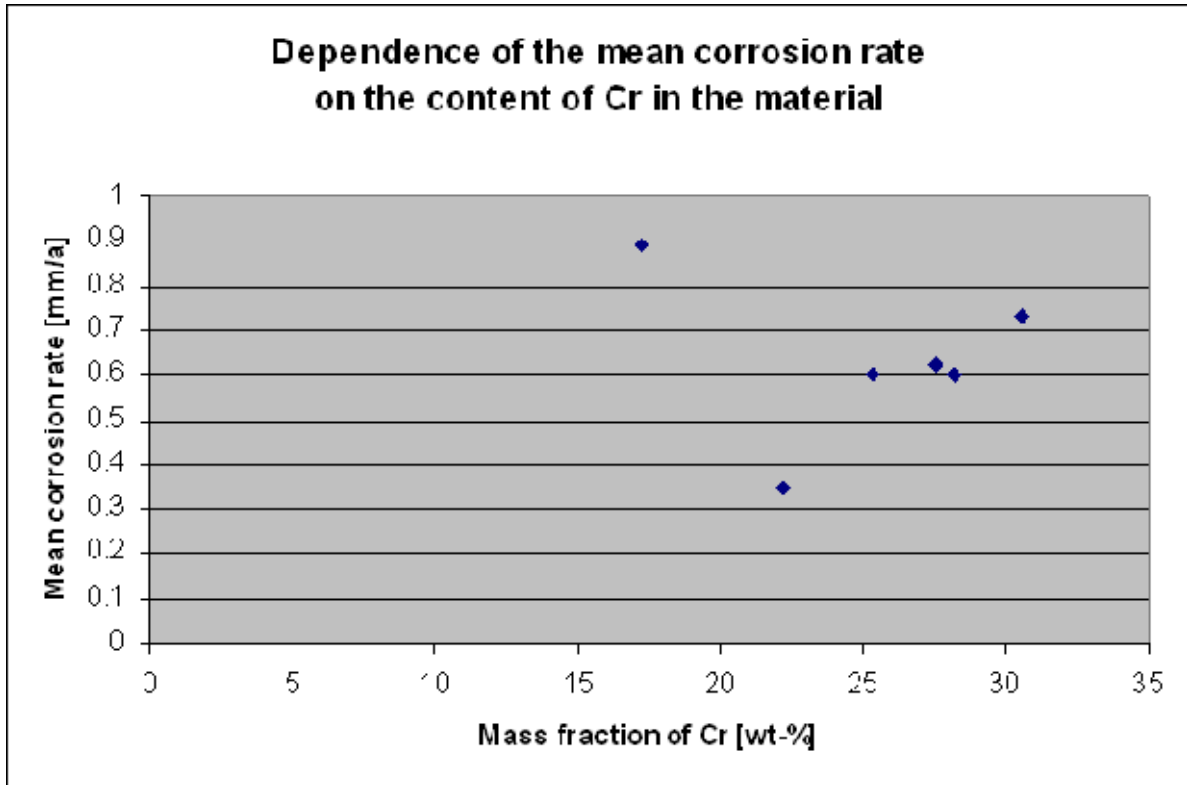


Figure 11. Dependence of mean corrosion rate on the content of Cr in the six materials tested in Probe 2. See Figure 10 above for reference.

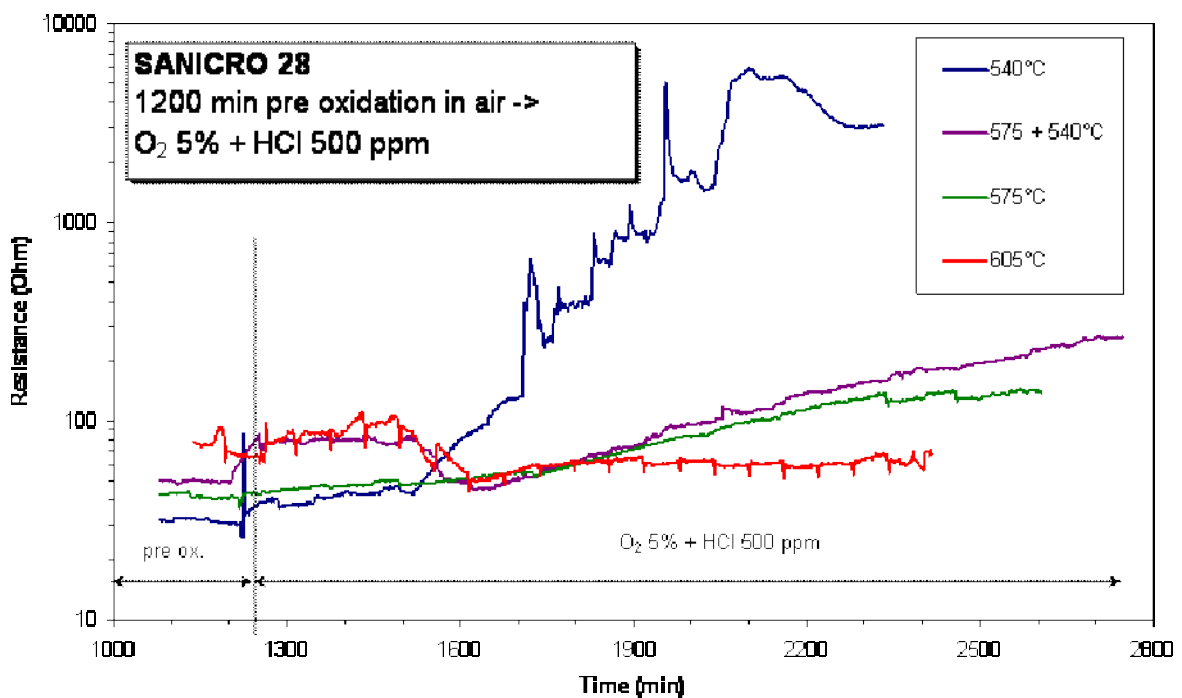


Figure 12. Results of a HT-CER study investigating the effect of specimen pre-oxidation in air to chloride-enhanced oxidation of various steels. The case of SAN 28. Ref. [8].

4 Thermodynamic calculations using FactSage 6.1

Quantitative elemental analyses are useful for corrosion mechanistic considerations using thermochemical equilibrium calculation programs, [11-15.]. Atmospheric oxidation of carbon and low alloy steels under alkali sulphate deposits with chloride contents is greatly enhanced even at material temperatures lower than the first melting point of the salt mixture, [1-4, 7-8].

A recent corrosion case of recovery boiler superheater tubing made of low-alloy steel showed catastrophic internal attack attributable to extremely rapid mass transport in a corrosion product mixture consisting of metallic phase, iron oxide phase, and complex oxide phase with alkali metal content, possibly intermixed with some chloride, [8]. The internal attack had proceeded partly laterally under a dense magnetite scale. The final corrosion product consisted, as usual, of porous oxide scale showing lateral sulphide striations, and enrichment of iron chloride on the metal surface. Similar kind of localised corrosion process but in a minute scale may be proposed to be active in various practical deposit corrosion cases of austenitic stainless steels and nickel alloys. This pragmatic proposition was applied to thermodynamic analysis of the corrosion problem under study. The enhanced corrosion attack of nickel alloys in the temperature range of from 450 °C to 500 °C due to alkali polysulphide type-melts, see refs. [12-15], should be considered to have of relevance here.

4.1 General considerations on deposit chemistry

Factually no single quantitative elemental deposit analysis corresponded to some linear combination of alkali sulphates and alkali chlorides. Assuming that some carbonate and/or sulphide are present, this discrepancy could be solved satisfactorily in various cases. Few attempts to calculate simplified phase equilibrium that would prevail under Ar-CO₂-H₂O model atmospheres were made. In the case of typical deposit for SAN 28 on the Windward side, the lowest melting point was found to be as high as 810 °C. At low CO₂-activities alkali carbonates did, however, dissociate resulting to high alkali oxide activities. In the case of deposit on the Leeward side of the sample SAN 28 the deposit was found to be under any Ar-CO₂-H₂O model atmosphere trial unstable. This matter of fact was due to very high partial pressure of sulphur trioxide and gaseous chlorine HCl(g) and Cl₂(g) at the equilibrium states predicted. Otherwise, under alkaline flue gas conditions, related for example to high-solids firing of liquors with low sulphidity, mixtures of alkali ferrites, carbonates and chlorides may form aggressive melt on the tube surface *in-situ* resulting to highly accelerated oxide scale growth. Alternating SO_x rich and SO_x deficient conditions may set out the most adverse operation conditions in the superheater area of recovery boilers [8].

4.1.1 Equilibrium calculations based on quantitative analyses performed

A number of phase equilibrium- or meta-stable phase-equilibriums were calculated based on detailed analyses of local areas within the metal, in the corrosion product layers and in the layers interim of corrosion products and deposited matter. The main interest was to make comparisons amongst little affected and heavily affected sides (or location) for the same material. Calculation results for SAN 28 are illustrated in Fig. 13. This material showed, at locations, the most severe and the most minute corrosion attack of all.

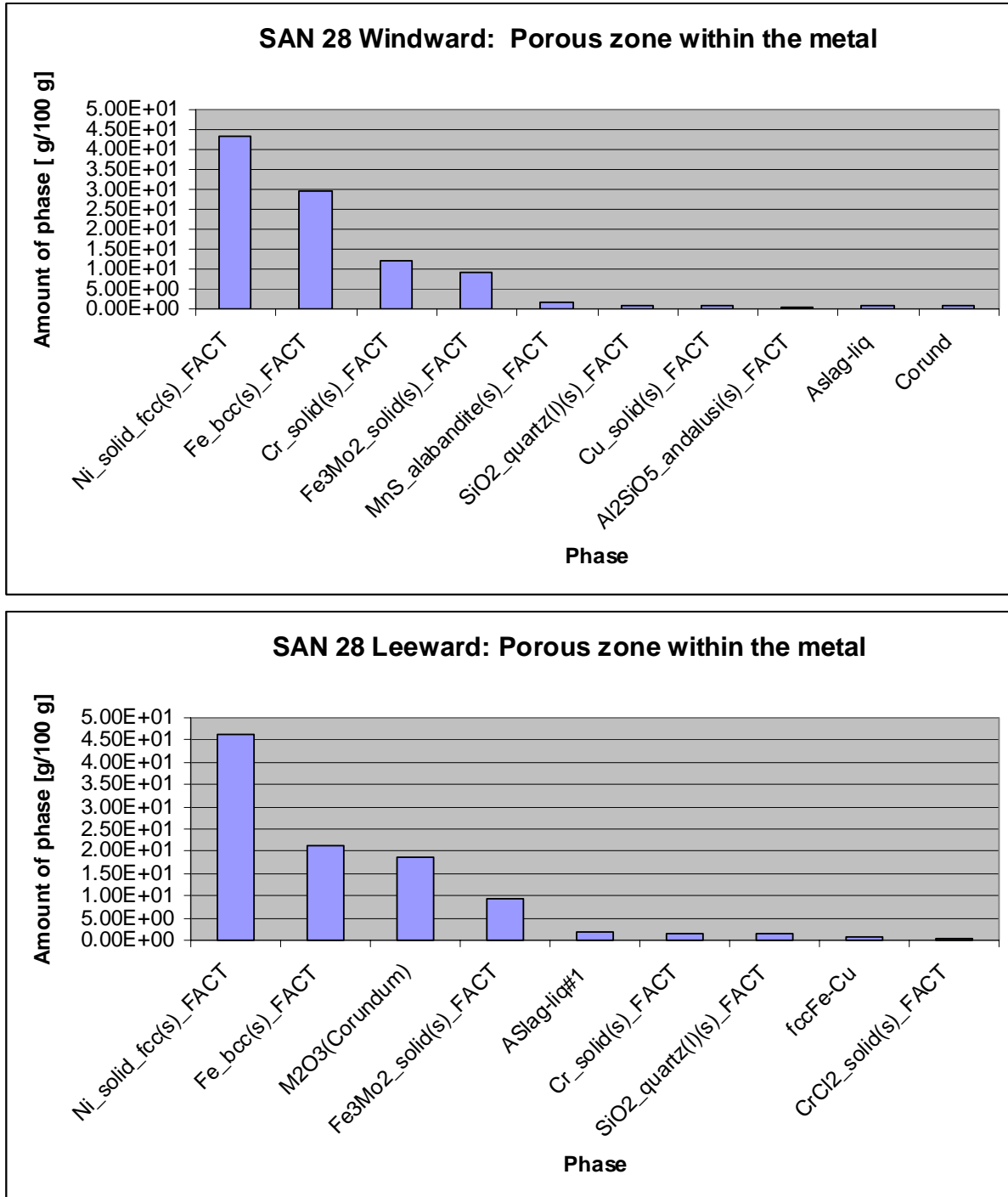


Figure 13. Calculated phase composition that corresponds to an areal analysis of porous (de-alloyed) zone on the Windward side (top picture) and Leeward side (bottom picture) of sample of SAN 28. Transport of oxygen and sulphur via molten phases inward is predicted to possibly occur. Chlorine, however, is if present bound as a solid compound CrCl_2 . (Phase equilibrium calculated for the temperature of 542°C .)

In the case of SAN 28, mixture phases allowing a rapid transport of metal and oxidant species are predicted to be present in the porous metal. There is, however, no guarantee that the model liquid phase ASlag-liq#1 in Fig. 13, or any other liquid, exists in the real physical equilibrium. Chlorine, when present as-analysed, tends to bound as a solid phase compound CrCl_2 causing that Cl_2 -activity is very low within the porous zone. Accordingly, chromium must be considered as a beneficial alloying element. In the subsurface layers and multiphase corrosion scales that may show relatively high oxygen activities, low melting mixtures of

metal chlorides and oxy-chlorides may be present. Alkali chlorides NaCl and KCl form with CrCl_2 various ternary eutectics in the temperature range of about from 604 °C to 548 °C.

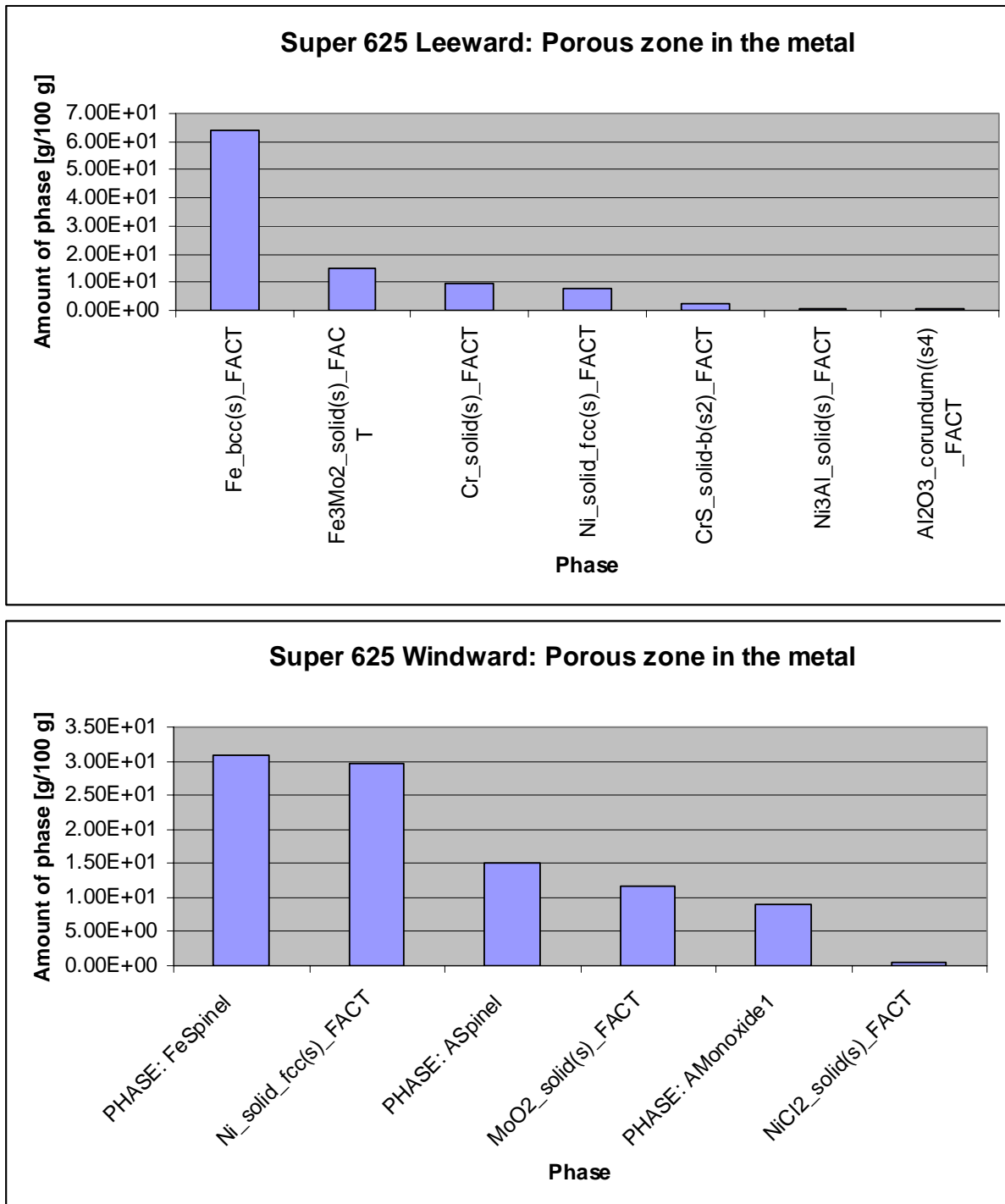


Figure 14. Calculated phase composition that corresponds to an areal analysis of porous (de-alloyed) zone on the Windward side (top picture) and Leeward side (bottom picture) of sample Super 625. Transport of oxygen and sulphur via molten phases inward may not readily occur (according to the prediction). Chlorine, if present, is bound as a solid compound NiCl_2 . (Phase equilibrium calculated for the temperature of 542 °C.)

In the case of Super 625 (Fig 14) no molten phases were predicted to be present in the porous zone within the metal at an equilibrium temperature of 542 °C applied. On the Windward side some chlorine together with a relatively high amount of oxygen was analysed. Chlorine was,

however, bound as a solid compound NiCl_2 with moderate vapour pressure at high material temperatures of recovery boiler superheater tubes. NiCl_2 form low-melting eutectics with NaCl and KCl at temperatures about of $563\text{ }^\circ\text{C}$ and $494\text{ }^\circ\text{C}$, for NaCl and KCl , respectively. In the system KCl-NiCl_2 there exists also a peritectic melting temperature about of $502\text{ }^\circ\text{C}$.

Equilibrium calculations based on areal or point analysis of outer corrosion scales did most often lead to unphysical equilibrium state-predictions showing very high equilibrium partial pressures of sulphur oxides and gaseous chlorine species, see for example the case of deposit analysis representing deposit/scale interaction zone on the Windward side of Super 625, Fig. 15 below.

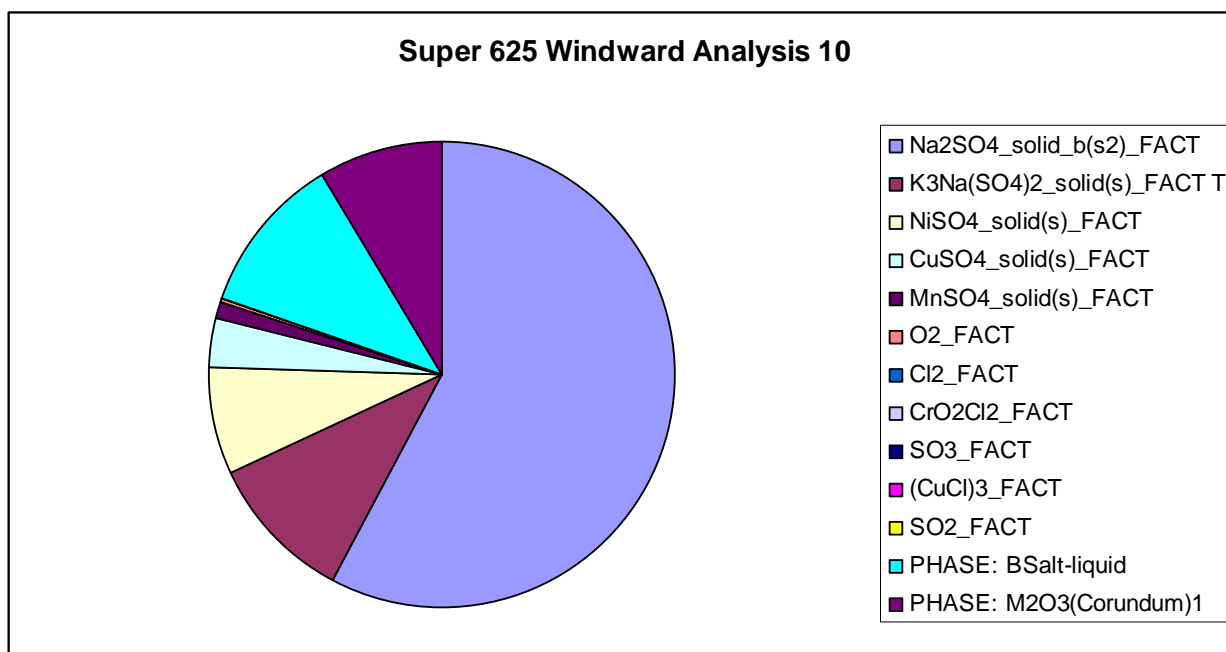


Figure 15. Calculated phase composition that corresponds to an areal analysis of corrosion scale/deposit on Windward side of Super 625 (top picture); the equilibrium state predicted is obviously non-physical due to high partial pressure of gaseous species SO_3 and Cl_2 .

This situation may be explained (i) by incomplete local reaction equilibrium amongst oxygen, sulphur and chloride species actually present and (ii) some amount of carbonate (and hydrogen) in the true elemental composition. The short operation cycle of proximate soot blowers makes it plausible that a non-equilibrium state is rather characteristic for the deposit conditions prevailing on the Leeward- and Up-side of the probe. Catalytic activity of various transition metal and trace metal species may cause that various kinetically restricted reactions advance towards equilibrium immediately on the tube outer surface (on/within the corrosion scale) and eventually in the permanent deposits.

From the corrosion point of view the actual ranges of partial pressure of chlorine and oxygen are of special importance. Phase equilibrium for Super 625 Windward side analysis No 10, Fig. 15, was recalculated assuming that some carbonate is actually present. Calculations were for qualitative purposes only; calculation results are thus not given here in more detail. Equilibrium amounts of various metallic chloride and oxy-chloride species were recorded in the phase equilibrium partial volume corresponding to the partial pressure range of gaseous chlorine (p_{Cl_2}) from 10^{-17} atm to 10^{-5} atm were noted. Transition metal chloride species of interest in the corrosion mechanism, that of active oxidation in particular, were found to be $(\text{CuCl})_3(\text{g})$, $\text{NiCl}_2(\text{g})$ and $\text{NaFeCl}_4(\text{g})$. Partial pressure of chromium oxy-chloride species $\text{CrClO}_2(\text{g})$ did become important but above the p_{Cl_2} range of 10^{-5} atm. The molten salt

mixture phase that was predicted to be stabilised in the high end of chlorine partial pressure mentioned above is rich in chlorides of potassium, iron, nickel and manganese.

4.1.2 Predictive calculations

In order to be able to study corrosion behaviour in a more generalised manner superheater deposit analyses relevant to Joutseno Recovery Boiler were referred to, [16, 17]. In the model calculations each of the six materials tested was exposed to the same model deposit with the content of chloride, potassium and carbonate in the range of 0.5 wt-% Cl, 5 wt-% K and 1.5 wt-% C, respectively. Equilibrium temperature was used as a variable. Oxide scale growth rate was considered to increase steeply at a limiting temperature above which a model melt with some content of transition metals elements of the alloy may co-exist with an oxide scale. In most cases studied such model melts did contain transition metal chlorides. It is interesting to note that sodium chromate (NaCr_2O_4) was a rather stable species. If one assumes that the ranking order of the materials in the deposit conditions in question is the same as the order of the limiting temperatures obtained by calculation, one gets a ranking order like the one shown in Fig. 16 below. The model ranking is similar to the ranking according to maximal corrosion attack observed, Fig. 17.

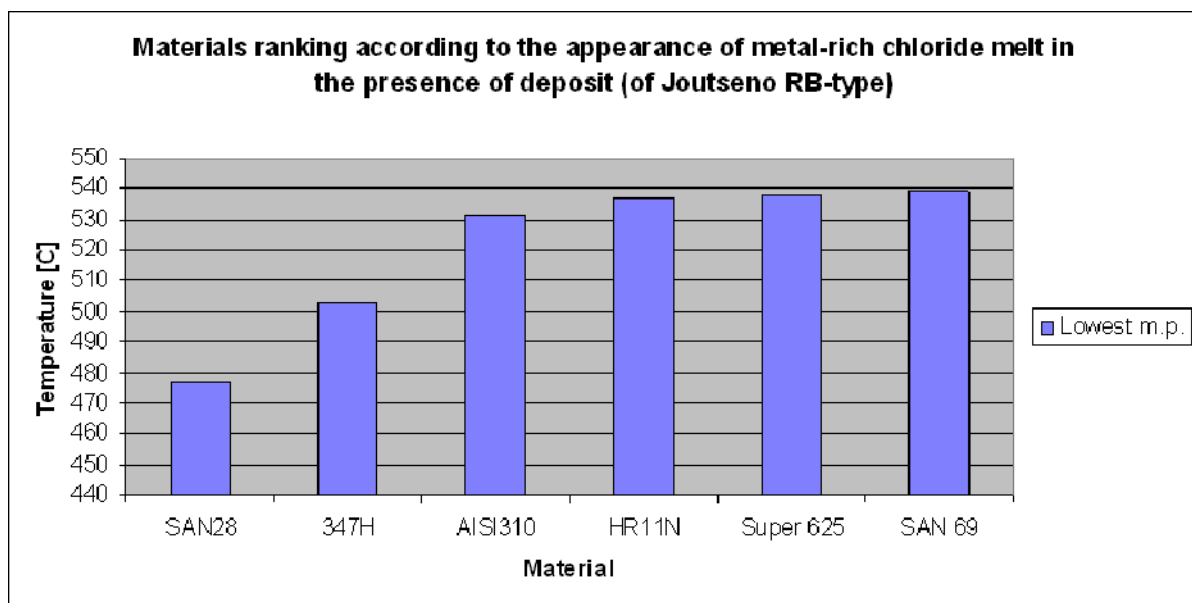


Figure 16. Calculated lowest temperature where a transition metal chloride-rich melt may exist within oxide scale in the presence of deposit of Joutseno recovery boiler type containing some carbonate. Transport of metal, sulphur, oxygen and chlorine ions is predicted to occur readily above the alloy-specific temperature indicated on the left axis.

The conceptual model used emphasizes, from the corrosion kinetic point of view, the role of various mass transport processes within the corroding metal and mature corrosion scales where partial pressure of oxygen is also in practice low. Thus the ranking shown above may not and is neither intended to reflect the materials behaviour in short term tests under an air atmosphere where chloride enhanced corrosion mechanisms are related to the mass transport phenomenon commonly named as “active oxidation” or “low temperature-oxidation” in a more direct manner, see for example refs. [19-21].

5 Discussion

5.1 Comparison to recent full-scale material exposure data

Interestingly, corrosion morphology and material wastage rates in question were found to correspond well to those observed before for various specimens of austenitic stainless steels AISI 310 and HRC, [7], or that of 347H, 310H and SAN 28, [9]. Extrapolated corrosion rates for obtained in the present study and in that of Keiser et al [2010], [9], are compared schematically in Figure 17.

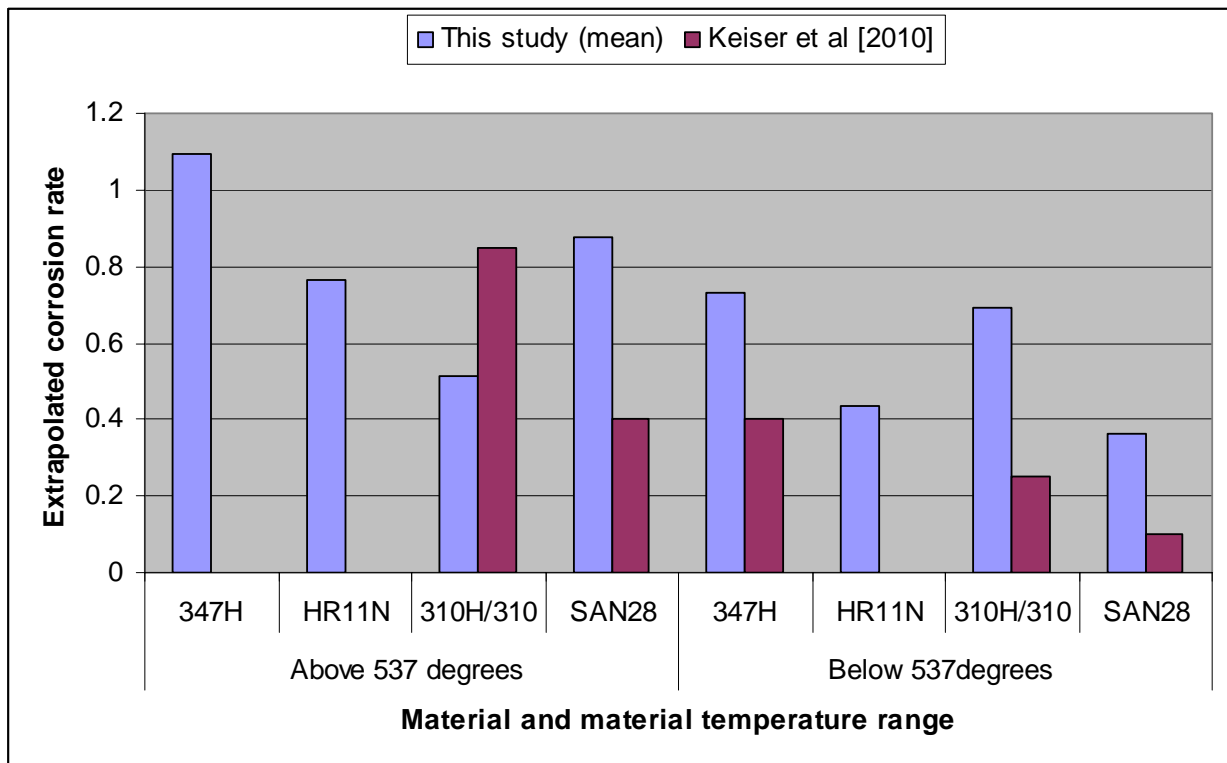


Figure 17. Schematic presentation of extrapolated corrosion data applied from two different sources. Experimental exposure time in RB superheater area in each case is as follows. This study: 600 h; Keiser et al [2010]: 1000 h.

Extrapolated corrosion rate for the same type high chromium alloys materials is found to be lower after the exposure time of 1000 h [9] compared to that of 600 h (this study). Related deposit chemistries are presented in Fig. 18 and the lowest melting temperature of deposits respectively in Fig. 19.

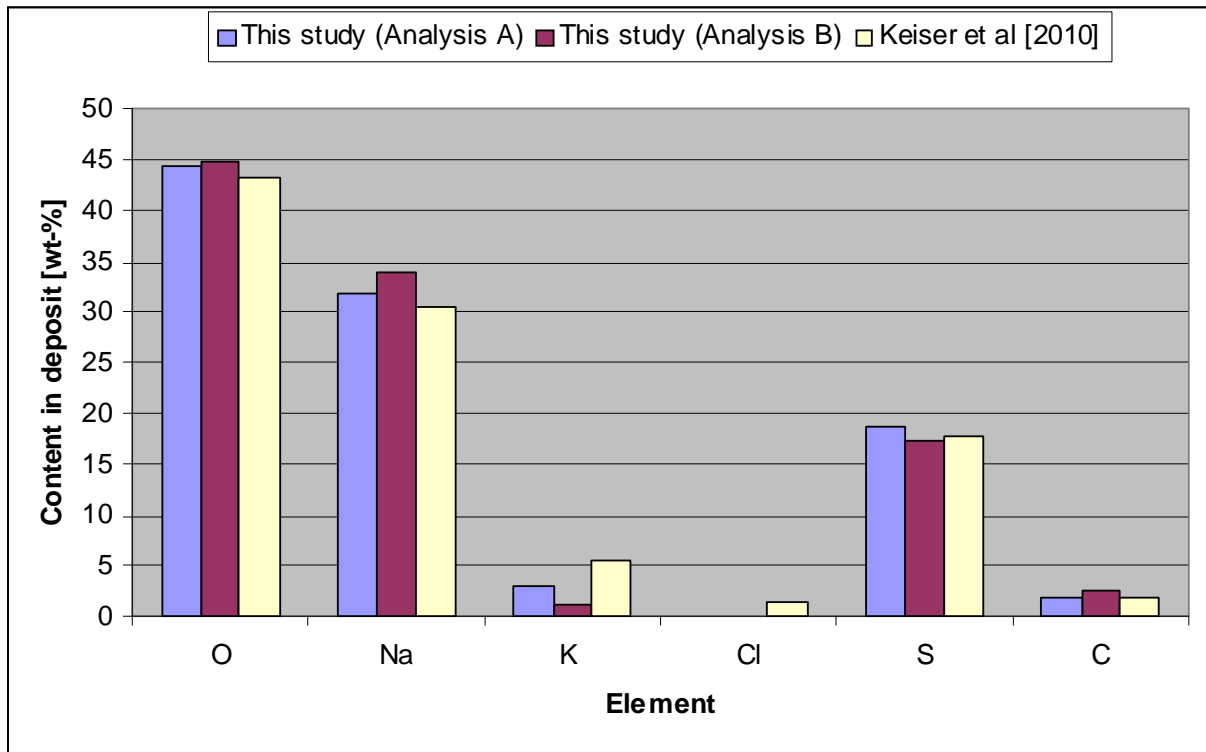


Figure 18. Deposit chemistry with reference to the various corrosion data presented in Figure 17.

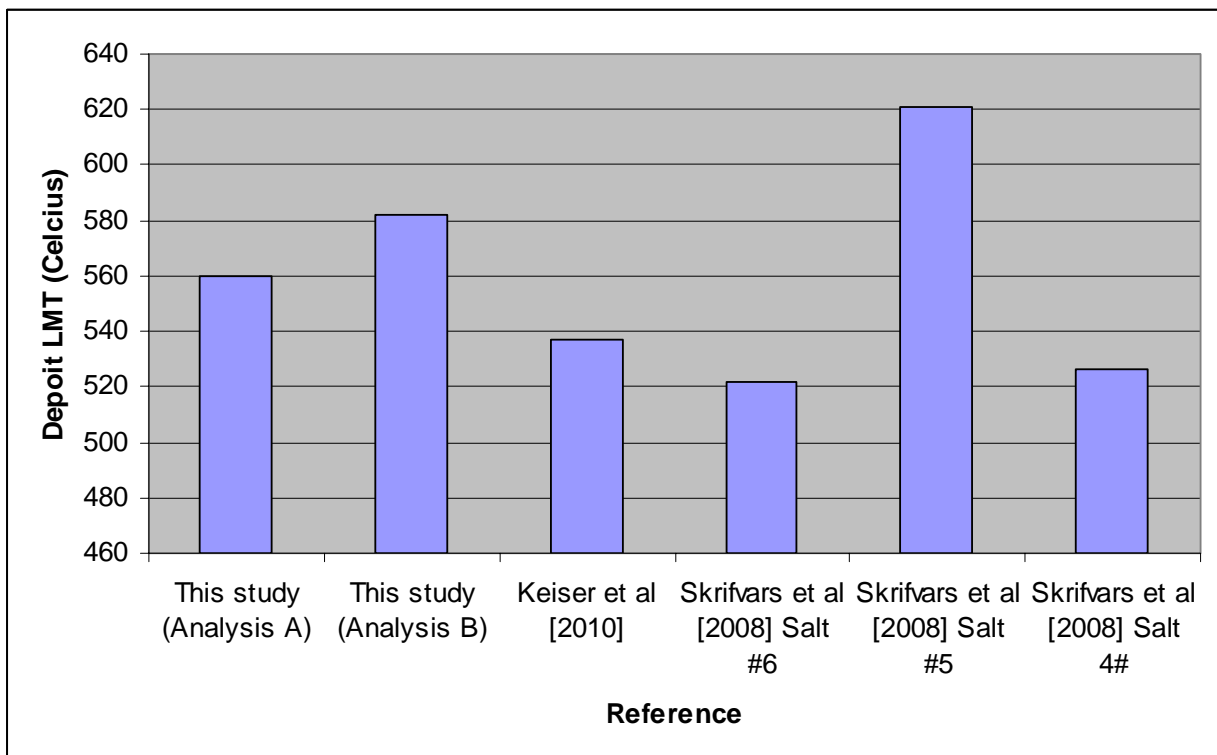


Figure 29. Lowest melting temperature (LMT) with reference to Fig. 17. LMT for this study and that of Keiser et al (2010), [9] have been re-calculated using the same FactSage 6.1 model for comparative purposes. Atmosphere of 90 % Ar – 10 % CO₂ – 2 O₂ was assumed. Other LMT-data is original, Skrifvars et al (2008), [19]

Alloys relying on the protective chromia scale show thin protective chromium-rich oxide films, or mixed-type oxide scales with inferior protective capability. In variably aggressive environments, as is the case for full scale material exposures in the recovery boiler superheater area, initiation conditions of localised corrosion attack and conditions of healing are also highly variable in respect of time and exact place. For example the contact resistance measured using HT-CER for SAN 28 specimens pre-oxidised at temperature of 605 °C in air is diminished rapidly in oxidizing-chloridizing environment exposure at the same temperature.

Oxide scale formed on SAN 28 is reported to be of dual structure showing an outer spinel type scale enriched in respect of manganese and inner corundum type scale, [20]. The performance of high chromium steels alloys exposed in laboratory to chlorine environments may at least in the short term depend decisively on the initial oxidation state of the specimen besides of its preparation using some accepted method.

5.2 Corrosion mechanistic considerations

Laboratory corrosion test atmosphere of ambient air can be considered as preliminary relevant for the case of high-solids firing of soft wood where SO₂ content of flue gases before ESP of less than 1 ppm have been reported, [21]. Pitting resistance of various high-chromium alloys (e.g., Super 625, SAN 28, AC66) is rather good when exposed to alkali sulphate-alkali chloride melt in laboratory under an air atmosphere.

In short term (65 h) alkali sulfate – chloride - carbonate melt exposures applying half immersed specimens made of steels mentioned above enhanced localised corrosion was observed post-exposure at locations proximate to the melt-air interface. In that location a thin molten salt film present and continuously replenished from the melt pool. The oxygen potential of the molten salt film is obviously high favouring basic fluxing of chromium and iron, [8]. Rate of localized metal loss of high-chromium steels and alloys may then reach, or even exceed, corrosion rate of low alloy and lower grade stainless steels. In the presence of KCl and CO₂ the role of chloride rich melts as compared to that of active oxidation is emphasized in the corrosion mechanism. Then, type 625 nickel alloys, and certain austenitic stainless steels alloyed highly with chromium but moderately with nickel seem to perform best. The role of molybdenum (and that of niobium) in the type 625 alloys is considered, preliminary, as beneficial but as intrinsic very complex at the same.

An interesting result of equilibrium calculations performed in this study was that any chlorine that is present at low partial pressures of both chlorine and oxygen is apt to retain in the metal preferably as CrCl₂ with extremely low vapour pressure. Important amounts of gaseous nickel chloride NiCl₂(g) and that of copper species (CuCl)₃ in particular predicted to be present even the conditions mentioned above. Copper originating from the corroding alloy itself (as SAN 28) or from external sources (liquor, soot blowing steam, corroding materials) may in theory be involved in transport of chlorine species within the corrosion scale and sub-scale volumes of the corroding high-chromium, high-nickel alloys. See analytical data for Super 625 and SAN 69 specimens exposed in this study; copper contamination during specimen handling and preparation is a possible but highly accidental source of copper.

5.3 Concluding remarks

The basic view taken in this study emphasizing the role of formation of complex melts with contents of various transition metals is basically in accord with the recent understanding of alkali chloride-alkali sulphate enhanced deposit corrosion of high-alloy steels in boilers, see [21]. Localised corrosion attack of highly chromium alloyed materials is considered, however, to be of statistical nature in the recovery boiler superheater area. Long-term progression of localised corrosion of high-alloy steels and nickel alloys can not be evaluated based on known behaviour of low-alloys steels and lower grade austenitic steels showing enhanced scale growth mainly. Perforation of tube walls of high pressure components such as superheaters is not acceptable. In continuation efforts to apply here statistical methods developed for predictive analysis of hot corrosion test data, e.g., [22], on larger data sets of corrosion depth measuring values are recommended.

6 Conclusions

The corrosion performance of materials 347H, AISI 310, HR11N, SAN 28, Super 625 and SAN 69 at high material temperatures of recovery boiler superheaters was studied. Full scale material exposures were carried out in Joutseno RB by September-October 2010. Two identical cooled probes with 6 material samples in each were exposed in the boiler for a time of one month. Nominal material temperatures on the exposed side of each probe were 530 °C and 570 °C. The boiler operated in high-solids firing mode using soft wood liquor with some 0.1 chlorine as fuel.

Corrosion conditions were found to be highly variable depending of the flue gas flow direction and the temperature exposure history. Maximum metal loss was typically observed to occur on the leeward side of the probe. The extent of metallic corrosion at locations was, however, related to the presence of chloride. Corrosion morphologies noticed are known as typical of each material tested in terms of oxide scale growth, grain boundary attack and internal penetration.

The materials ranking according to the maximum total metal loss typically found on the leeward side of the probe for each material tested was considered to be as: SAN 28 < 347H < AISI 310 < HR11N < SAN 69 ~ Super 625 (best). Predictive calculations referring to deposit conditions with about 0.5 % chloride, 5 % potassium and certain amount of carbonate resulted to a similar ranking considered to be as: SAN 28 < 347H < AISI 310 < HR11N < Super 625 ~ SAN 69 (best).

Performance of the six materials tested is considered as unsatisfactory, Super 625 and possibly SAN 69 excluded, in the actual test conditions; i.e., at such conditions where the probes were exposed to steam blowing from a close vertical distance and at average tube material temperatures of about 570 and 540 °C, peaking for short time up to 590 °C. There exist, however, no major quantitative or qualitative differences between the results of the present study and recent full scale recovery boiler and laboratory test data available in the open literature taking in regard the temperature sensitivity of the corrosion phenomena in question and the statistical nature of the extent of localised corrosion in place and time.

References

1. Alexander, P.A., *Laboratory Studies of the Effects of Sulphates and Chlorides on the Oxidation of Superheater Alloys*, *Dummy Tijdschrift*, 1963, 571-582.
2. Ross, W., Umland, F., *Untersuchung chlorid-induzierter Hoch-Temperaturkorrosion an Eisen-, Nickel-, Cobalt-Basislegierungen*, *Werkstoffe und Korrosion*, 35, 1984, 47-54
3. Shinata, Y., Nishi, Y., *NaCl-induced Accelerated Oxidation of Chromium*, *Oxidation of Metals*, 26, 1986, ³/₄, 201-211.
4. E. Reese, E.M. Muller-Lorenz and H.J. Grabke, *Investigation of the transient state of oxidation-chloridation*, *JOURNAL DE PHYSIQUE IV*, Volume 3, Colloque C9, supplément au *Journal de Physique* 111, Volume 3, décembre 1993, 133-141
5. H. E. Evans, A. T. Donaldson and T. C. Gilmour, *Mechanisms of Breakaway Oxidation and Application to a Chromia-Forming Steel*, *Oxidation of Metals*, Volume 52, Numbers 5-6, 379-402
6. James M. Rakowski, Charles P. Stinner, *Prediction Of Oxidation-Limited Lifetime Of Stainless Steel Foils For Primary Surface Recuperators*, Paper Number 07463, *CORROSION* 2007, March 11 - 15, 2007, Nashville, Tennessee, 2007. NACE International. 12 p.
7. Mäkipää, M., Oksa, M and Koivisto, L., *Superheater Tube Corrosion in Changing Operation Conditions of Recovery Boilers*, Paper NACE 01424-01-T-5H.
8. Mäkipää, M., Lind, T., Pyykönen, J., McKeough, P., Oksa, M., Malkow, Th., Fordham, R.J., Baxter, D., Koivisto, L., Saviharju, K. and Vakkilainen, E., *Superheater tube corrosion in recovery boilers*, *10th International Symposium on Corrosion in the Pulp and Paper Industry (10th ISCPPI)*. Helsinki, 21 - 24 August 200, Hakkarainen, Tero (ed.), 2001. VTT Manufacturing Technology, Espoo.
9. James R. Keiser; Joseph R. Kish, Douglas L. Singbeil, *RECOVERY BOILER SUPERHEATER CORROSION FIELD STUDY*, *CORROSION* 2010, March 14 - 18, 2010, San Antonio, TX. 2010, NACE International
10. Chyrkin, A., Schulze, S. L., Pirón-Abella, J., Bleck W., Singheiser. L. Quadackers, W.J., *Oxidation Limited Lifetime of Ni-Base Metal Foams in the Temperature Range 700–900 °C*, *Advanced Engineering Materials*, Volume 12, Issue 9, pages 873–883, September, 2010
11. V. Buscaglia, P. Nanni and C. Bottino, *The mechanism of sodium sulphate-induced low temperature hot corrosion of pure iron*, *Corrosion Science*, Volume 30, Issues 4-5, 1990, Pages 327-333, 335-349.
12. MÄKIPÄÄ, M., MÄKINEN, S., BACKMAN, R., and HÄMÄLÄINEN, M., "Corrosion of BLRB Floor Tubes in Reduced Kraft Smelts: Experimental and Theoretical Studies", in: *TAPPI Proceedings, 1996 Engineering Conference, Book 2*. TAPPI Press, Atlanta, USA, 682-691 (1996).
13. M. Mäkipää, S. Mäkinen, R. Backman, M. Hämäläinen. *Material performance in reducing sulfur containing environments*. Report VALC207. VTT Manufacturing Technology, Espoo. 1996, 17 p.
14. Mäkipää, M., and Backman, R., *Proceedings of the 9th International Symposium on Corrosion in the Pulp and Paper Industry*, CPPA, Montreal, PQ, p. 199-207 (1998).

15. K. Hack and T. Jantzen, *Development of databases and generation of stability diagrams pertaining to the modelling of processes during hot corrosion of heat exchanger component*, *Materials and Corrosion* 2006, 57, No. 3
16. Wm. James. Frederick Jr., Esa K. Vakkilainen, *Sintering and Structure Development in Alkali Metal Salt Deposits Formed in Kraft Recovery Boilers*, *Energy & Fuels* 2003, 17, 1501-1509
17. Wm. James. Frederick Jr., Esa K. Vakkilainen, *The Conditions for Boiler Bank Plugging by Submicrometer Sodium Salt (Fume) Particles in Kraft Recovery Boilers* *Energy & Fuels* 2004, 18, 795-803
18. B.-J. Skrifvars,, R. Backman a, M. Hupa a, K. Salmenoja b, E. Vakkilainen, *Corrosion of superheater steel materials under alkali salt deposits Part 1: The effect of salt deposit composition and temperatur*, *Corrosion Science* 50 (2008) 1274–1282.
19. B.-J. Skrifvar,, M. Westén-Karlsson,, M. Hupa, K. Salmenoja, *Corrosion of super-heater steel materials under alkali salt deposits. Part 2: SEM analyses of different steel materials* *Corrosion Science* 52 (2010) 1011–1019
20. C. Pettersson, T. Jonsson, C. Proff, M. Halvarsson, J.-E. Svensson and L.-G. Johansson, *High Temperature Oxidation of the Austenitic (35Fe27Cr31Ni) Alloy Sanicro 28 in O₂ + H₂O Environment*, *Oxidation of Metals*, Volume 74, Numbers 1-2, 93-111,
21. David A. Tillman, Dao Duong, Bruce Miller, *Chlorine in Solid Fuels Fired in Pulverized Fuel, Boilers s Sources, Forms, Reactions, and Consequences: a Literature Review* *Energy & Fuels* 2009, 23, 3379–3391
22. J.R. Nicholls and P. Hancock, *Prediction of high-temperature corrosion performance using statistical analysis techniques*. In: J. E. Srutt and J.R. Nicholls (eds.) *Plant Corrosion Prediction of Mateials Performance*. Institution of Corrosion Science/Ellos Horwood Limited, 1987. pp 258-273
23. Pirita Mikkanen, Esko I. Kauppinen, Jouni Pyykönen, Jorma K. Jokiniemi, Minna Aurela, Esa K. Vakkilainen, Kauko Janka, *Alkali Salt Ash Formation in Four Finnish Industrial Recovery Boilers*, *Energy & Fuels* 1999, 13, 778-795

Appendix

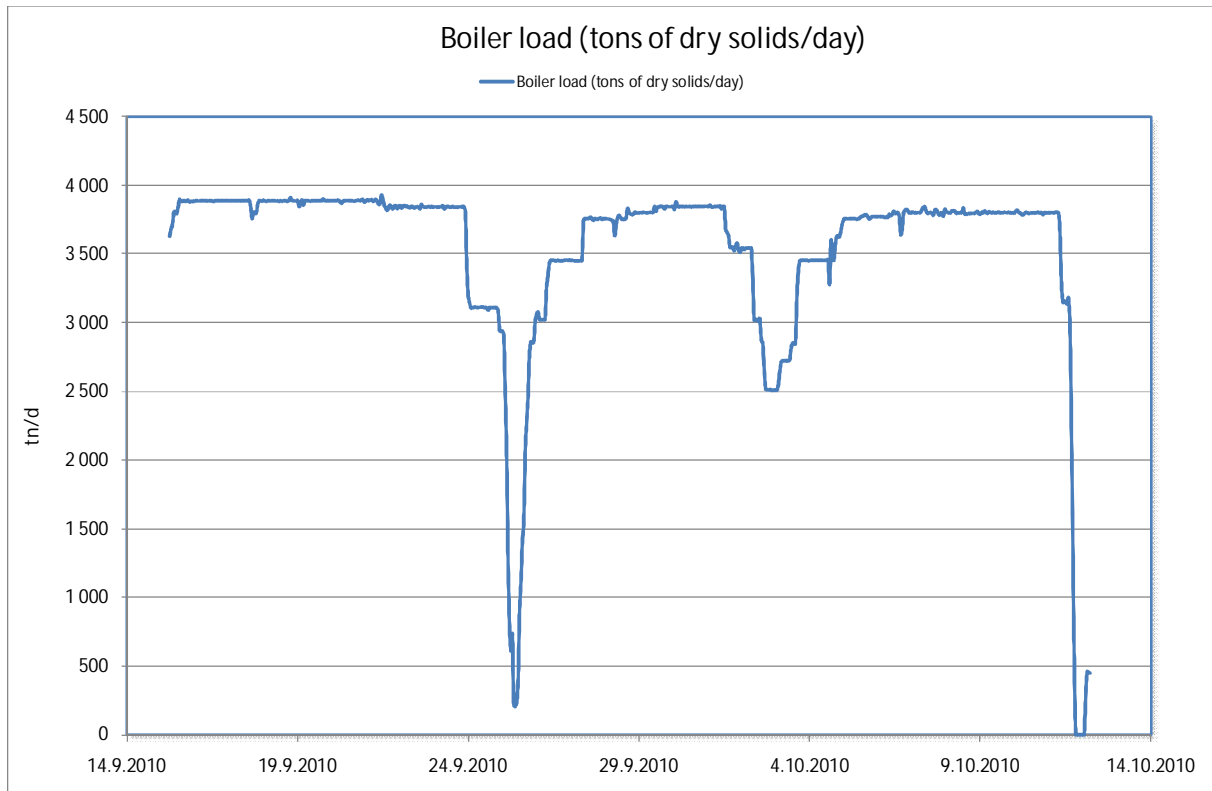


Figure 1. Boiler load (tons of dry solids/day) during the measurement period.

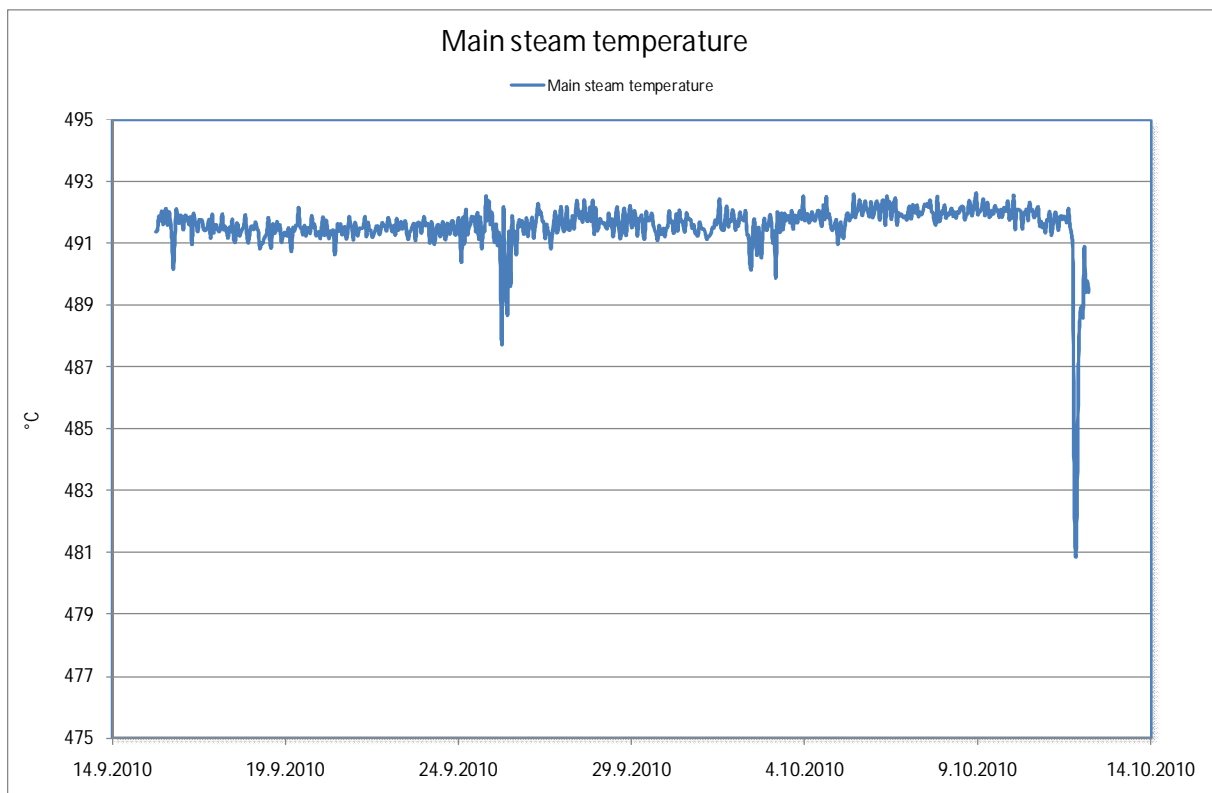


Figure 2. Main steam temperature during the measurement period.

Appendix

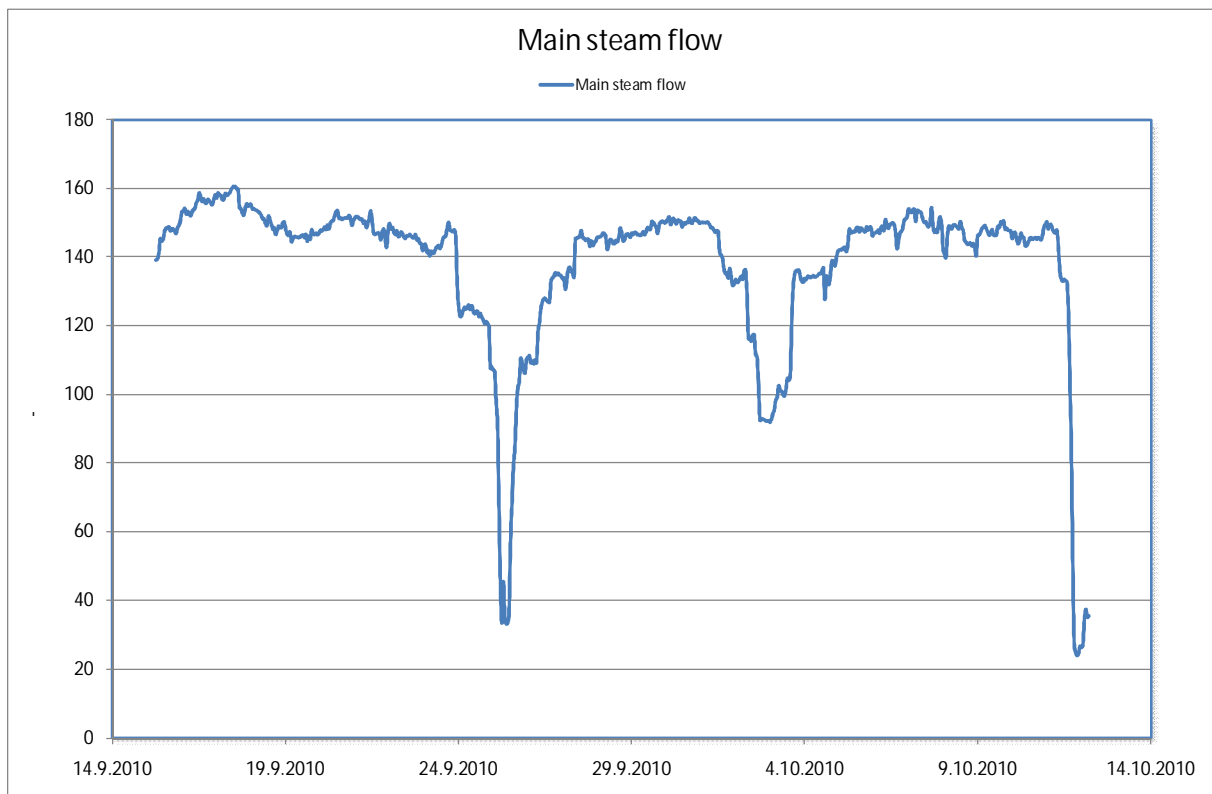


Figure 3. Main steam flow during the measurement period.

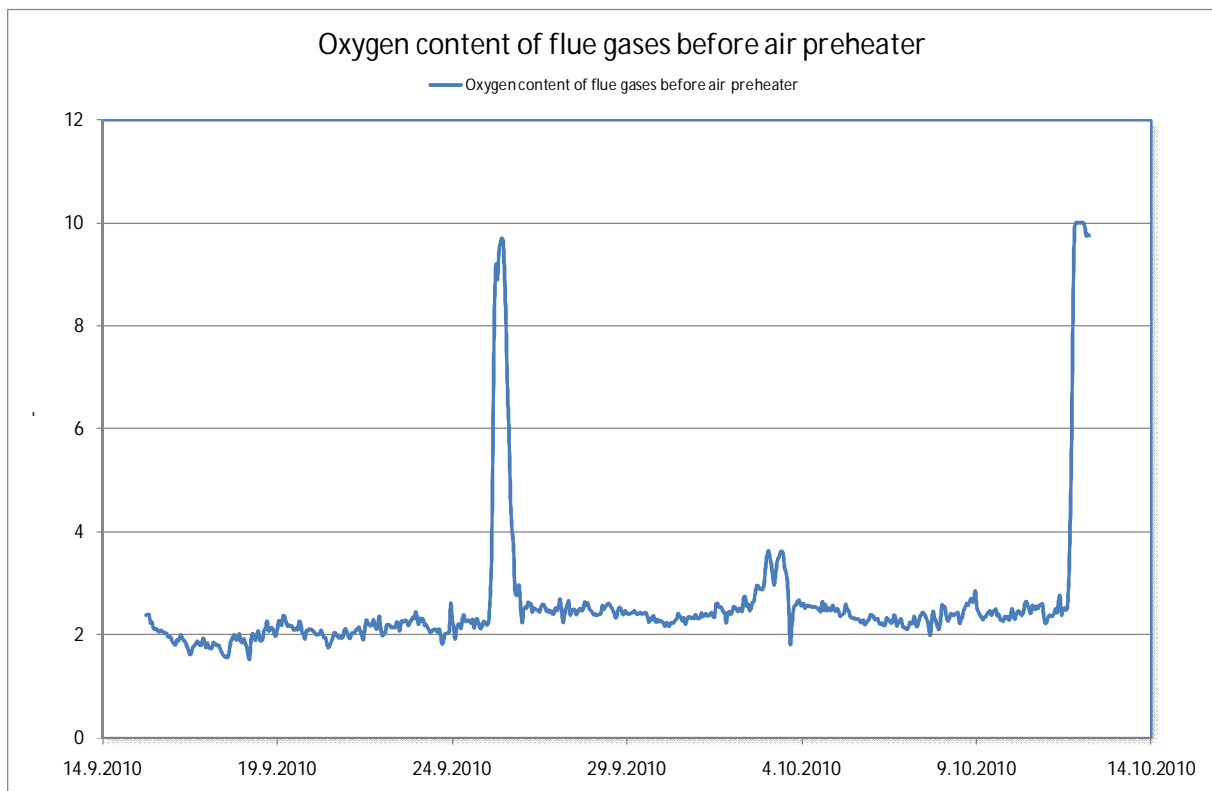


Figure 4. Oxygen content of flue gases before air preheater during the measurement period.

Appendix

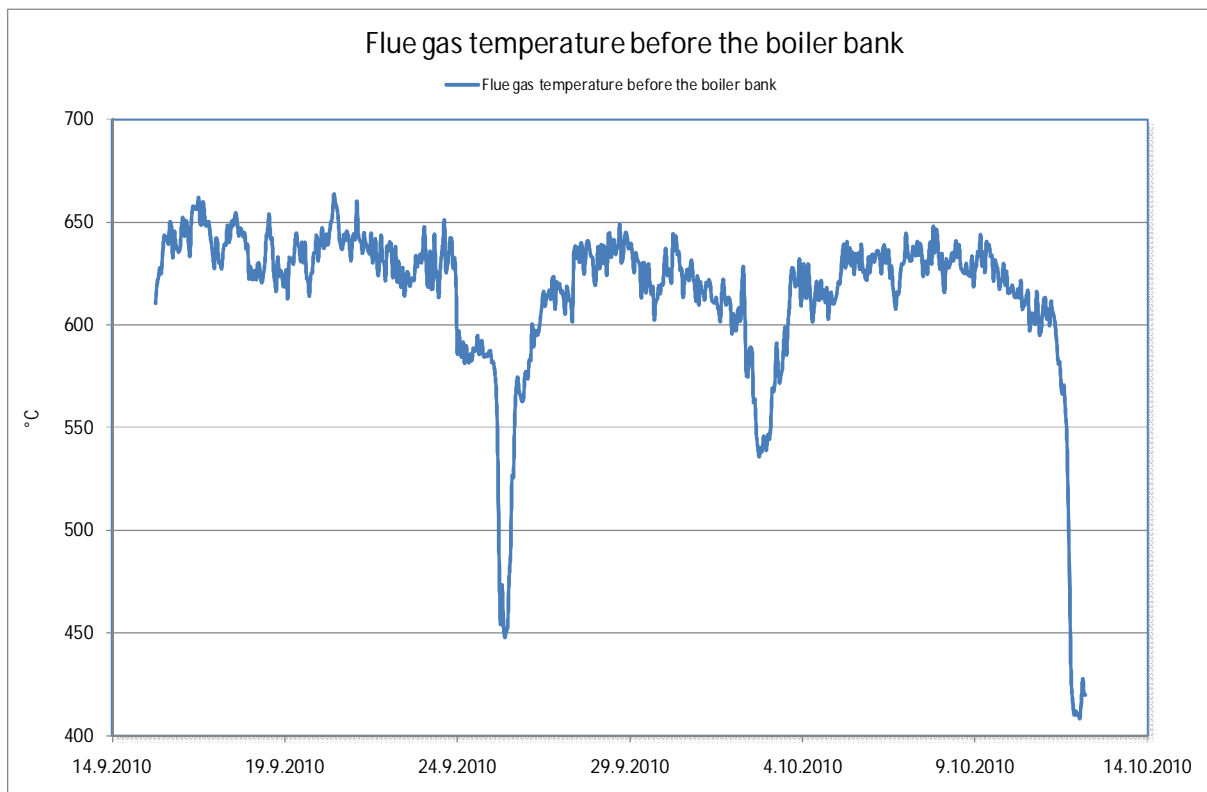


Figure 5. Flue gas temperature before the boiler bank during the measurement period.

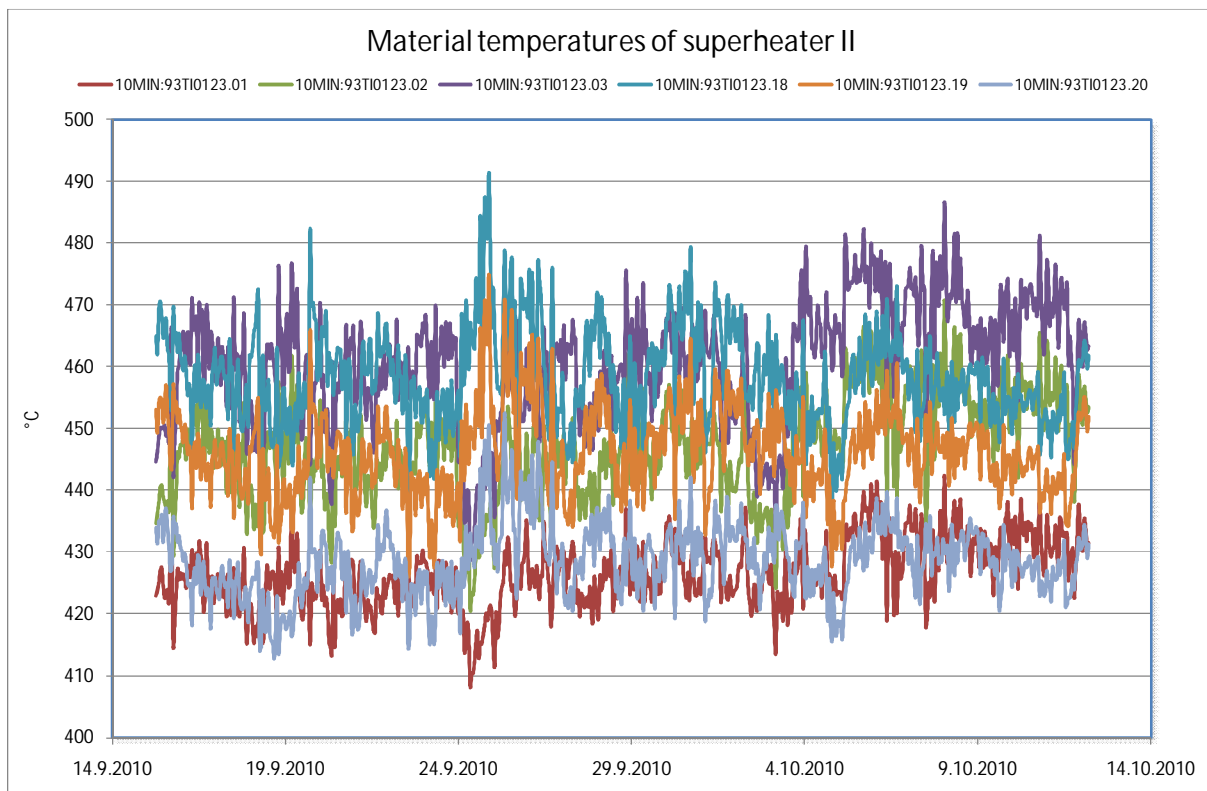


Figure 6. Material temperatures of superheater II during the measurement period.

Appendix

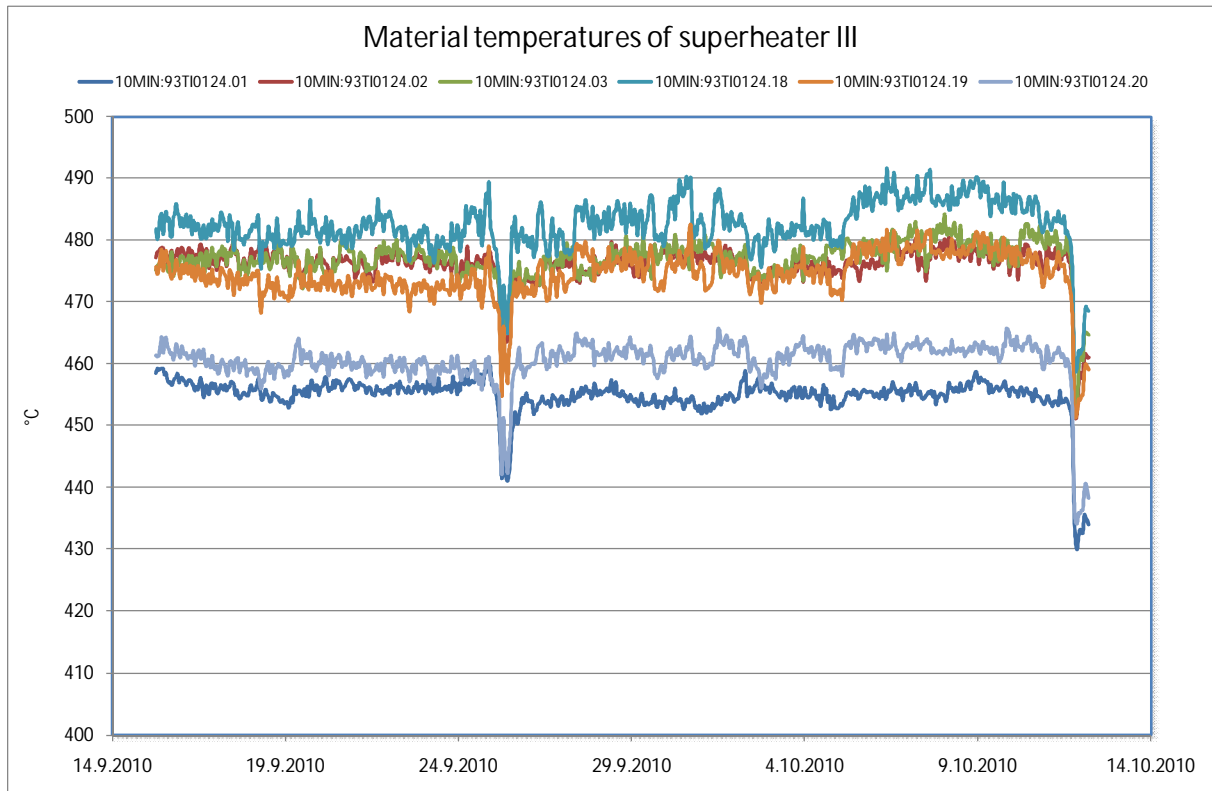


Figure 7. Material temperatures of superheater III during the measurement period.

Appendix

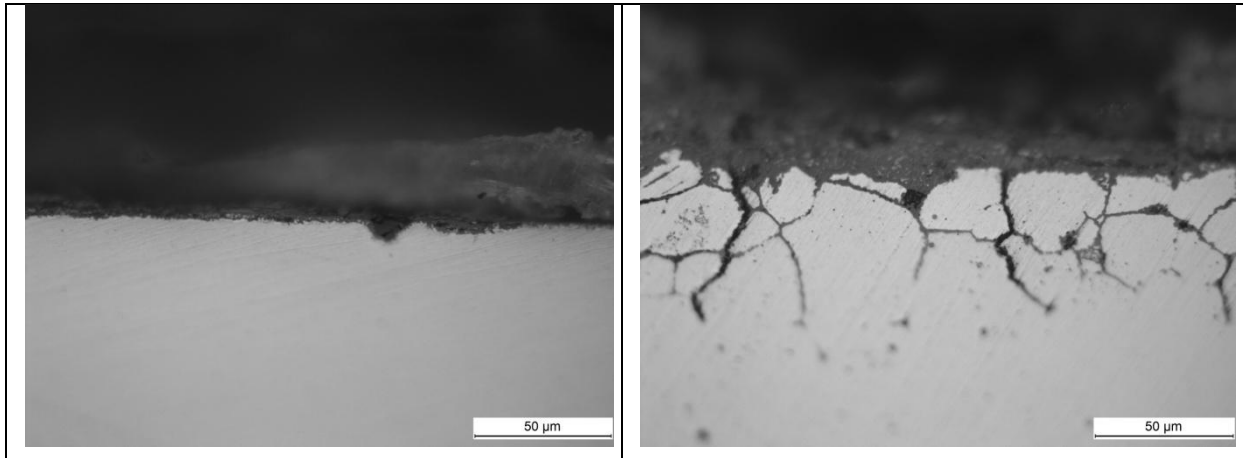


Figure 8. Cross sectional views of the material 347H exposed in the Probe 1: Windward position, left picture; Leeward position, right picture. Un-etched specimen.

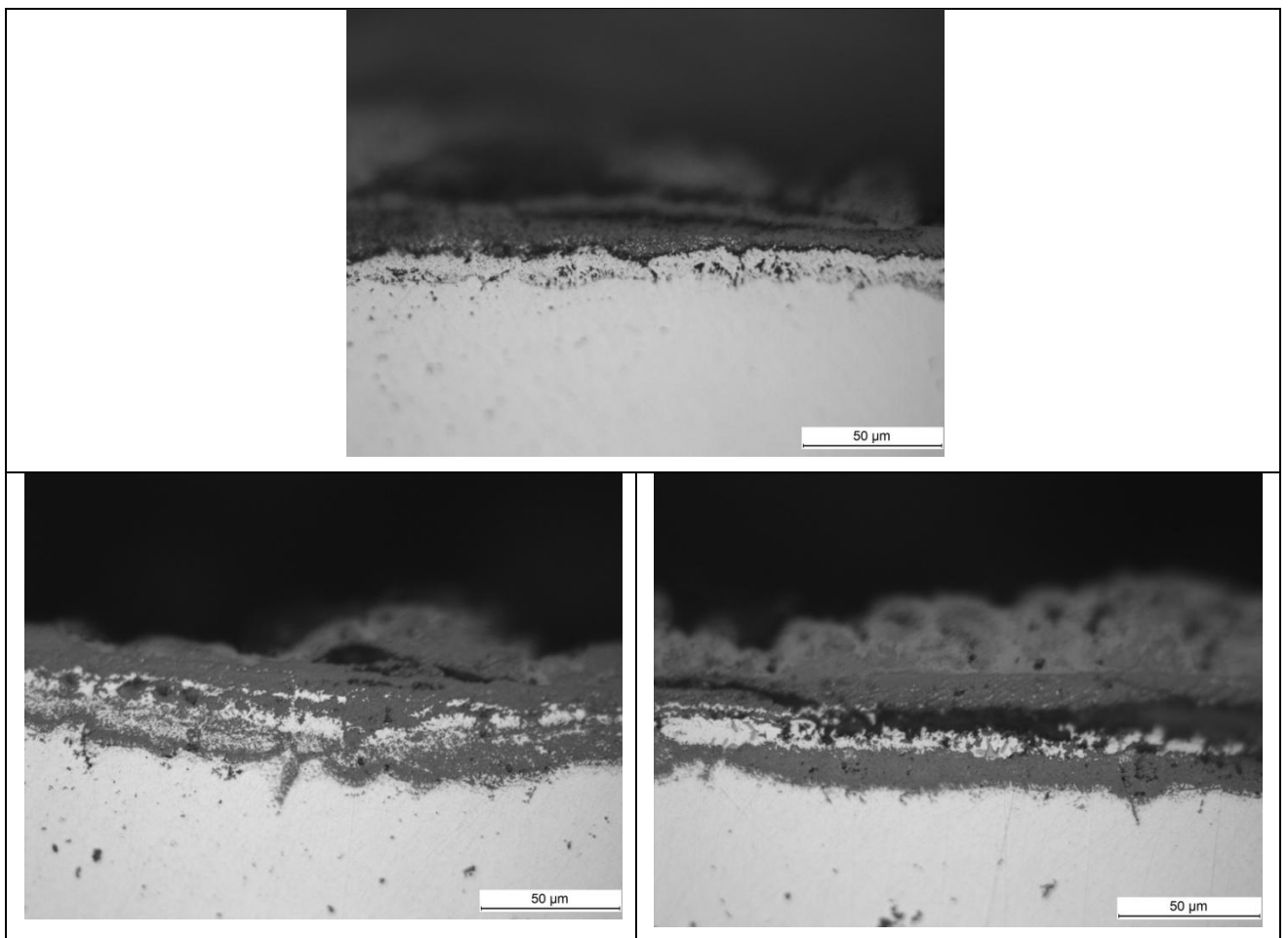


Figure 9. Cross sectional views of the material SAN 28 exposed in the Probe 1: Windward position, top picture; Leeward position, two bottom pictures. Un-etched specimen.

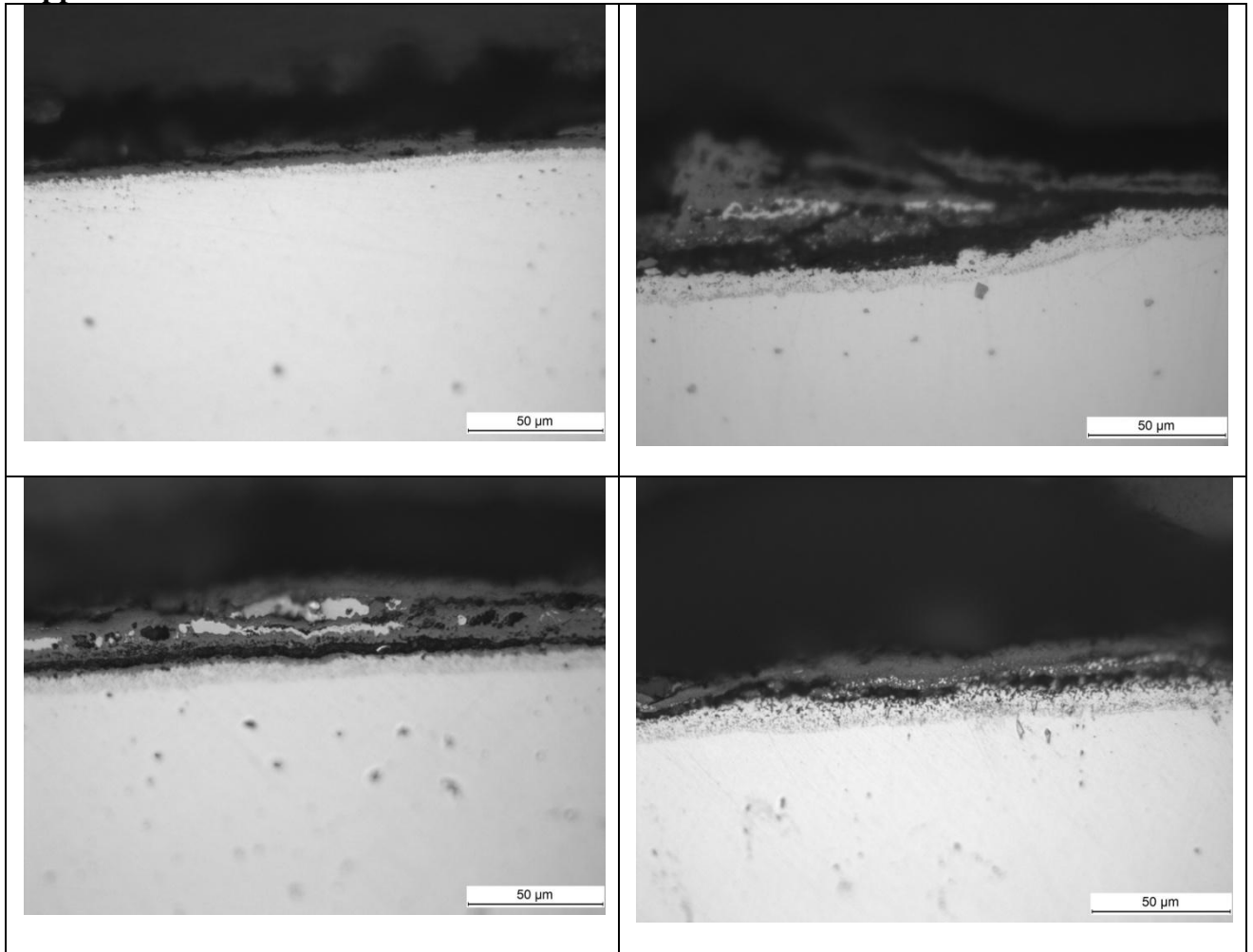
Appendix


Figure 10. Cross sectional views of the material Super 625 exposed in the Probe 1. Top row: Windward position, left picture; Leeward position, right picture. Bottom row: 30 degrees Up from Windward position, left picture; 30 degrees Down from Windward position, right picture. Un-etched specimen.

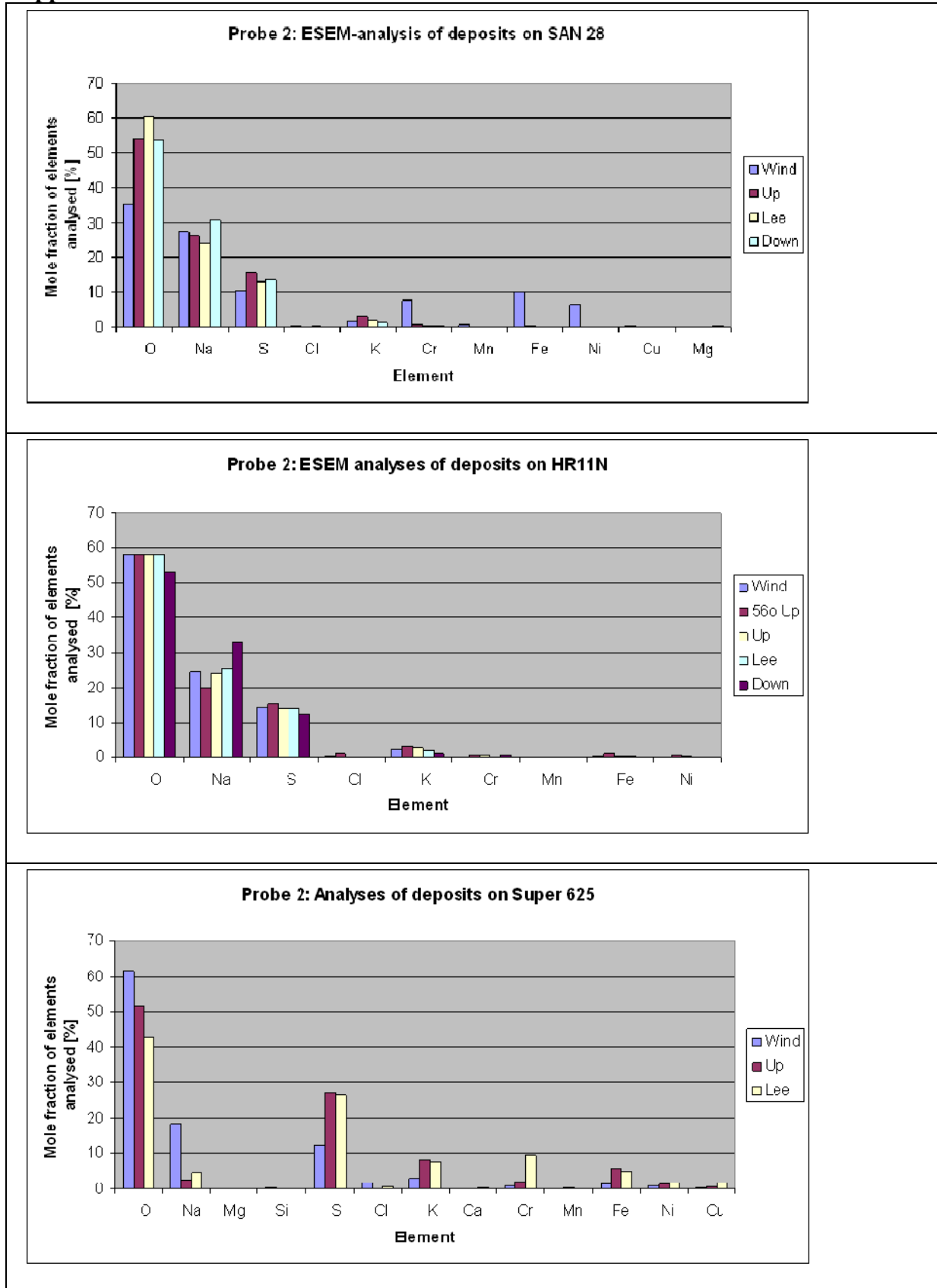
Appendix


Figure 11. Representative deposit analyses for the material samples SAN 28, HR11N and Super 625 exposed in Probe 2.

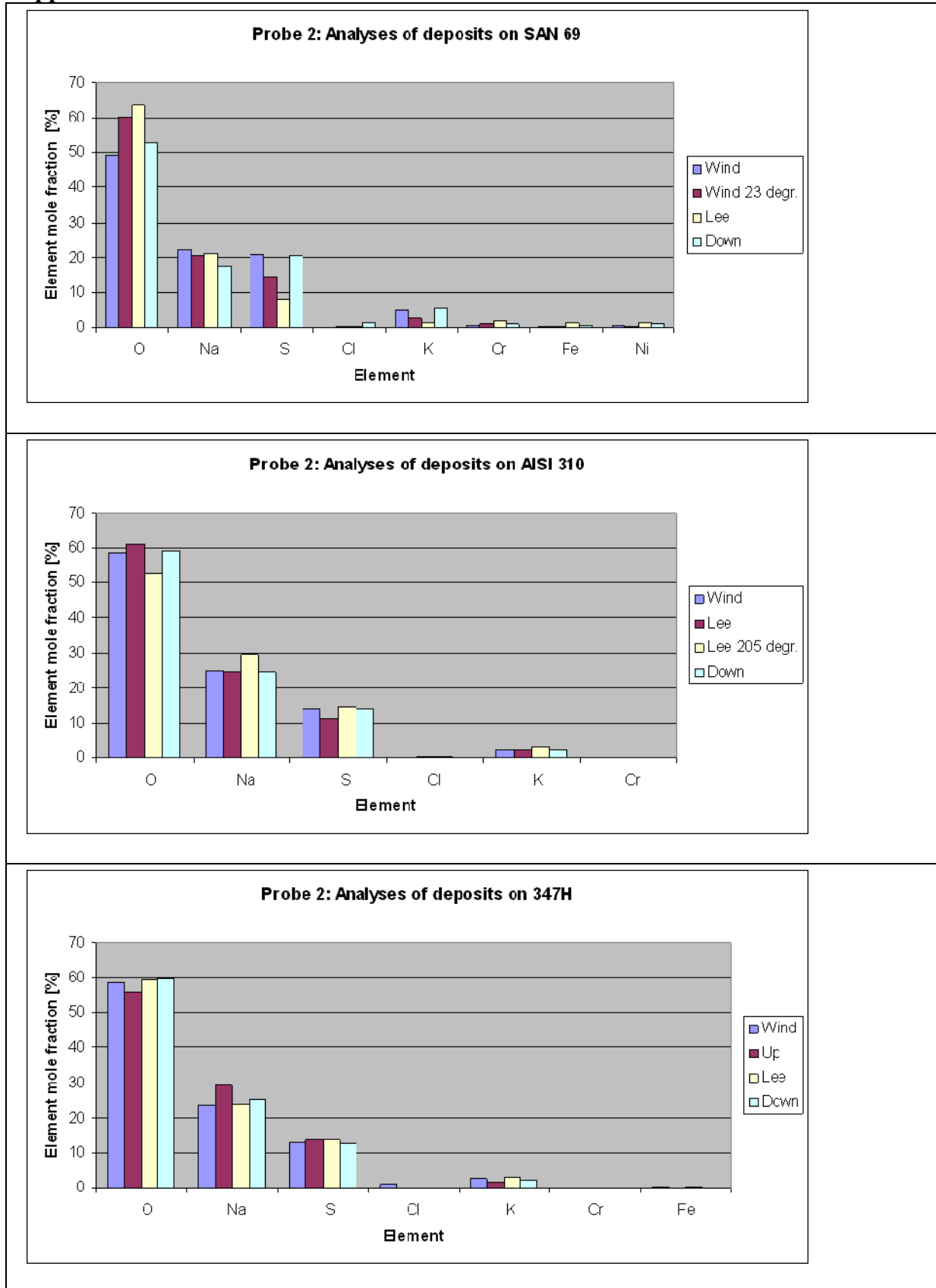
Appendix


Figure 12. Representative deposit analyses for the material samples SAN 69, AISI 310 and 347H exposed in Probe 2.

Appendix

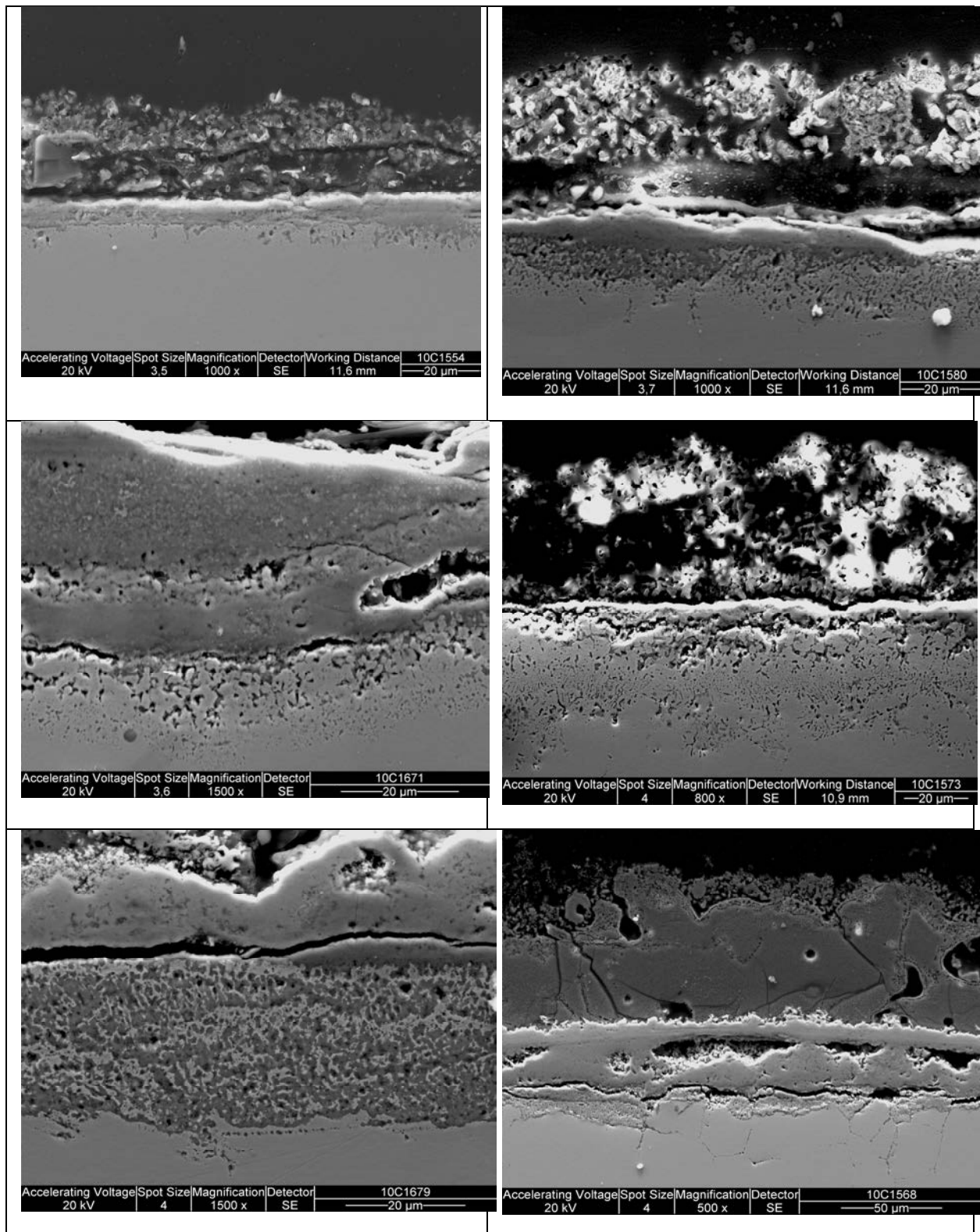


Figure 13. Cross-sectional view showing the total thickness of internally attacked zones and oxide scales observed on the Windward side for each material sample exposed in Probe 2. Left column from top to bottom: SAN 28, Super 625, AISI 310. Right column from top to bottom: HR11N, SAN 69, 347H. Note different magnifications. Material surface temperature in average 562°C. Estimated metal losses range from 0.1 mm (357H) to 0.01 mm (SAN 28).

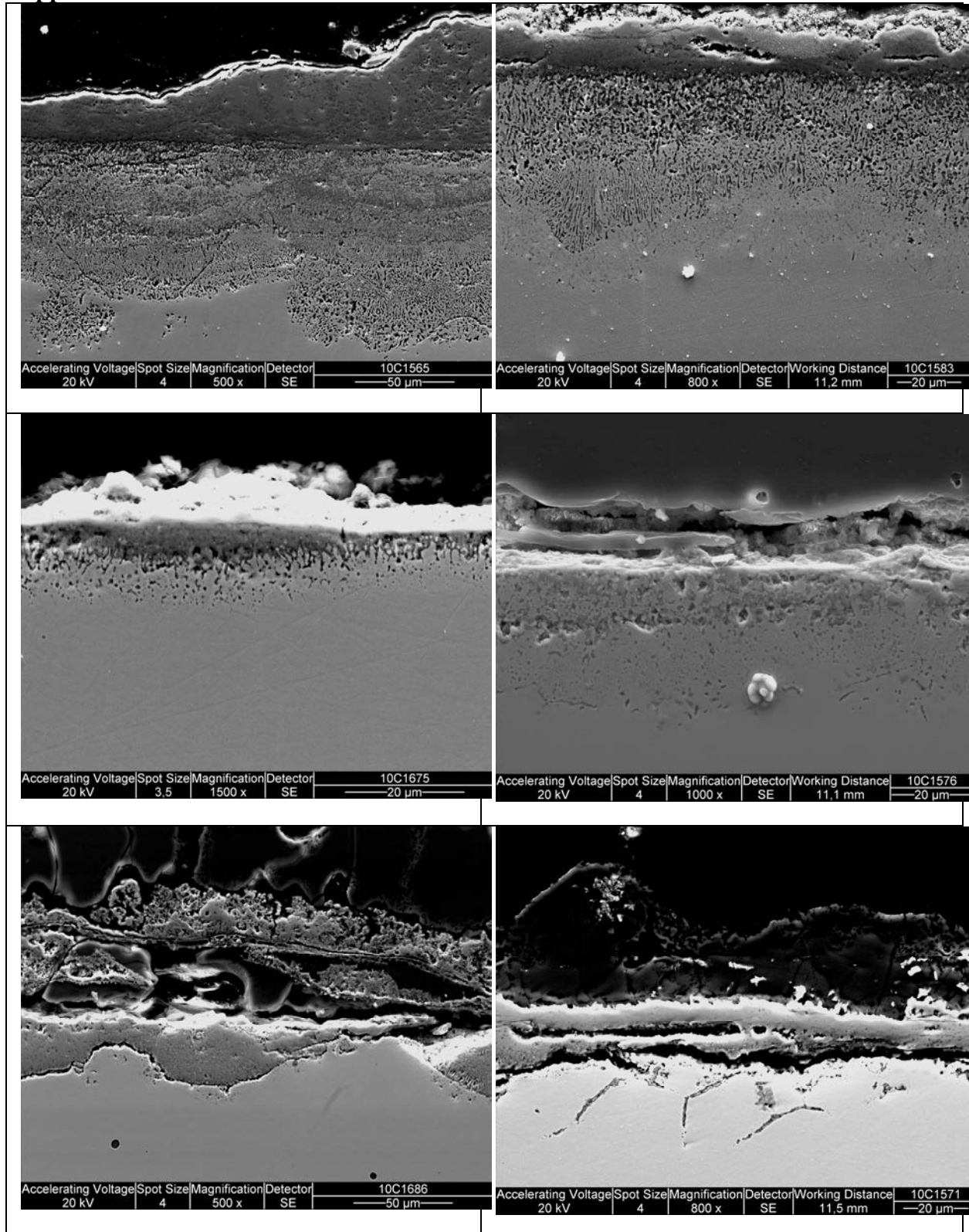
Appendix


Figure 14. Cross-sectional view showing the total thickness of internally attacked zones and oxide scales observed on the Leeward side for each material sample exposed in Probe 2. Left column from top to bottom: SAN 28, Super 625, AISI 310. Right column from top to bottom: HR11N, SAN 69, 347H. Note different magnifications. Material surface temperature in average 542°C. Estimated metal losses range from 0.11 mm (SAN 28) to 0.015 mm (Super 625).

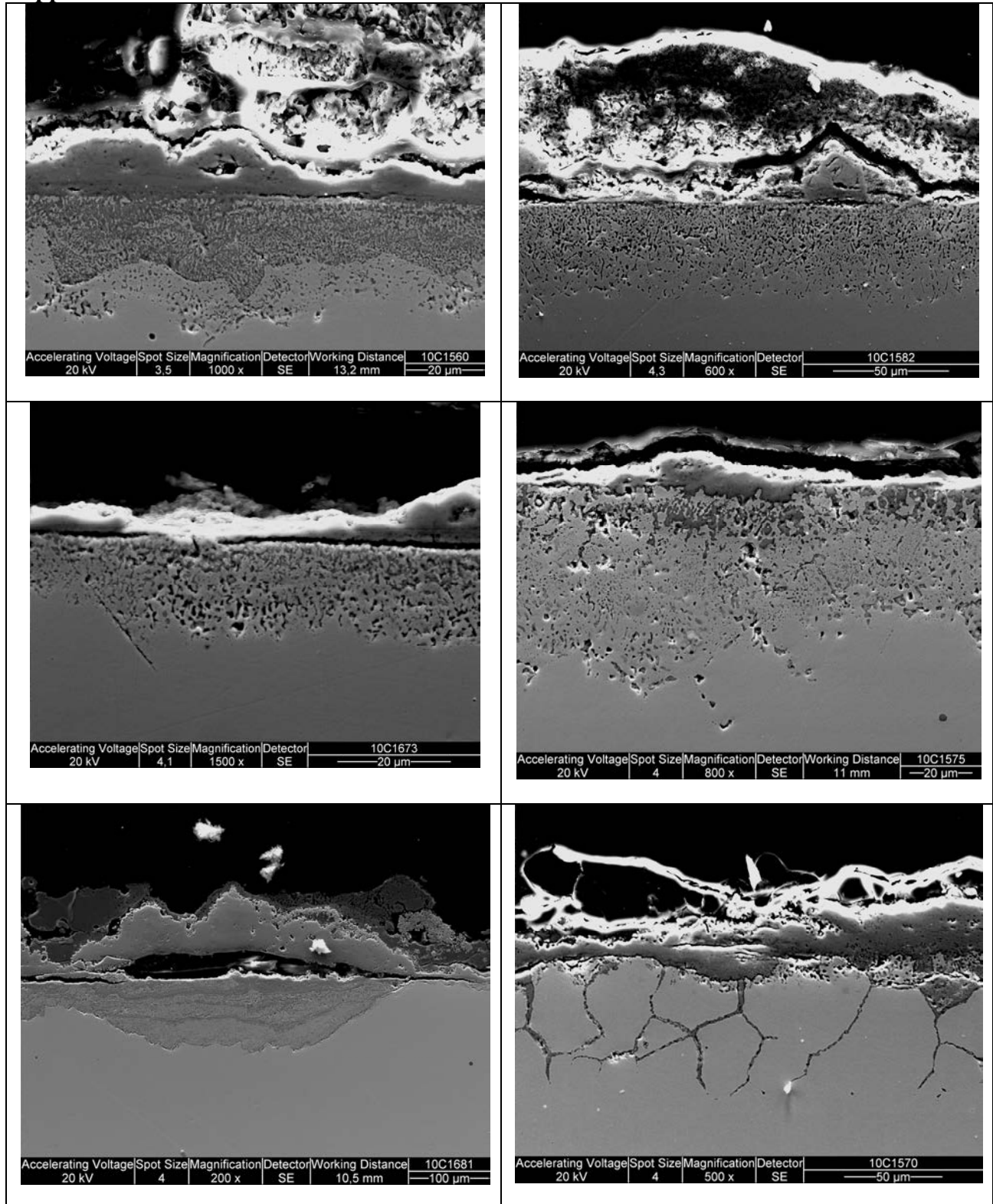
Appendix


Figure 15. Cross-sectional view showing the total thickness of internally attacked zones and oxide scales observed on the Up side for each material sample exposed in Probe 2. Left column from top to bottom: SAN 28, Super 625, AISI 310. Right column from top to bottom: HR11N, SAN 69, 347H. Note different magnifications. Material surface temperature in average 518°C. Estimated metal losses range from 0.09 mm (AISI 310) to 0.025 mm (Super 625).

Appendix

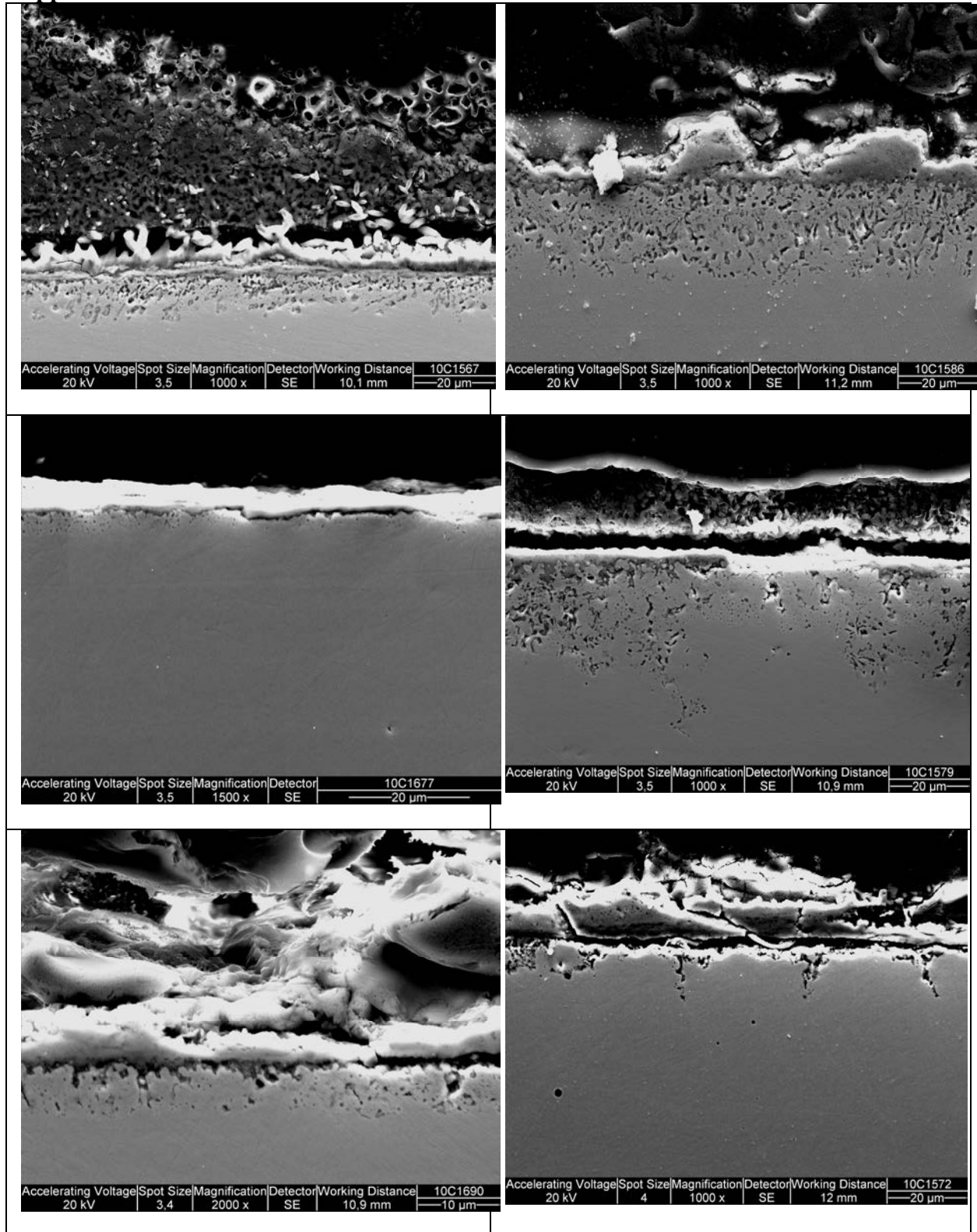


Figure 16. Cross-sectional view showing the total thickness of internally attacked zones and oxide scales observed on the Down side for each material sample exposed in Probe 2. Left column from top to bottom: SAN 28, Super 625, AISI 310. Right column from top to bottom: HR11N, SAN 69, 347H. Note different magnifications. Material surface temperature in average 508°C. Estimated metal losses range from 0.040 mm (SAN 69) to 0.005 mm (Super 625 and AISI 310).

Appendix

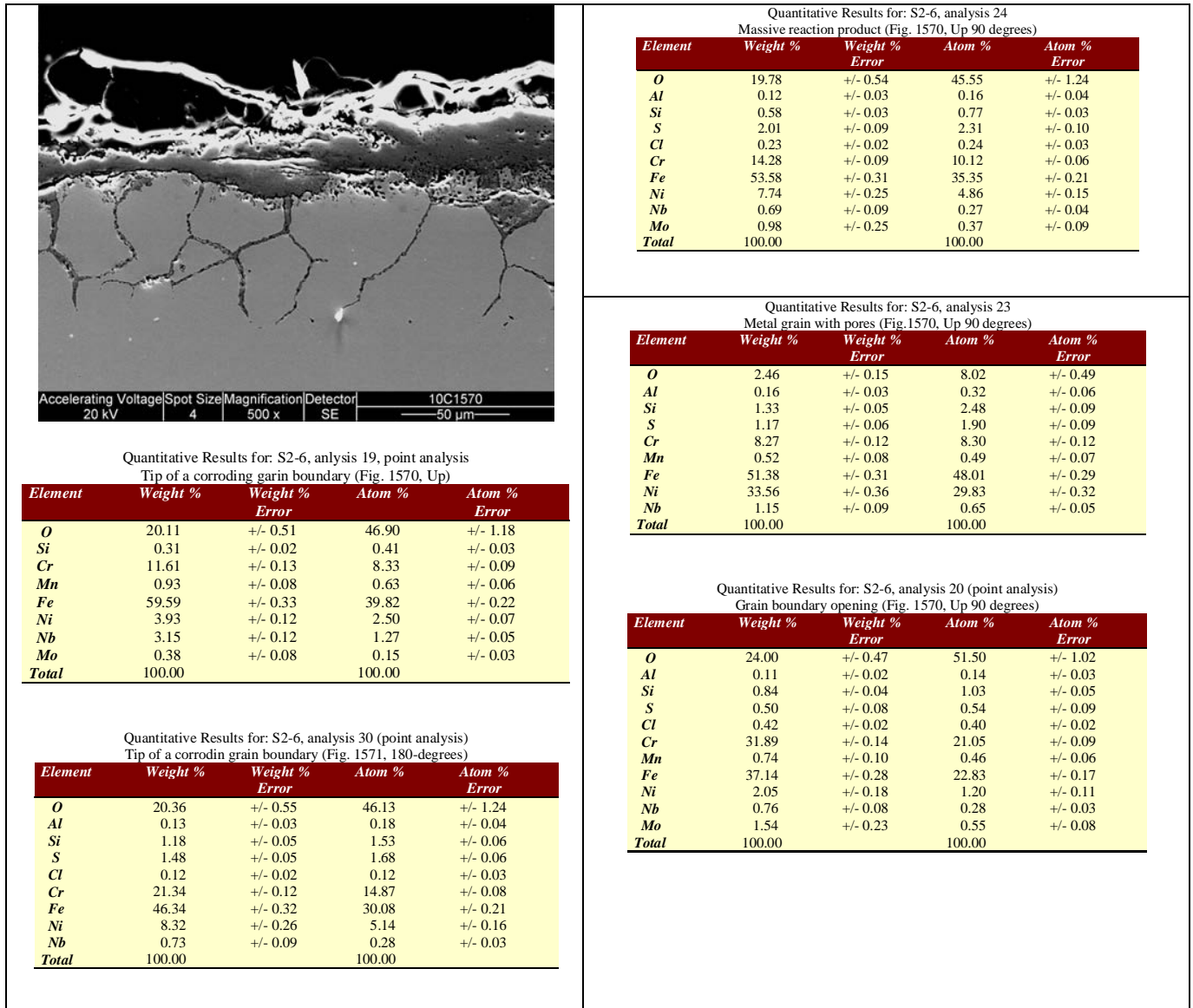


Figure 19. Cross sectional view featuring morphologies and compositional characteristics of grain boundary attack, de-alloying of superficial metal grains, and enhanced oxide growth typical of the exposed sample of material 347H. Note that the conventional detection limit for Cl is 0.1 wt-%. SEM-picture.

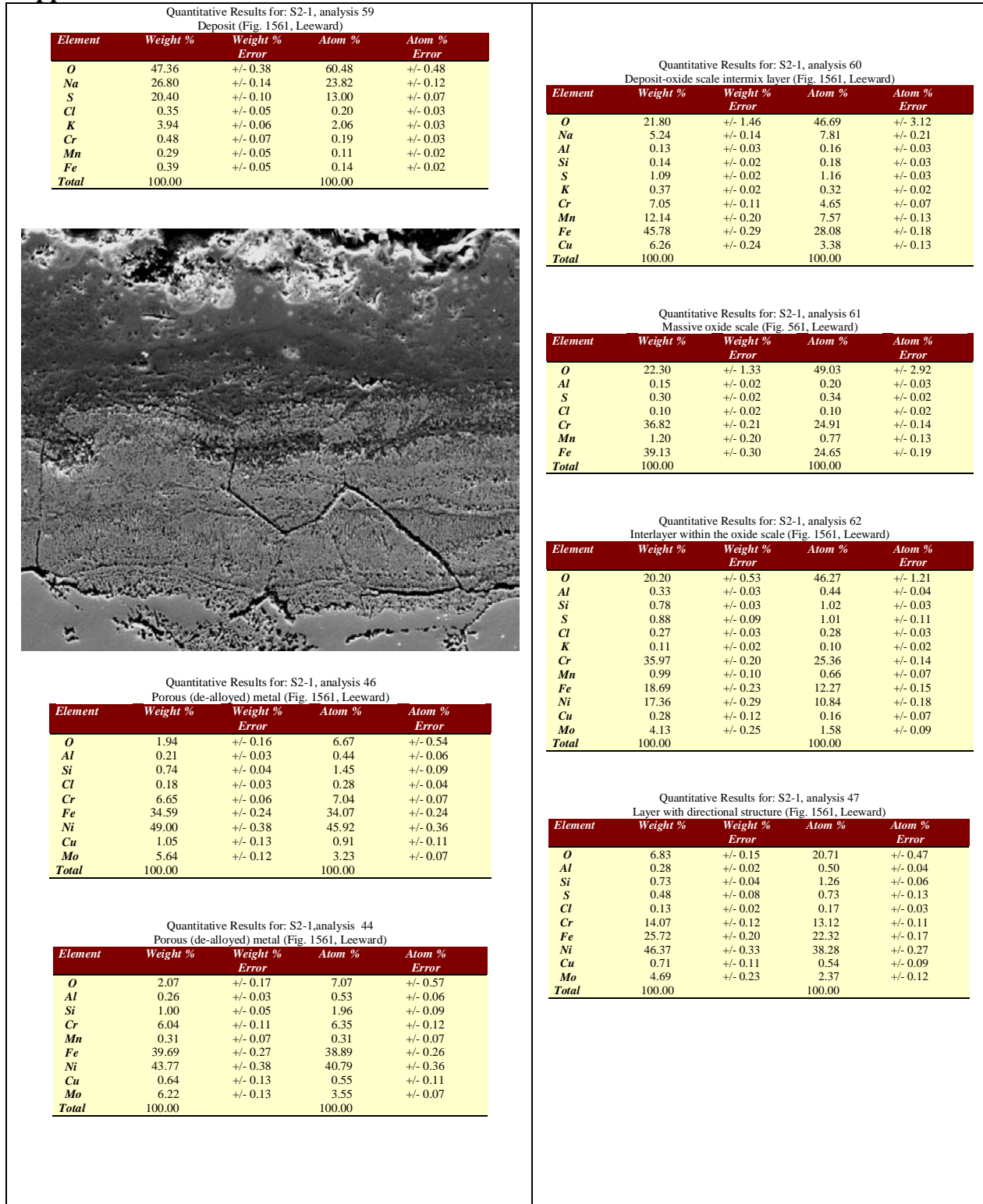
Appendix


Figure 20. Cross sectional view featuring morphologies and compositional characteristics of locally enhanced corrosion of SAN 28. Outer scale of mixed iron-chromium oxide type, and various oxygen, sulphur and chlorine penetrated de-alloyed zones in the ale metal are typical also of locally enhanced corrosion of HR11N, AISI 310, SAN 69 and Super 625. Corrosion performance at high temperatures is severely reduced due to depletion of chromium.

Appendix

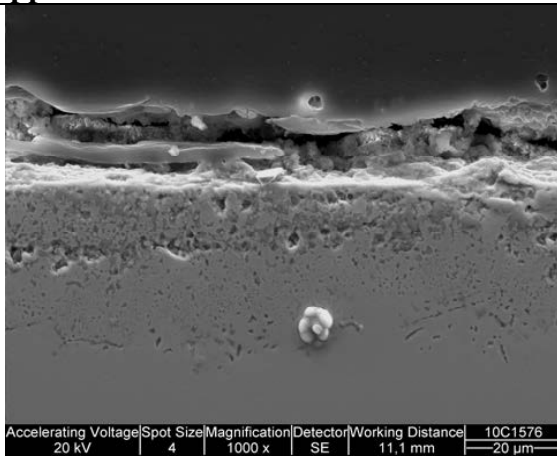
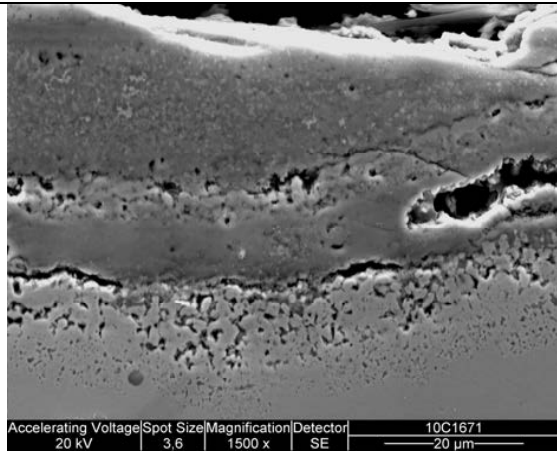
 <p>Quantitative Results for: S2-4, point analysis 22 Metal chloride rich protrusion (Fig. 1576, Leeward)</p> <table border="1"> <thead> <tr> <th>Element</th> <th>Weight %</th> <th>Weight % Error</th> <th>Atom %</th> <th>Atom % Error</th> </tr> </thead> <tbody> <tr><td>O</td><td>28.49</td><td>+/- 0.79</td><td>53.79</td><td>+/- 1.50</td></tr> <tr><td>Al</td><td>0.26</td><td>+/- 0.03</td><td>0.29</td><td>+/- 0.03</td></tr> <tr><td>Si</td><td>0.10</td><td>+/- 0.02</td><td>0.10</td><td>+/- 0.03</td></tr> <tr><td>Cl</td><td>19.97</td><td>+/- 0.12</td><td>17.02</td><td>+/- 0.10</td></tr> <tr><td>Cr</td><td>36.22</td><td>+/- 0.23</td><td>21.04</td><td>+/- 0.13</td></tr> <tr><td>Fe</td><td>2.12</td><td>+/- 0.16</td><td>1.14</td><td>+/- 0.09</td></tr> <tr><td>Ni</td><td>12.84</td><td>+/- 0.28</td><td>6.61</td><td>+/- 0.14</td></tr> <tr><td>Total</td><td>100.00</td><td></td><td>100.00</td><td></td></tr> </tbody> </table>	Element	Weight %	Weight % Error	Atom %	Atom % Error	O	28.49	+/- 0.79	53.79	+/- 1.50	Al	0.26	+/- 0.03	0.29	+/- 0.03	Si	0.10	+/- 0.02	0.10	+/- 0.03	Cl	19.97	+/- 0.12	17.02	+/- 0.10	Cr	36.22	+/- 0.23	21.04	+/- 0.13	Fe	2.12	+/- 0.16	1.14	+/- 0.09	Ni	12.84	+/- 0.28	6.61	+/- 0.14	Total	100.00		100.00		<p>Quantitative Results for: S2-4, analysis 3 Porous (de-alloyed) metal (Fig. 1573, Windward)</p> <table border="1"> <thead> <tr> <th>Element</th> <th>Weight %</th> <th>Weight % Error</th> <th>Atom %</th> <th>Atom % Error</th> </tr> </thead> <tbody> <tr><td>O</td><td>1.15</td><td>+/- 0.13</td><td>3.97</td><td>+/- 0.46</td></tr> <tr><td>Al</td><td>0.20</td><td>+/- 0.03</td><td>0.41</td><td>+/- 0.06</td></tr> <tr><td>Si</td><td>0.37</td><td>+/- 0.03</td><td>0.72</td><td>+/- 0.05</td></tr> <tr><td>Cl</td><td>0.12</td><td>+/- 0.02</td><td>0.18</td><td>+/- 0.03</td></tr> <tr><td>Cr</td><td>16.16</td><td>+/- 0.09</td><td>17.14</td><td>+/- 0.10</td></tr> <tr><td>Fe</td><td>11.21</td><td>+/- 0.16</td><td>11.07</td><td>+/- 0.16</td></tr> <tr><td>Ni</td><td>70.80</td><td>+/- 0.41</td><td>66.50</td><td>+/- 0.38</td></tr> <tr><td>Total</td><td>100.00</td><td></td><td>100.00</td><td></td></tr> </tbody> </table> <p>Quantitative Results for: S2-4, point analysis 13 Tip of corrosion penetration deep in the metal (Fig. 1575, Up)</p> <table border="1"> <thead> <tr> <th>Element</th> <th>Weight %</th> <th>Weight % Error</th> <th>Atom %</th> <th>Atom % Error</th> </tr> </thead> <tbody> <tr><td>O</td><td>3.03</td><td>+/- 0.14</td><td>9.84</td><td>+/- 0.47</td></tr> <tr><td>Al</td><td>0.23</td><td>+/- 0.03</td><td>0.44</td><td>+/- 0.06</td></tr> <tr><td>Si</td><td>1.23</td><td>+/- 0.05</td><td>2.27</td><td>+/- 0.09</td></tr> <tr><td>S</td><td>0.13</td><td>+/- 0.02</td><td>0.21</td><td>+/- 0.04</td></tr> <tr><td>Cl</td><td>0.51</td><td>+/- 0.03</td><td>0.75</td><td>+/- 0.04</td></tr> <tr><td>Cr</td><td>16.84</td><td>+/- 0.16</td><td>16.86</td><td>+/- 0.16</td></tr> <tr><td>Mn</td><td>0.26</td><td>+/- 0.08</td><td>0.24</td><td>+/- 0.08</td></tr> <tr><td>Fe</td><td>9.23</td><td>+/- 0.18</td><td>8.60</td><td>+/- 0.17</td></tr> <tr><td>Ni</td><td>68.56</td><td>+/- 0.45</td><td>60.78</td><td>+/- 0.40</td></tr> <tr><td>Total</td><td>100.00</td><td></td><td>100.00</td><td></td></tr> </tbody> </table>	Element	Weight %	Weight % Error	Atom %	Atom % Error	O	1.15	+/- 0.13	3.97	+/- 0.46	Al	0.20	+/- 0.03	0.41	+/- 0.06	Si	0.37	+/- 0.03	0.72	+/- 0.05	Cl	0.12	+/- 0.02	0.18	+/- 0.03	Cr	16.16	+/- 0.09	17.14	+/- 0.10	Fe	11.21	+/- 0.16	11.07	+/- 0.16	Ni	70.80	+/- 0.41	66.50	+/- 0.38	Total	100.00		100.00		Element	Weight %	Weight % Error	Atom %	Atom % Error	O	3.03	+/- 0.14	9.84	+/- 0.47	Al	0.23	+/- 0.03	0.44	+/- 0.06	Si	1.23	+/- 0.05	2.27	+/- 0.09	S	0.13	+/- 0.02	0.21	+/- 0.04	Cl	0.51	+/- 0.03	0.75	+/- 0.04	Cr	16.84	+/- 0.16	16.86	+/- 0.16	Mn	0.26	+/- 0.08	0.24	+/- 0.08	Fe	9.23	+/- 0.18	8.60	+/- 0.17	Ni	68.56	+/- 0.45	60.78	+/- 0.40	Total	100.00		100.00																																																																																						
Element	Weight %	Weight % Error	Atom %	Atom % Error																																																																																																																																																																																																																																			
O	28.49	+/- 0.79	53.79	+/- 1.50																																																																																																																																																																																																																																			
Al	0.26	+/- 0.03	0.29	+/- 0.03																																																																																																																																																																																																																																			
Si	0.10	+/- 0.02	0.10	+/- 0.03																																																																																																																																																																																																																																			
Cl	19.97	+/- 0.12	17.02	+/- 0.10																																																																																																																																																																																																																																			
Cr	36.22	+/- 0.23	21.04	+/- 0.13																																																																																																																																																																																																																																			
Fe	2.12	+/- 0.16	1.14	+/- 0.09																																																																																																																																																																																																																																			
Ni	12.84	+/- 0.28	6.61	+/- 0.14																																																																																																																																																																																																																																			
Total	100.00		100.00																																																																																																																																																																																																																																				
Element	Weight %	Weight % Error	Atom %	Atom % Error																																																																																																																																																																																																																																			
O	1.15	+/- 0.13	3.97	+/- 0.46																																																																																																																																																																																																																																			
Al	0.20	+/- 0.03	0.41	+/- 0.06																																																																																																																																																																																																																																			
Si	0.37	+/- 0.03	0.72	+/- 0.05																																																																																																																																																																																																																																			
Cl	0.12	+/- 0.02	0.18	+/- 0.03																																																																																																																																																																																																																																			
Cr	16.16	+/- 0.09	17.14	+/- 0.10																																																																																																																																																																																																																																			
Fe	11.21	+/- 0.16	11.07	+/- 0.16																																																																																																																																																																																																																																			
Ni	70.80	+/- 0.41	66.50	+/- 0.38																																																																																																																																																																																																																																			
Total	100.00		100.00																																																																																																																																																																																																																																				
Element	Weight %	Weight % Error	Atom %	Atom % Error																																																																																																																																																																																																																																			
O	3.03	+/- 0.14	9.84	+/- 0.47																																																																																																																																																																																																																																			
Al	0.23	+/- 0.03	0.44	+/- 0.06																																																																																																																																																																																																																																			
Si	1.23	+/- 0.05	2.27	+/- 0.09																																																																																																																																																																																																																																			
S	0.13	+/- 0.02	0.21	+/- 0.04																																																																																																																																																																																																																																			
Cl	0.51	+/- 0.03	0.75	+/- 0.04																																																																																																																																																																																																																																			
Cr	16.84	+/- 0.16	16.86	+/- 0.16																																																																																																																																																																																																																																			
Mn	0.26	+/- 0.08	0.24	+/- 0.08																																																																																																																																																																																																																																			
Fe	9.23	+/- 0.18	8.60	+/- 0.17																																																																																																																																																																																																																																			
Ni	68.56	+/- 0.45	60.78	+/- 0.40																																																																																																																																																																																																																																			
Total	100.00		100.00																																																																																																																																																																																																																																				
 <p>Quantitative Results for: S2-3, analysis 1 Analysis of base metal Super 625 (Fig. 1668, Windward)</p> <table border="1"> <thead> <tr> <th>Element</th> <th>Weight %</th> <th>Weight % Error</th> <th>Atom %</th> <th>Atom % Error</th> </tr> </thead> <tbody> <tr><td>Al</td><td>0.29</td><td>+/- 0.03</td><td>0.63</td><td>+/- 0.06</td></tr> <tr><td>Si</td><td>0.37</td><td>+/- 0.04</td><td>0.77</td><td>+/- 0.08</td></tr> <tr><td>Ti</td><td>0.21</td><td>+/- 0.03</td><td>0.25</td><td>+/- 0.04</td></tr> <tr><td>Cr</td><td>22.18</td><td>+/- 0.15</td><td>24.66</td><td>+/- 0.16</td></tr> <tr><td>Fe</td><td>16.82</td><td>+/- 0.19</td><td>17.42</td><td>+/- 0.19</td></tr> <tr><td>Ni</td><td>52.48</td><td>+/- 0.36</td><td>51.68</td><td>+/- 0.35</td></tr> <tr><td>Mo</td><td>7.64</td><td>+/- 0.13</td><td>4.61</td><td>+/- 0.08</td></tr> <tr><td>Total</td><td>100.00</td><td></td><td>100.00</td><td></td></tr> </tbody> </table>	Element	Weight %	Weight % Error	Atom %	Atom % Error	Al	0.29	+/- 0.03	0.63	+/- 0.06	Si	0.37	+/- 0.04	0.77	+/- 0.08	Ti	0.21	+/- 0.03	0.25	+/- 0.04	Cr	22.18	+/- 0.15	24.66	+/- 0.16	Fe	16.82	+/- 0.19	17.42	+/- 0.19	Ni	52.48	+/- 0.36	51.68	+/- 0.35	Mo	7.64	+/- 0.13	4.61	+/- 0.08	Total	100.00		100.00		<p>Quantitative Results for: S2-3, analysis 18 Oxide scale, outer layer (Fig. 1671, 45 degrees)</p> <table border="1"> <thead> <tr> <th>Element</th> <th>Weight %</th> <th>Weight % Error</th> <th>Atom %</th> <th>Atom % Error</th> </tr> </thead> <tbody> <tr><td>O</td><td>20.19</td><td>+/- 0.63</td><td>46.06</td><td>+/- 1.43</td></tr> <tr><td>Al</td><td>0.27</td><td>+/- 0.03</td><td>0.36</td><td>+/- 0.04</td></tr> <tr><td>Si</td><td>0.28</td><td>+/- 0.03</td><td>0.37</td><td>+/- 0.03</td></tr> <tr><td>S</td><td>4.07</td><td>+/- 0.20</td><td>4.64</td><td>+/- 0.22</td></tr> <tr><td>Cl</td><td>0.25</td><td>+/- 0.03</td><td>0.26</td><td>+/- 0.03</td></tr> <tr><td>K</td><td>0.20</td><td>+/- 0.02</td><td>0.19</td><td>+/- 0.02</td></tr> <tr><td>Ti</td><td>0.27</td><td>+/- 0.03</td><td>0.20</td><td>+/- 0.02</td></tr> <tr><td>Cr</td><td>34.80</td><td>+/- 0.20</td><td>24.43</td><td>+/- 0.14</td></tr> <tr><td>Fe</td><td>11.88</td><td>+/- 0.21</td><td>7.76</td><td>+/- 0.14</td></tr> <tr><td>Ni</td><td>21.40</td><td>+/- 0.31</td><td>13.30</td><td>+/- 0.19</td></tr> <tr><td>Mo</td><td>6.39</td><td>+/- 0.41</td><td>2.43</td><td>+/- 0.15</td></tr> <tr><td>Total</td><td>100.00</td><td></td><td>100.00</td><td></td></tr> </tbody> </table> <p>Quantitative Results for: S2-3, analysis 16 Oxide scale, inner layer (Fig. 1671, 45 degrees)</p> <table border="1"> <thead> <tr> <th>Element</th> <th>Weight %</th> <th>Weight % Error</th> <th>Atom %</th> <th>Atom % Error</th> </tr> </thead> <tbody> <tr><td>O</td><td>25.27</td><td>+/- 0.58</td><td>53.76</td><td>+/- 1.23</td></tr> <tr><td>Al</td><td>0.16</td><td>+/- 0.03</td><td>0.20</td><td>+/- 0.04</td></tr> <tr><td>Si</td><td>0.35</td><td>+/- 0.03</td><td>0.43</td><td>+/- 0.03</td></tr> <tr><td>S</td><td>0.53</td><td>+/- 0.05</td><td>0.56</td><td>+/- 0.05</td></tr> <tr><td>Cl</td><td>0.12</td><td>+/- 0.03</td><td>0.12</td><td>+/- 0.02</td></tr> <tr><td>K</td><td>0.16</td><td>+/- 0.02</td><td>0.14</td><td>+/- 0.02</td></tr> <tr><td>Ti</td><td>0.20</td><td>+/- 0.03</td><td>0.14</td><td>+/- 0.02</td></tr> <tr><td>Cr</td><td>11.79</td><td>+/- 0.14</td><td>7.72</td><td>+/- 0.09</td></tr> <tr><td>Mn</td><td>0.60</td><td>+/- 0.09</td><td>0.37</td><td>+/- 0.05</td></tr> <tr><td>Fe</td><td>47.02</td><td>+/- 0.33</td><td>28.66</td><td>+/- 0.20</td></tr> <tr><td>Ni</td><td>13.33</td><td>+/- 0.30</td><td>7.73</td><td>+/- 0.18</td></tr> <tr><td>Nb</td><td>0.48</td><td>+/- 0.08</td><td>0.17</td><td>+/- 0.03</td></tr> <tr><td>Total</td><td>100.00</td><td></td><td>100.00</td><td></td></tr> </tbody> </table> <p>Quantitative Results for: S2-3, analysis 12 Porous metal, inner layer (Fig. 1671, 45 degrees)</p> <table border="1"> <thead> <tr> <th>Element</th> <th>Weight %</th> <th>Weight % Error</th> <th>Atom %</th> <th>Atom % Error</th> </tr> </thead> <tbody> <tr><td>O</td><td>0.46</td><td>+/- 0.18</td><td>1.64</td><td>+/- 0.63</td></tr> <tr><td>Al</td><td>0.28</td><td>+/- 0.03</td><td>0.59</td><td>+/- 0.07</td></tr> <tr><td>Si</td><td>0.26</td><td>+/- 0.03</td><td>0.53</td><td>+/- 0.06</td></tr> <tr><td>S</td><td>2.96</td><td>+/- 0.21</td><td>5.24</td><td>+/- 0.37</td></tr> <tr><td>Cr</td><td>8.53</td><td>+/- 0.08</td><td>9.30</td><td>+/- 0.09</td></tr> <tr><td>Fe</td><td>13.03</td><td>+/- 0.20</td><td>13.22</td><td>+/- 0.20</td></tr> <tr><td>Ni</td><td>68.07</td><td>+/- 0.47</td><td>65.70</td><td>+/- 0.45</td></tr> <tr><td>Mo</td><td>6.39</td><td>+/- 0.44</td><td>3.78</td><td>+/- 0.26</td></tr> <tr><td>Total</td><td>100.00</td><td></td><td>100.00</td><td></td></tr> </tbody> </table>	Element	Weight %	Weight % Error	Atom %	Atom % Error	O	20.19	+/- 0.63	46.06	+/- 1.43	Al	0.27	+/- 0.03	0.36	+/- 0.04	Si	0.28	+/- 0.03	0.37	+/- 0.03	S	4.07	+/- 0.20	4.64	+/- 0.22	Cl	0.25	+/- 0.03	0.26	+/- 0.03	K	0.20	+/- 0.02	0.19	+/- 0.02	Ti	0.27	+/- 0.03	0.20	+/- 0.02	Cr	34.80	+/- 0.20	24.43	+/- 0.14	Fe	11.88	+/- 0.21	7.76	+/- 0.14	Ni	21.40	+/- 0.31	13.30	+/- 0.19	Mo	6.39	+/- 0.41	2.43	+/- 0.15	Total	100.00		100.00		Element	Weight %	Weight % Error	Atom %	Atom % Error	O	25.27	+/- 0.58	53.76	+/- 1.23	Al	0.16	+/- 0.03	0.20	+/- 0.04	Si	0.35	+/- 0.03	0.43	+/- 0.03	S	0.53	+/- 0.05	0.56	+/- 0.05	Cl	0.12	+/- 0.03	0.12	+/- 0.02	K	0.16	+/- 0.02	0.14	+/- 0.02	Ti	0.20	+/- 0.03	0.14	+/- 0.02	Cr	11.79	+/- 0.14	7.72	+/- 0.09	Mn	0.60	+/- 0.09	0.37	+/- 0.05	Fe	47.02	+/- 0.33	28.66	+/- 0.20	Ni	13.33	+/- 0.30	7.73	+/- 0.18	Nb	0.48	+/- 0.08	0.17	+/- 0.03	Total	100.00		100.00		Element	Weight %	Weight % Error	Atom %	Atom % Error	O	0.46	+/- 0.18	1.64	+/- 0.63	Al	0.28	+/- 0.03	0.59	+/- 0.07	Si	0.26	+/- 0.03	0.53	+/- 0.06	S	2.96	+/- 0.21	5.24	+/- 0.37	Cr	8.53	+/- 0.08	9.30	+/- 0.09	Fe	13.03	+/- 0.20	13.22	+/- 0.20	Ni	68.07	+/- 0.47	65.70	+/- 0.45	Mo	6.39	+/- 0.44	3.78	+/- 0.26	Total	100.00		100.00	
Element	Weight %	Weight % Error	Atom %	Atom % Error																																																																																																																																																																																																																																			
Al	0.29	+/- 0.03	0.63	+/- 0.06																																																																																																																																																																																																																																			
Si	0.37	+/- 0.04	0.77	+/- 0.08																																																																																																																																																																																																																																			
Ti	0.21	+/- 0.03	0.25	+/- 0.04																																																																																																																																																																																																																																			
Cr	22.18	+/- 0.15	24.66	+/- 0.16																																																																																																																																																																																																																																			
Fe	16.82	+/- 0.19	17.42	+/- 0.19																																																																																																																																																																																																																																			
Ni	52.48	+/- 0.36	51.68	+/- 0.35																																																																																																																																																																																																																																			
Mo	7.64	+/- 0.13	4.61	+/- 0.08																																																																																																																																																																																																																																			
Total	100.00		100.00																																																																																																																																																																																																																																				
Element	Weight %	Weight % Error	Atom %	Atom % Error																																																																																																																																																																																																																																			
O	20.19	+/- 0.63	46.06	+/- 1.43																																																																																																																																																																																																																																			
Al	0.27	+/- 0.03	0.36	+/- 0.04																																																																																																																																																																																																																																			
Si	0.28	+/- 0.03	0.37	+/- 0.03																																																																																																																																																																																																																																			
S	4.07	+/- 0.20	4.64	+/- 0.22																																																																																																																																																																																																																																			
Cl	0.25	+/- 0.03	0.26	+/- 0.03																																																																																																																																																																																																																																			
K	0.20	+/- 0.02	0.19	+/- 0.02																																																																																																																																																																																																																																			
Ti	0.27	+/- 0.03	0.20	+/- 0.02																																																																																																																																																																																																																																			
Cr	34.80	+/- 0.20	24.43	+/- 0.14																																																																																																																																																																																																																																			
Fe	11.88	+/- 0.21	7.76	+/- 0.14																																																																																																																																																																																																																																			
Ni	21.40	+/- 0.31	13.30	+/- 0.19																																																																																																																																																																																																																																			
Mo	6.39	+/- 0.41	2.43	+/- 0.15																																																																																																																																																																																																																																			
Total	100.00		100.00																																																																																																																																																																																																																																				
Element	Weight %	Weight % Error	Atom %	Atom % Error																																																																																																																																																																																																																																			
O	25.27	+/- 0.58	53.76	+/- 1.23																																																																																																																																																																																																																																			
Al	0.16	+/- 0.03	0.20	+/- 0.04																																																																																																																																																																																																																																			
Si	0.35	+/- 0.03	0.43	+/- 0.03																																																																																																																																																																																																																																			
S	0.53	+/- 0.05	0.56	+/- 0.05																																																																																																																																																																																																																																			
Cl	0.12	+/- 0.03	0.12	+/- 0.02																																																																																																																																																																																																																																			
K	0.16	+/- 0.02	0.14	+/- 0.02																																																																																																																																																																																																																																			
Ti	0.20	+/- 0.03	0.14	+/- 0.02																																																																																																																																																																																																																																			
Cr	11.79	+/- 0.14	7.72	+/- 0.09																																																																																																																																																																																																																																			
Mn	0.60	+/- 0.09	0.37	+/- 0.05																																																																																																																																																																																																																																			
Fe	47.02	+/- 0.33	28.66	+/- 0.20																																																																																																																																																																																																																																			
Ni	13.33	+/- 0.30	7.73	+/- 0.18																																																																																																																																																																																																																																			
Nb	0.48	+/- 0.08	0.17	+/- 0.03																																																																																																																																																																																																																																			
Total	100.00		100.00																																																																																																																																																																																																																																				
Element	Weight %	Weight % Error	Atom %	Atom % Error																																																																																																																																																																																																																																			
O	0.46	+/- 0.18	1.64	+/- 0.63																																																																																																																																																																																																																																			
Al	0.28	+/- 0.03	0.59	+/- 0.07																																																																																																																																																																																																																																			
Si	0.26	+/- 0.03	0.53	+/- 0.06																																																																																																																																																																																																																																			
S	2.96	+/- 0.21	5.24	+/- 0.37																																																																																																																																																																																																																																			
Cr	8.53	+/- 0.08	9.30	+/- 0.09																																																																																																																																																																																																																																			
Fe	13.03	+/- 0.20	13.22	+/- 0.20																																																																																																																																																																																																																																			
Ni	68.07	+/- 0.47	65.70	+/- 0.45																																																																																																																																																																																																																																			
Mo	6.39	+/- 0.44	3.78	+/- 0.26																																																																																																																																																																																																																																			
Total	100.00		100.00																																																																																																																																																																																																																																				

Figure 21. Cross sectional view featuring morphologies and compositional characteristics of locally enhanced corrosion of SAN 69 (top field) and Super 625 (bottom field). Mixed-type oxide scales and sub-scale zones depleted in chromium are typical.

APPENDIX 7

**Boildec Oy
Field testing of furnace materials
offer extra tests
25.1.2011**



Markus Nieminen
Soodakattilayhdistys

25.1.2011

TULIPESÄSONDIPROJEKTIN LISÄKOE/-KOKEET

Toimituksen sisältö

Boildec tarjoaa lisäkokeiden tekoa niin, että Boildec järjestää koepalojen asennuksen koelaitteistoon, koelaitteiston asennukset MB Joutsenon tehtaan soodakattilaan, kokeiden valvonnan sekä kokeen päätyttyä koelaitteiston purkamisen ja koepalojen toimittamisen VTT:lle analyysijä varten.

Aikataulu

Koe pyritään suorittamaan tilaajan asettamassa aikataulussa niin, että koe voidaan aloittaa kuukauden kuluessa siitä, kun VTT toimittaa Boildecille mittoihin leikatut, asennusvalmiit koepalat. Kun kokeen kesto on n. 1000 tuntia, saadaan koe päätökseen tällöin n. kuuden viikon kuluttua laitteiston asennuksesta. Koelaitteiston purkamiseen ja siirtoon varataan aikaa kaksi viikkoa, joten koestetut koepalat voidaan tällöin toimittaa kolmen kuukauden kuluttua siitä, kun Boildec on saanut käyttöönsä asennusvalmiit koepalat. Tehtaan seisokit saattavat luonnollisesti aiheuttaa aikatauluun viiveitä.

Kustannukset

Kustannukset ovat 20 000 € (+ alv.) per koe.

Laskutus

Työ laskutetaan, kun koepalat on toimitettu VTT:lle ja kokeen valvontareportti on toimitettu SKY:n kestoisuustyöryhmän puheenjohtajalle ja sihteerille.

Boildec Oy
jous

Tar-



2 (2)

Vantaalla, 25.1.2011

Timo Karjunen

APPENDIX 8

**VTT: Pekka Pohjanne
Analyses of furnace materials
offer extra tests
11.2.2011**



Tulipesän sondikoenäytteiden analysointi ja korroosionopeuksien määrittäminen

– 1. Lisänäytteet

| Asiakas Suomen Soodakattilayhdistys ry



Suomen Soodakattilayhdistys ry
Markus Nieminen
PL 4
01621 Vantaa

Tulipesän sondikoenäytteiden analysointi ja korroosionopeuksien määrittäminen – 1. Lisänäytteet

Kiitämme tarjouspyynnöstänne ja tarjoamme teille Boildec Oy:n toteuttaman yhden lisäsondikokeen näytteiden analysoinnin ja korroosionopeuden määrittämisen alla kuvatun suunnitelman mukaisesti.

Tutkimuksen sisältö:

- Osallistuminen sondinäytteiden valmistukseen (koneistus- ja hiontaohjeet sekä valmiiden näytteiden hyväksyntä, Protopshop Oy). (4 näytettä/sondi sekä 4 referenssinäytettä 0-näytteiksi metallografiin tutkimuksiin, yhteensä 8 näytettä)
- Sondiin asennettavien 4 näytteen paksuusprofiilimittaukset, pinta-alamääritykset, punnitukset ja valokuvaus sekä näytteiden toimitus Protopshop Oy:lle sondiin asennettavaksi.
- Sondinäytteiden paksuusprofiilimittaukset kokeen jälkeen sekä korroosionopeuksien määrittäminen paksuusmittaustuloksista (4 näytettä)
- Korroosionmuodon, korroosiotuotekerrosten koostumuksen/rakenteen analysointi pyyhkäisyelektronimikroskoopilla (SEM/EDS koostumusanalyysi) (4 sondinäytettä + 4 referenssinäytettä)
- Tulosten raportointi suomen-/englanninkielisenä tutkimusselostuksena.

Hinta ja laskutus

Tutkimuksen hinta on 11 500 €. Hintaan lisätään kulloinkin voimassaoleva arvonlisävero.

Työ laskutetaan yhdessä erässä, kun työ on tehty ja kirjallinen raportti on toimitettu asiakkaalle.

Mikäli työ edellyttää matkustamista niin syntyneet matka- ja majoituskustannukset sekä päivärahat veloitetaan valtion matkustussäännön mukaisesti ja ne laskutetaan erikseen.

Maksuehdot

Maksuehto on 21 päivää laskun päiväyksestä. Viivästyskorko on korkolain mukainen.

Aikataulu ja raportointi

Aikataulu on riippuvainen mm. koemateriaalien saatavuudesta ja Boildec Oy:n sondikokeiden toteutusaikataulusta.

Tulokset raportoidaan lyhyesti VTT:n suomen-/englanninkielisenä tutkimusraporttina kolmenkuukauden kuluessa sondikokeessa olleiden näytteiden toimituksesta VTT:lle analysoitavaksi.

Muut ehdot

Sondinäytteille ennen koetta tehtäviin paksuusmittauksiin tulee varata riittävästi aikaa. Boildec Oy:n tulee ilmoittaa VTT:lle näytteiden valmistuksen aloituksesta aina vähintään 4 viikkoa ennen suunniteltua kokeenaloitusta. Kokeiden jälkeen näytteet toimitetaan VTT:lle sondista irtileikattuina. Näytteiden irrotus tulee tehdä kuivana, ts. leikkauksessa/sahauksessa ei saa käyttää leikkuunestettä/vettä.

VTT:llä on oikeus mainita toimeksiannon ja toimeksiantajan nimet referenssinään.

Tätä tarjousta tai sen sisältämiä tietoja saa hyödyntää vain VTT:n ja tarjouksen saajan välisessä suhteessa. Tämän tarjouksen osittainenkin kopioiminen, muuttaminen, edelleen luovuttaminen tai käyttäminen muuhun tarkoitukseen ilman VTT:n lupaa on kielletty.

Toimeksiannon ulkopuoliset työt veloitetaan erikseen VTT:n laskutushintojen mukaan.

Muutoin noudatetaan VTT:n yleisiä sopimusehtoja (liite 1).

Yhteyshenkilö

VTT:ssä asiaa hoitavat Pekka Pohjanne, puhelin: 020 722 6863, sähköposti: pekka.pohjanne.@vtt.fi.

Voimassaolo

Tarjouksemme on voimassa edellä mainituin ehdoin 15.03.2011 asti. VTT laatii tilausvahvistuksen, jos tilaus poikkeaa tarjouksesta tai tilaus on suullinen. Näissä tapauksissa tilaus astuu voimaan, kun VTT on sen vahvistanut.

VTT, Valtion teknillinen tutkimuskeskus


Pentti Kauppinen
Teknologiapäällikkö


Pekka Pohjanne
Erikoistutkija 

LIITTEET

1 VTT yleiset sopimusehdot

TOIMEKSIANTOSOPIMUS

- 1.1 Näitä sopimusehtoja sovelletaan osana VTT:n ja toimeksiantajan (jäljempänä sopijapuolet) sopimusta, jolla nämä sopivat VTT:n tekemästä työstä tai tuottamasta palvelusta. Silloinkin, kun toimeksiannon tarkoituksena on kehittää laite tai väline, toimeksiantaja ostaa VTT:ltä kehittämistyötä.
- 1.2 VTT Groupiin katsotaan kuuluvaksi Valtion teknillinen tutkimuskeskus (VTT) sekä sellaiset organisaatiot, joissa VTT käyttää välitöntä tai välillistä määräysvaltaa.
- 1.3 Tarjous, johon VTT:n yleiset sopimusehdot on liitetty, on voimassa yhden (1) kuukauden sen päiväyksestä.
- 1.4 Sopimusta ei voida siirtää kolmannelle osapuolelle ilman toisen sopijapuolen suostumusta.
- 1.5 Sopijapuolet voivat sopia kirjallisesti näiden ehtojen yksittäisten määräysten muuttamisesta tai poissulkemisesta.
- 1.6 Mikäli sopimusasiakirjat ovat sisältöltään ristiriitaisia, on niiden pätevyysjärjestys seuraava: 1) sopimus, 2) tilausvahvistus, 3) tarjous, 4) tilaus, 5) nämä yleiset sopimusehdot ja 6) tarjouspyyntö. Mikäli muu taho kuin sopijapuolet rahoittaa toimeksiantoa, sellaiseen rahoitukseen liittyvät erityiset ehdot sijoittuvat pätevyysjärjestyksessä kaikkien muiden sopimusasiakirjojen edelle.

2. YHTEISTOIMINTAORGANISAATIO

- 2.1 Sopijapuolet asettavat toimeksiantoa varten vastuuhenkilönsä. Vastuuhenkilön muutoksesta on ilmoitettava toiselle sopijapuolelle.
- 2.2 Mikäli toimeksianto suoritetaan projektiorganisaatiossa, toimeksiannon suoritusta ohjaa johtoryhmä, johon sopijapuolet nimeävät edustajansa.
- 2.3 Johtoryhmän tehtävänä on käsitellä projektia koskevia asioita sekä erityisesti valvoa ja ohjata projektin toteuttamista sopimuksen rajaamissa puitteissa. Tätä varten johtoryhmä:
 - täsmentää projektille asetetut tavoitteet ja hyväksyy projektia koskevat suunnitelmat,
 - käsittelee projektisuunnitelman tarkistukset ja muutokset sekä tarvittaessa esittelee ne sopijapuolten hyväksyttäväksi,
 - valvoo projektin edistymistä ja tukee projektipäällikön toimintaa,
 - hyväksyy projektin tulokset ja toteaa projektin loppuunsaorituksen
- 2.4 Johtoryhmä ei voi muuttaa sopimusta tai sen liitettä, ellei sopijapuolten kesken siitä erikseen kirjallisesti sovita.

3. VELOITUS

- 3.1 Sopimusasiakirjoissa sovitaan toimeksiannon veloituksista. Hinta ilmaistaan euroina.
- 3.2 Arvonlisävero sekä mahdolliset ulkomaiset verot ja viranomaismaksut lisätään sovittuun hintaan.
- 3.3 Mikäli toimeksiannon tavoitetta tai aikataulua muutetaan taikka sopimuksen voimassaoloaikana tapahtuu toimeksiantajan ja VTT:n yhteisesti toteamia olennaisia kustannustason muutoksia, tarkistetaan veloitusta vastaavasti ko. ajankohdasta.
- 3.4 Ellei laskutusaikataulusta ole muuta sovittu, VTT laskuttaa sovitun hinnan toimeksiannon aikataulua vastaavissa kuukausierissä.
- 3.5 VTT:llä on oikeus toimittaa toimeksiannon tulokset postiennakkolla tai vaatia osittaisia ennakkomaksua.
- 3.6 VTT:llä on oikeus pitää hallussaan toimeksiannon tulokset, kunnes toimeksianto on kokonaan maksettu.
- 3.7 Maksu on suoritettava 21 päivän kuluessa laskun päiväyksestä. Viivästyskorko on voimassaolevan korkolain (20.8.1982/633) mukainen viivästyskorko. Laskuun lisätään mahdolliset perintäkulut. Laskun huomautusaika on 8 päivää.

4. LUOTTAMUKSELLISUUS

- 4.1 Sopijapuolet sitoutuvat pitämään salassa sopimuksen voimassaolon lakattua toimeksiannon yhteydessä tai siihen liittyen toiselta sopijapuolelta saadut liike- ja ammattisalaisuudet ja muut luottamukselliset tiedot. Salassapitovelvoite lakkaa kymmenen (10) vuoden kuluttua sopimuksen voimassaolon päättymisestä, ellei sopimuksessa ole sovittu lyhyempää aikaa.

- 4.2 Salassapitovelvoitteesta huolimatta VTT:llä on tarvittaessa oikeus antaa luottamuksellisia tietoja hyväksytyille alihankkijoilleen sekä VTT Groupiin kuuluville organisaatioille edellyttäen, että VTT huolehtii näiden sitouttamisesta vastaavan laajuisiin salassapitovelvoitteisiin.
- 4.3 VTT:llä on oikeus mainita toimeksiannon ja toimeksiantajan nimet referenssinään.

5. OMISTUS- JA KÄYTTÖOIKEUDET

- 5.1 Sopijapuolen toiselle sopijapuolelle luovuttama tieto, ideat, menetelmät, ratkaisumallit, laitteet, aineet ja muu aineisto, riippumatta siitä ovatko ne suojattuja tai suojattavissa immateriaalioikeudellisesti, jotka ovat syntyneet toimeksiannon ulkopuolella (tausta-aineisto), kuuluvat luovuttavalle sopijapuolelle. Mikäli VTT:n tausta-aineistoa tarvitaan toimeksiannon tulosten hyödyntämiseen, tausta-aineiston käyttöoikeuden ehdoista sovitaan kirjallisesti erikseen.
- 5.2 Tieto, ideat, menetelmät, ratkaisumallit, laitteet, aineet ja muu aineisto, riippumatta siitä ovatko ne suojattuja tai suojattavissa immateriaalioikeudellisesti, jotka VTT esittää toimeksiannon toteuttamista varten, mutta jotka eivät tule osaksi toimeksiannon tulosta, ovat VTT:n omaisuutta.
- 5.3 Tieto, ideat, menetelmät, ratkaisumallit, laitteet, aineet ja muu aineisto, mukaan lukien syntyneet raportit ja selvitykset, riippumatta siitä ovatko ne suojattuja tai suojattavissa immateriaalioikeudellisesti, jotka ovat syntyneet toimeksiannon yhteydessä ja tulevat osaksi toimeksiannon tulosta (tulosaaineisto) ovat toimeksiantajan omaisuutta, ellei sopimuksessa ole todettu toimeksiannon kohteena olevan VTT:n ydinteknologia (core technology). Jälkimmäisessä tapauksessa VTT saa omistusoikeuden tuloksiin ja toimeksiantaja saa tuloksiin erikseen määritellyn käyttöoikeuden toimeksiantajan kannalta järkevässä laajuudessa.
- 5.4 Mikäli VTT rahoittaa toimeksiantoa tai hankkii toimeksiannolle muuta julkista rahoitusta, VTT saa toteutunutta julkista rahoitusosuutta vastaavan ja/tai rahoitusehtojen mukaisen omistusoikeuden toimeksiannon tuloksiin.
- 5.5 Omistus-, immateriaali- ja muut oikeudet toimeksiannon yhteydessä syntyneeseen tietokoneohjelmaan, tietokantaan, integroidun piirin piirimalliin ja biotekniisiin löydöksiin kuuluvat VTT:lle. Toimeksiantaja saa tällaisiin tuloksiin erikseen määritellyn käyttöoikeuden toimeksiantajan kannalta järkevässä laajuudessa.
- 5.6 Sopijapuolet saavat käyttää toimeksiannon suorittamista varten käyttöönsä saamaansa toisen sopijapuolen tausta-aineistoa vain sopimuksen mukaisten tehtävien suorittamisessa.
- 5.7 Toimeksiantoa varten VTT:n itselleen hankkimat työvälineet ja laitteet ovat VTT:n omaisuutta.
- 5.8 VTT:llä on oikeus käyttää hyväkseen toimeksiannon yhteydessä saavutettua ammattitaitoa ja kokemusta myös muussa kuin sopimuksen tarkoittamassa toiminnassa.
- 5.9 Tulosaaineiston kuulussa toimeksiantajalle omistusoikeus siirtyy toimeksiantajalle, kun toimeksianto on kokonaan maksettu.

6. OIKEUS KEKSINTÖÖN

- 6.1 Toimeksiantaja saa oikeuden sellaisiin keksintöihin, jotka toimeksiannon tuloksina tulevat toimeksiantajan omaisuudeksi sopimuksen ja näiden ehtojen mukaisesti.
- 6.2 Keksijä tekee työsuhtekeksintöläin (29.12.1967/656) mukaisen kirjallisen ilmoituksen työsuhtekeksinnöstä omalle työnantajalleen.
- 6.3 Sopijapuolen on viipymättä ilmoitettava kirjallisesti toiselle sopijapuolelle tehdystä keksinnöstä.
- 6.4 Mikäli toimeksiantaja haluaa oikeuden keksintöön, hänen on ilmoitettava kirjallisesti VTT:lle vaatimuksensa keksintöön kahden (2) kuukauden kuluessa saatuaan tiedon keksinnöstä uhalla, että VTT saa kaikki oikeudet keksintöön.
- 6.5 Sopijapuolet toimivat siten, että keksinnön ennenaikainen julkiseksi tulo estyy.
- 6.6 Keksijä tunnustetaan keksinnön tekijäksi. Keksijä on oikeutettu saamaan kohtuullisen korvauksen tehdystä keksinnöstä. Kaikki patentista aiheutuvat kustannukset ja korvauksen keksijälle maksa se sopijapuoli, jolla on tai joka saa oikeuden keksintöön.

APPENDIX 9

**Teollisuuden Vesi Oy
Water recommendation
introduction and table of contents
14.1.2011**

Veden ja höyryn laatusuositukset soodakattilalaitoksille

1. Johdanto

Vedenkäsittely ja vesikemia ovat olleet mukana Soodakattilayhdistyksen projekteissa vuosien ajan, sillä ne liittyvät oleellisesti soodakattilan turvalliseen käyttöön. Hyvällä vesikemialla voidaan vähentää mm. kerrostumien syntymistä kattilassa ja siten myös riskejä kattilan vaurioitumiselle. Veden laadun seuranta soodakattilalaitoksilla on perustunut pitkälti DENÅn esitettyihin ohjearvoihin sekä kattilatoimittajilta saatuihin arvoihin. Usea laitos on soveltanut vesikemiaa näiden ohjeiden pohjalta ja luonut omat laitoskohtaiset ohjearvonsa. Lisäksi kemikaalitoimittaja on saattanut antaa omia ohjearvoja esim. pH:lle ja jäännöskemikaaleille. Käytetyt arvot ovat hyvin pitkälle toisiaan vastaavia, mutta lukujen alkuperä on saattanut vaipua hämärän peittoon. Osa ohjearvokokoelmista on myös puutteellisia tai riittämättömiä vesikemian hallintaan.

Tässä ohjearvosuosituksessa tuodaan esille nykytilanne ohjearvoista ja sovelletaan niitä soodakattilaympäristöön painealueelle 60...160 bar. Vertailupohjana on käytetty sekä VGB:n, EPRI:n että Värmeforskin julkaisemia ohjearvosuosituksia. Höyryn laatuvaatimuksissa on viitattu IEC:n raporttiin. Näiden ohjearvoraporttien lisäksi työssä on käytetty tukena v. 2003 vahvistettua paineastioiden turvalliseen käyttöön tähtäävää standardia EN12952-12. EU:n standardien ja muiden ohjearvokokoelmien välillä suurin ero on se, että EU-standardin paneutuessa laitosten turvalliseen käyttöön muut ohjearvot pyrkivät edistämään laitosten taloudellista käyttöä. Sama linja otetaan käyttöön tässä suosituksessa. Suosituksia kirjattaessa on ajateltu erityisesti taloudellisen käytön varmistamista turvallisen käytön lisäksi.

Verrattuna voimalaitoksiin ja lämpökattiloihin soodakattilalaitoksilla on prosessin tuomia erityispiirteitä, jotka on huomioitu suosituksia rakennettaessa. Niitä ovat korkea tulipesärasitus kattilassa, höyryn käyttö polttoilman esilämmittimissä, prosessilauhteiden mahdollinen kontaminoituminen, lisäveden suuri suhteellinen osuus syöttövedessä sekä orgaanisten kemikaalien käyttö. Yhdeksi keskeiseksi tavoitteeksi työssä on asetettu vesihöyrykierron kontrollin ja valvonnan lisääminen tilanteissa, joissa kierrolle tunnusomaista on suuret orgaanisen aineen pitoisuudet, mahdolliset vuodot lauhteisiin ja lisäveden suuri määrä.

Toinen keskeinen osa ohjearvotyössä on vesihöyrykierron laadun valvonnan ohjeistaminen. Se painottuu jatkuvatoimisten mittalaitteiden mahdollisimman kattavaan ja luotettavaan käyttöön yhdistettynä käsin tehtäviin laboratoriomäärityksiin. Varsin mittaviin ja aikaa vieviin mittausrutiineihin on etsitty vaihtoehtoja muista standardeista esim. ASME ja EPRI. Tavoitteena on ollut hakea mittauksille riittävä vähimmäistaso painottaen tehtävien mittausten laatua ja tarkoituksenmukaisuutta määrän sijaan.

Varsinaisten ohjearvojen ja valvontaohjeiden ohella tuodaan esille arvioita, mitä etuja/hyötyjä paremmalla veden laadulla sekä kattilalle että turbiinille on hyötysuhteen, korroosion tai kerrostumien kannalta. Lisäksi on taulukoitu mahdollisia syitä ohjearvojen alitukseen tai ylityksiin, tuotu esille poikkeamien vakavuutta sekä kerrottu tarkistus- ja toimintaohjeita poikkeamatilanteisiin.

Lauhteenkäsittely ja sen tekniikka liittyy oleellisesti soodakattilaympäristöön, sillä ajoittainen huono prosessilauhteiden laatu sekä orgaanisten kattilavesikemikaalien käyttö tekee siitä vaativan ajettavan sekä seurattavan. Tämä koskee sekä sekavaihdinta että pehmennyssuodatinta. Lauhteiden laatua, lauhteenkäsittelyn tasoa, soveltuvuutta ja tarpeellisuutta on käsitelty omana kokonaisuutenaan.

Suosituksissa ei ole otettu kantaa siihen, miten lisävesi käsitellään haluttuun tasoon. On lähdetty siitä, että kaikesta raakavedestä voidaan puhdistaa vaatimusten mukaista vettä, mutta sekä tekniikat että kustannukset veden valmistuksessa voivat muuttua. Tämä tulee ottaa huomioon uutta laitosta suunniteltaessa. Vanhoilla laitoksilla lisäveden laatua voidaan tarvittaessa parantaa eri tekniikoilla (esim. humussuodatin, UV-käsittely ja kalvotekniikat).

Raportti on jäsennelty niin, että se toimii samalla vesikemian oppaana ja työkirjana. Suositukset on esitetty sekä kuvina että taulukoina, jolloin oman laitoksen arvoja on hyvä verrata niihin. Tavoitteena on ollut helppolukuinen raportti, josta löytyvät tänä päivänä laitoksilla tarvittavat vesikemian tiedot sekä perusteet kemikaalien, mittauspisteiden, mitattavien suureiden sekä lauhteenkäsittelyn valinnalle ja lisäveden laadulle.

Sisällysluettelo

Yhteenveto

1. Johdanto
2. Ohjearvojen soveltuvuus, rajaukset, tulkinta ja käyttö
3. Vesikemian perusteet
 - 3.1. Vesi-/höyrykierto
 - 3.2. Korroosion perusteet
 - 3.3. Vesikemian tavoitteet
4. Vesikemian valinta
 - 4.1. Prosessi ja käytetyt materiaalit
 - 4.2. Höyry
 - 4.3. Kattila
 - 4.3.1. fosfaattikemia
 - 4.3.2. lipeäkemia
 - 4.3.3. amiinikemia
 - 4.4. Syöttövesi ja lauhde
 - 4.4.1. ammoniakki
 - 4.4.2. amiinit
 - 4.4.3. hapenpoisto
 - 4.5. Lauhteidenkäsittely
5. Vesihöyrykierron valvonta
 - 5.1. Valvonnan perusteet
 - 5.2. Näytepisteet ja edustava näytteenotto
 - 5.3. Vesihöyrykierron mittaukset ja seurattavat komponentit
 - 5.4. Vähimmäisvaatimukset valvonnalle
6. Ohjearvot ja toimintarajat
 - 6.1. Toimintarajat
 - 6.2. Höyry
 - 6.3. Kattilavesi
 - 6.4. Syöttövesi
 - 6.5. Lauhde
 - 6.6. Lisävesi
7. Ohjearvojen ylitys- ja alitustilanteet
 - 7.1. Poikkeamatilanteet
 - 7.2. Tarkistus- ja toimintaohjeet

APPENDIX 10

**Åbo Akademi: Nikolai DeMartini, Patrik Yrjas, Tor Lauren, Mikko Hupa
Dew point measurements
Offer
8.12.2010**



Proposal for Dew point Measurements

8 Dec 2010

This is a proposal to make dew point measurements, SO₃ measurements and corrosion measurements in two boilers: one Kraft boiler with the possibility of operating with low and high SO₂ and O₂; and Heinola's NSSC boiler with extremely high SO₂. Measurements would be taken behind the ESP, before any scrubber.

The purpose is to get reliable information of the low temperature corrosion conditions in recovery boiler flue gases being cooled further.

1. Dew point measurements will be made with a commercial instrument ("Land" etc). The question here is the sensitivity of the electrical signal at the low concentrations of condensing sulfuric acid normally present in kraft boiler flue gases.
2. Corrosion measurements will be made with our air-cooled probes and samples will be analyzed with SEM-EDS. Careful control of the probe temperature will be required. Also open questions relate to the exposure time.
3. Flue gas samples will be bubbled through an isopropyl alcohol (IPA) water mixture for capture of SO₃ and subsequent analysis of the sulfate ion concentration - according to the standard methods for SO₃ analysis. The challenge here is to exclude any escape of particulate material in the IPA solution. Dust sulfate carryover to the IPA solution will disturb the SO₃ analysis.

The cost for this work is €30 000 (+VAT) and is contingent on one of the two dew point analyzers we have access to (1 at ÅAU, 1 from LUT) working. We will test both before starting the project and if major repairs or a new unit is needed we will make a new proposal accordingly before starting the project.

Prepared by:

Nikolai DeMartini
Patrik Yrjas
Tor Lauren
Mikko Hupa

Senior Researcher
Senior Researcher
Mill Measurement Expert
Professor